Springer Theses
Recognizing Outstanding Ph.D. Research

Nobuyuki Matsumoto

Classical Pendulum Feels Quantum Back-Action

Springer

Springer Theses

Recognizing Outstanding Ph.D. Research

Aims and Scope

The series "Springer Theses" brings together a selection of the very best Ph.D. theses from around the world and across the physical sciences. Nominated and endorsed by two recognized specialists, each published volume has been selected for its scientific excellence and the high impact of its contents for the pertinent field of research. For greater accessibility to non-specialists, the published versions include an extended introduction, as well as a foreword by the student's supervisor explaining the special relevance of the work for the field. As a whole, the series will provide a valuable resource both for newcomers to the research fields described, and for other scientists seeking detailed background information on special questions. Finally, it provides an accredited documentation of the valuable contributions made by today's younger generation of scientists.

Theses are accepted into the series by invited nomination only and must fulfill all of the following criteria

- They must be written in good English.
- The topic should fall within the confines of Chemistry, Physics, Earth Sciences, Engineering and related interdisciplinary fields such as Materials, Nanoscience, Chemical Engineering, Complex Systems and Biophysics.
- The work reported in the thesis must represent a significant scientific advance.
- If the thesis includes previously published material, permission to reproduce this must be gained from the respective copyright holder.
- They must have been examined and passed during the 12 months prior to nomination.
- Each thesis should include a foreword by the supervisor outlining the significance of its content.
- The theses should have a clearly defined structure including an introduction accessible to scientists not expert in that particular field.

More information about this series at http://www.springer.com/series/8790

Nobuyuki Matsumoto

Classical Pendulum Feels Quantum Back-Action

Doctoral Thesis accepted by
The University of Tokyo, Tokyo, Japan

Springer

Author
Dr. Nobuyuki Matsumoto
Department of Physics
The University of Tokyo
Tokyo
Japan

Supervisor
Assoc. Prof. Masaki Ando
The University of Tokyo
Tokyo
Japan

ISSN 2190-5053 ISSN 2190-5061 (electronic)
Springer Theses
ISBN 978-4-431-55880-4 ISBN 978-4-431-55882-8 (eBook)
DOI 10.1007/978-4-431-55882-8

Library of Congress Control Number: 2015957122

Printed on acid-free paper

This Springer imprint is published by SpringerNature
The registered company is Springer Japan KK

Parts of this thesis have been published in the following journal articles:

- Matsumoto, N., Michimura, Y., Aso, Y., & Tsubono, K. Optically trapped mirror for reaching the standard quantum limit. *Opt. Express* **22**, 12915 (2014).
- Matsumoto, N., Komori, K., Michimura, Y., Hayase, G., Aso, Y., & Tsubono, K. 5-mg suspended mirror driven by measurement-induced backaction. *Phys. Rev. A* **92**, 033825 (2015).

Supervisor's Foreword

By using the interactions between optical radiation and mechanical motion, it is possible to explore and to manipulate the quantum behavior of a macroscopic object. This Ph.D. thesis by Nobuyuki Matsumoto takes a significant step in this newly emerging research field, called *Optomechanics*, by experiments with a triangular optical cavity with a mirror with 5 mg mass.

One of the main motivations for this thesis was to take the first step to test quantum mechanics on a macroscopic scale. Although quantum mechanics is successful in explaining physics on a microscopic scale, its validity on the macroscopic scale is still being debated. An issue of quantum decoherence, the transition from the microscopic quantum world to the macroscopic "classical" world, is not clearly solved. To test it experimentally, a macroscopic system, in which any classical noise contributions are well suppressed, is required.

Another motivation for this thesis was to obtain knowledge to improve the sensitivity of precision measurement such as with gravitational-wave antennae. With extremely high transmissivity, observation of gravitational waves will give us new insights into the astrophysical phenomena and the birth and history of the universe itself. Sensitivity of laser interferometric gravitational-wave antennae under construction now will be limited by optical quantum fluctuations. Although several schemes to reduce optical quantum noises are being proposed, they have not been tested experimentally because of the difficulty in developing a prototype interferometer with a sensitivity limited only by optical quantum noises.

The key step for these investigations is a direct observation of quantum back-action (quantum radiation pressure fluctuation) of a laser beam acting on a suspended macroscopic mirror. For that purpose, several groups have been trying to develop an optical cavity with high circulating laser power comprising a tiny mirror to enhance the back-action effect. However, high intra-cavity power and a low-noise mirror cannot be achieved simultaneously in a straightforward manner because of an effect called Siddles–Sigg instability (see the thesis for details).

Dr. Matsumoto came up with the idea that this problem could be solved by using a triangular optical cavity and developed an experimental setup based on that

concept. In addition, he implemented several state-of-the-art precision measurements so as to stabilize the cavity and to avoid various kinds of noises: an optical spring by an additional laser beam, suspension with low-mechanical loss to reduce thermal noise, vibration isolation stages to reduce seismic noise, and others. As a result, Dr. Matsumoto successfully realized an experimental setup in which the quantum back-action level is 1.4 times larger than suspension thermal fluctuation.

This was the first time to achieve suppression of thermal fluctuation below the optical quantum radiation pressure fluctuation in a macroscopic scale of 5 mg mass. I hope readers will grasp the idea and experimental schemes and will enjoy them.

Tokyo, Japan
August 2015

Assoc. Prof. Masaki Ando

Acknowledgments

The research described in this thesis advanced under the supervision of KimioTsubono until he retired in 2012. As my former supervisor, Prof. Tsubono had enabled me to apply myself to research. When I was a member of the Tsubono laboratory, I never worried about lack of research equipment, research fund, and so on. He also provided some opportunities to work as a T.A. He prepared the best academic research environment not only for me but for everybody in the laboratory. This environment has been maintained by the incredible support of Yoichi Aso and my present supervisor, Masaki Ando, even after his retirement. I would like to thank Prof. Aso for his abundant advice, especially for building the experimental apparatus. I am thankful to Prof. Ando for being interested in my experiment and for his encouragement. I am not sure I would have been able to finish this work without their help.

I have had the greatest good fortune to work with talented and inspiring people. First, I have to mention Noriaki Ohmae. In 2011, when I had almost finished my work, he provided me with a great deal of advice, some of which led to the present research. I was able to find the theme of this research as a result of his advice.

Kenshi Okada and Yuta Michimura were incredible supporters with whom I argued most about the experiment, the future, and so on. Kenshi Okada is a man of executive ability, and an unconventional discussion with him proved to be the most fun for me. I also thank him for his appreciation whenever possible. Yuta Michimura is a person who can move things along steadily. He and I joined the laboratory at about the same time, and together we studied various matters together. He has always been the first person with whom I discuss various issues. I also thank him for telling me how to use the spectrum analyzer and giving me much other useful information. Their help was useful not only from a research aspect but also in other ways.

Ayaka Shoda, Takafumi Ushiba, and Masayuki Nakano were the members of the seminar when the idea of a triangular cavity occurred to me. I would like to thank them for useful discussions at that time. Takafumi also has worked with me to develop the high Q-value pendulum after 2014.

Kentaro Komori and Yuya Kuwahara, respectively, have worked together with me on different projects after 2014. Kentaro has helped me to measure and analyze the data presented in this thesis. Without his incredible contribution, this thesis would not have been possible. Yuya has played a central role in the development of the high Q-value pendulum.

I would like to thank Gen Hayase, who became famous as the developer of the marshmallow-like gel. At the beginning, the experiment using a new low-density mirror made of silica aerogel had been planned, and he had been advancing its development. That plan is still in progress. I would also like to thank Kazuyoshi Kanamori and Kazuki Nakanishi for their help. Kazuki Nakanishi recommended that I use a thin mirror. I was truly surprised and impressed by the aerogel that they were developing.

I am grateful to Shigenori Moriwaki, Kei Oikawa, and Norikatsu Mio for their help. When I tried to attach a wire to the tiny mirror, they let me use a microscope that they had been using. I would also like to thank Shigenori Moriwaki for his advice.

I also thank Michiko Kudoh and Ami Ito. They always supported me. I am sorry for not beginning this acknowledgment with gratitude to Michiko Kudo. I am grateful to Koji Ishidoshiro and Wataru Kokuyama for their help to me. I also thank other colleagues in the Ando laboratory: Kazunori Shibata and Kodai Tejima.

I would like to thank members of the Kawamura laboratory at ICRR: Seiji Kawamura, Shihori Sakata, Takumi Mori, Kazuhiro Agatsuma, Daniel Friedrich, and Masayuki Nakano for making me do the seminar. Based on the findings of Shihori's doctoral thesis, I was able to design the experiment.

I thank Kentaro Somiya for giving me the opportunity to go to Germany.

I am thankful to Yutaka Shikano for providing me with opportunities to join the workshop. I also thank Yutaka for giving much advice for writing a paper, a theoretical understanding of the quantum measurement problem, and so on. He is an impressive man and also fun to work with.

Sigmakoki Co., Ltd., Mirapro Co., Ltd., and Ultra Finich Technology Co., Ltd. (UFT) are companies that are working together. Sigmakoki developed the 5 mg mirror and now is developing the special-order product for our next experiment. Mirapro and UFT developed the vacuum chamber, inside which electrochemical buffing (ECB) was performed, for our next experiment.

I have personally admired the doctoral theses by Kenji Numata, Yoichi Aso, Keisuke Goda, Kirk Mackenzie, Henning Vahlbruch, Thomas Corbitt, and Haixing Miao, as their quality was extremely important for my research.

This research was supported by a Grant-in-Aid for JSPS Fellows No. 13J10490.

Finally, I am thankful to my parents for their patient encouragement and support.

Contents

Chapter 1
Introduction

Abstract In recent years, significant improvements in optical and mechanical elements have led to the development of the field of *optomechanics*, where mechanical oscillators couple optical fields via the radiation pressure of light. In this chapter, we provide a short history of study about optomechanical effects, and explain briefly about a part of optomechanical effects, e.g., cavity-assisted cooling, instability, measurement limit for continuous measurement, ponderomotive squeezing, and entanglement. Especially, the measurement limit for continuous measurement is explained in detail, because the quantum back-action was inferred from the noise analysis in our estimation. This chapter presents the historical and physical background of this research.

Keywords Optomechanics · Quantum back-action · Measurement limit · Continuous measurement

1.1 Optomechanical Effects

Light has momentum, and thus can exert pressure on objects through the exchange of momentum between the light and the objects. These forces were hypothesized by Johannes Kepler in the 17th century, on the basis of the fact that dust tails of comets pointed away from the Sun during a comet transit [1]. James Clerk Maxwell theoretically predicted radiation pressure by his Maxwell's equations in 1873. On the other hand, Adolfo Giuseppe Bartoli predicted the same result as Maxwell based on the second law of the thermodynamics in 1876 [2]. The first experimental demonstration of the *stationary* pressure of light was made by Peter Lebedew in 1901, by using a torsional balance, which was set in the vacuum tank ($\sim 10^{-2}$ Pa) to eliminate the radiometer effect [3]. In 1903, Ernest Nichols and Gordon Hull also conducted a similar, but advanced in terms of mitigating the radiometer effect, experiment [4].[1]

[1]This experiment was introduced in the novel entitled as "Sanshirō", which was written by the Japanese famous writer Natsume Sōseki in 1908. In the novel, Nonomiya-sensei performed the Nichols's experiment in the basement of the University of Tokyo. Our experiment was also performed in the basement of the University of Tokyo to measure the pressure of light, similarly to that

N. Matsumoto, *Classical Pendulum Feels Quantum Back-Action*,
Springer Theses, DOI 10.1007/978-4-431-55882-8_1

They improved the setup by increasing reflectance of the torsional balance's surface (Ag coating) in order to increase the pressure of light acting on the torsion balance, and tuned pressure inside the tank (∼2 kPa) such that the direction of the force due to the radiometer effect added to both arms of a torsional balance becomes opposite (and they are canceled each other). In 1909, Albert Einstein derived the statistics of the radiation pressure force fluctuations imposed on a movable mirror including the "radiation friction" [5]. From this analysis, he revealed the dual wave-particle nature of blackbody radiation.

Since then, various types of optomechanical effects have been both theoretically and experimentally explored using various types of optomechanical devices. Examples are given below.

- **Cooling**
  The cooling of an object by a laser is one of the most attractive features of optomechanics. This cooling effect mainly occurs due to the frictional (damping) force of light. Because a laser field is almost in its ground state (e.g., infrared optical field having an effective temperature of about 15,000 K), this damping force reduces the velocity of the object without introducing other thermal fluctuating forces (i.e., this effect is similar to "cold" damping described in Ref. [6]). As a result, the object is effectively cooled. This effect can also be understandable by scattering picture, as shown in the caption of Fig. 1.1.
  So far, the cooling method has been widely used from atom-scale to kg-scale objects, partially for trapping [7–9], achieving the ground state [10–12] and eliminating technical limitations [13–16]. Another aspect of the cooling is the optical spring effect [17–21], which not only changes the damping constant of the mechanical system, but it also changes the spring constant. This effect is certainly useful for examining the quantum behavior of mechanical oscillators *free* from external control, see also in Sect. 2.2.2.
- **Instability**
  The first cavity optomechanical experiment demonstrated bistability induced by the radiation-pressure force acting on a macroscopic mirror in the optical domain [22]. Since then, various types of instability, such as parametric instability [23, 24], have been reported. In our case, overcoming an optical anti-torsional effect (so-called Siddles-Sigg instability [25, 26]) was one of two technical features in the experiment. We realized it by an optical torsional spring effect in a triangular cavity, which was independently shown by Daniel Sigg and myself, see also in Chap. 4.
- **Measurement limit**
  Braginsky represented the fundamental consequences of the Heisenberg uncertainty principle (HUP) [27], and demonstrated that it imposes a limit on any force measurement since the 1960s [28, 29]. This fundamental quantum limit for the measurement sensitivity is called the standard quantum limit (SQL). SQL is the

(Footnote 1 continued)
written in Sanshirō. The difference is that Nonomiya-sensei's target was the *stationary* pressure of the light but our target was the *fluctuated* pressure of the light.

sum of components derived from the quantization of light, and of a mechanical oscillator, which lead to the generation of inevitable fluctuation, called *vacuum fluctuation* of the light and *zero-point fluctuation* of the oscillator, respectively (details are described in the next subsection). SQL applies universally to all devices that use a mechanical oscillator as a probe mass.

To overcome this limit, various types of techniques, such as input-squeezing [30–32], modification of the dynamics of the mechanical oscillator by an optical spring [33–35] and the measurement of a conserved dynamical quantity of the mechanical oscillator [36, 37], have been proposed. Today, all of them, which can overcome the SQL imposed on the free mass (so-called free-mass SQL) within a certain frequency range, are called QND (quantum nondemolition) measurements [38]. The QND measurement is a stronger necessary condition than the observation of quantum back-action for the generation of macroscopic entanglement states in laser interferometer [39].

- **Squeezing**
  When an oscillator is fluctuated by quantum radiation pressure fluctuation (i.e., observation of quantum back-action), a quadrature variance of the light is squeezed due to self-phase modulation, like that of Kerr squeezing in fibers [40, 41]. This effect is called ponderomotive squeezing, and has been observed using cold atoms [42], a NEMS oscillator [43] and a MEMS oscillator [14] after the observation of quantum back-action. Ponderomotive squeeing has a key to perform the QND measurement, see also in Sect. 3.1.1.
- **Entanglement**
  Entanglement is a physical phenomenon in which multiple subsystems can only be described with reference to each other. In other words, entanglement can be considered as to be correlations between small quantum fluctuations around a carrier field in the frequency domain [44]. Entanglement is at the heart of physical investigations not just because of its critical role in marking the boundary between classical and quantum world, but also because of its key role for realizing quantum information processing.

  Optomechanical coupling via radiation pressure is a promising approach to generate entanglement states, e.g. entanglement between mechanical degrees of freedom [39, 44–46] and entanglement between a light field and a mechanical oscillator [47–50].

In addition, optomechanical effects have been expected to be utilized as an engine via radiation pressure [51] and as a form of quantum memory [52, 53], and so on [54–57]. Especially, the first one was excellently realized as a space solar sail. IKAROS (Interplanetary Kite-craft Accelerated by Radiation Of the Sun) of the Japan Aerospace Exploration Agency (JAXA) [58] is the first spacecraft to successfully demonstrate the solar-sail technology in interplanetary space.

As described above, the optomechanical effects have a potential to allow for breakthroughs in a large variety of fields, such as precise weak-force measurements, quantum information, fundamental tests of quantum mechanics, and even satellite development. Effects induced by *stationary* radiation pressure, such as laser cool-

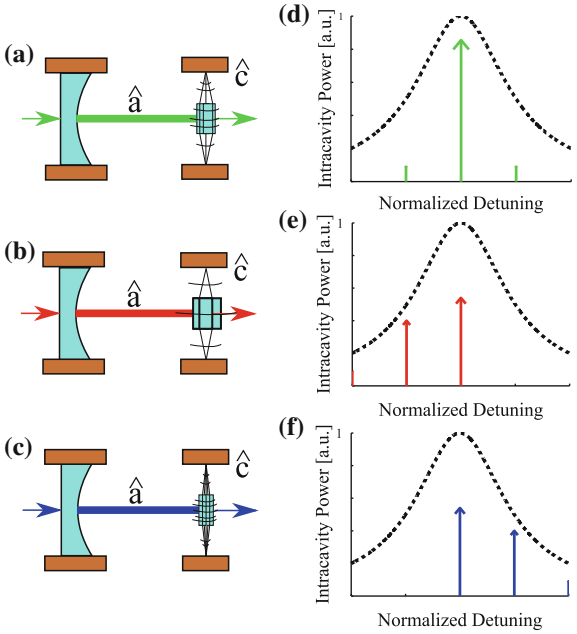

Fig. 1.1 Basic cavity optomechanical effects. Consider an optical cavity that consists of fixed and movable mirrors. **a–c** These figures are respectively schematic representations of three types of detuning: on-resonance, *red*-detuning (i.e., the frequency of the input light is lower than the resonant frequency of the optical cavity) and *blue*-detuning (i.e., the frequency is higher than the resonant). Here, $\hat{a}$ is a photon annihilation operator and $\hat{c}$ is a phonon annihilation operator of the movable mirror (see also in Sects. 2.1.1 and 2.2.1). **a** The input light is modulated by the resonant frequency of the movable mirror, such that the upper (lower) sideband component of the light acquires (sheds) energy from the mirror. (This is analogous to the generation of Stokes and anti-Stokes sidebands in Raman scattering.) As a result, there is no exchange of energy between the light and the mirror. This interaction can be characterized by $(\hat{a} + \hat{a}^\dagger)\hat{x}$, and thus it can be used as the displacement measurement. Here, $\hat{x}$ represents the position of the movable mirror. **b** The upper sideband component is enhanced by the optical cavity, and thus the motion of the mirror is damped (cooling). This interaction can be characterized by $\hat{a}^\dagger\hat{c} + \hat{a}\hat{c}^\dagger$, and thus it can be used to coherently transfer the state between the light and the mirror [56, 57]. **c** The lower sideband component is enhanced by the optical cavity, and thus the motion of the mirror is anti-damped (heating). This interaction can be characterized by $\hat{a}\hat{c} + \hat{a}^\dagger\hat{c}^\dagger$, and thus it can be used to create the various types of entanglement states [44–49]. **d–f** These figures show the intra-cavity power as a function of the detuning normalized by a resonant frequency of the movable mirror, when the cavity is tuned (d), the *red*-detuned (e), and the *blue*-detuned (f), respectively.

ing, instability and the solar sail have been experimentally realized. However effects induced by quantum *fluctuation* of radiation pressure, such as the generation of entanglement states, squeezed states and reaching/beating the SQL are still challenging to be realized, particularly in the macroscopic regime.

1.1.1 Quantum Noise Limit

Measuring weak forces is at the heart of modern physics from the macroscopic scale to the atomic scale, e.g. gravitational-wave (GW) detectors [59–62] and atomic-force microscopy [63]. In spite of the progress of lasers, optical components and mechanical oscillators, no optomechanical systems have yet reached the *free-mass* SQL [64]. The free-mass SQL is a next goal after the observation of quantum back-action, because it not only limits the sensitivity, but also defines a benchmark noise spectral density at which the door is opened to experimentally investigate macroscopic quantum mechanics, such as the generation of macroscopic entanglement states [39]. Here, we show the details of the SQL.

The force noise (double-sided) spectral density of the SQL, $S^{(2)}_{\mathrm{FF,SQL}}$ is given by [65]

$$S^{(2)}_{\mathrm{FF,SQL}}(\omega) = \hbar|\chi_{\mathrm{m}}(\omega)|^{-1} + 2\hbar\omega_{\mathrm{m}}\gamma_{\mathrm{m}}m. \tag{1.1}$$

Here, ω is the angular frequency, $\hbar$ the Dirac constant, m the mass of the oscillator, γ_{m} the amplitude mechanical decay rate (i.e., the mechanical quality factor Q_{m} is given by $Q_{\mathrm{m}} = \omega_{\mathrm{m}}/2\gamma_{\mathrm{m}}$) and χ_{m} the mechanical susceptibility. The first term arises from the quantization of light and the second term arises from mechanical quantization. This equation represents that the effect of the oscillator's quantization can be easily removed at above the resonant frequency [65, 66] if the mechanical decay rate is small (i.e., high mechanical quality factor), as shown in Fig. 1.2. It is worth pointing out that this is close to the actual situation of GW detectors, in which a quasi-freely suspended mirror with the resonant frequency of around 1 Hz and a very high quality factor about $10^7 - 10^9$, are monitored at above 10 Hz. Therefore, Eq. (1.1) is usually written as $S^{(2)}_{\mathrm{FF,SQL}}(\omega) = \hbar|\chi_{\mathrm{m}}(\omega)|^{-1}$ in the field of GW detectors; this is just called "the SQL" in the field (in this thesis, we use the term 'usual SQL' as meaning this). Also, this equation tells us that: (i) both of the components in Eq. (1.1) are equal at the resonance; and (ii) the usual SQL, the free-mass SQL, and the SQL are all equal far above the resonance of the mechanical oscillator.

The part of the SQL derived from the quantization of light is understandable, as described below. Light is a continuous electromagnetic wave, and its energy is delivered in discrete packets, called photon. Concerning the light emitted by a laser, which is a good approximation to a coherent state and has Poissonian statistics, the photons arrive randomly on a mirror. This randomness, which is called the "vacuum fluctuation", produces both direct phase noise and indirect phase noise, called shot noise and radiation pressure shot noise, respectively. The vacuum fluctuation of the *phase* quadrature (orthogonal to a carrier field) directly gives rise to phase noise (i.e., sensing noise), which is inversely proportional to the optical power, while the vacuum fluctuation of the *amplitude* quadrature (parallel to the carrier) creates a random radiation-pressure force on the mirror (i.e., force noise) that results in optical phase noise, which is directly proportional to the optical power. In general, the shot noise dominates at higher frequency and the radiation pressure shot noise dominates at lower frequency because the mechanical susceptibility of an oscillator

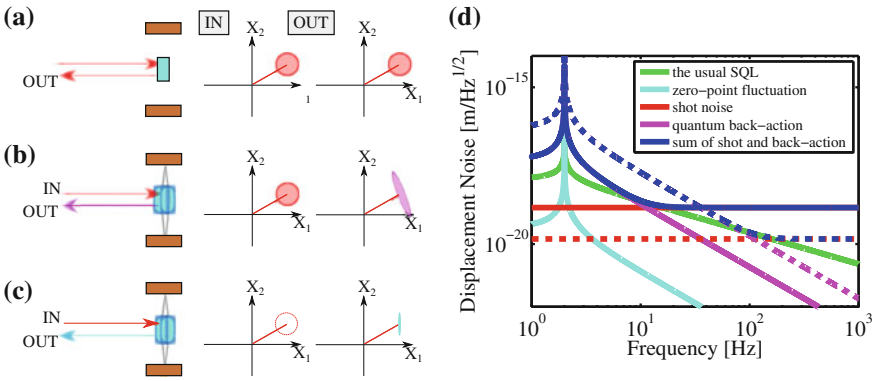

Fig. 1.2 Various types of quantum noise. Consider measurement of weak force imposed on a mirror (the force is encoded in the sequence of displacements) using an interferometer. **a**, **b**, **c** Schematic representations, which are called *ball-on-stick* pictures, of quantum noise. The amplitude of the laser is represented as a stick, while the fluctuation of light is represented as a ball on the stick. Here, X_1 is the amplitude quadrature and X_2 is the phase quadrature. In the conventional scheme, the displacement fluctuation is read out using information concerning the phase quadrature. **a** Shot noise is drawn. It limits the sensitivity, even if there is no zero-point fluctuation of the mirror, because it is just the *optical* effect. **b** Quantum back-action is drawn. It limits the sensitivity even if there is no zero-point fluctuation because it is the *optomechanical* effect induced by the quantum radiation pressure fluctuation through the mechanical susceptibility. Due to the self-phase modulation, the state of light is squeezed such that the noise level of the phase quadrature increases. This effect is enhanced at lower frequency according to the frequency dependence of the mechanical susceptibility. As a result, the noise level of the quantum back-action is equal to the shot noise and more, at low frequency region. **c** Zero point-fluctuation is drawn. It limits the sensitivity even if there is no vacuum fluctuation of light because it is just the *mechanical* effect. **d** Shows the amplitude power spectrum of the quantum noise for a 1 kg test mass. The contribution of the zero-point fluctuation subtracted from the SQL [(usual for the field of the GW detectors) depicted as a green line], the contribution of zero-point fluctuation (*cyan*), quantum back-action (*magenta*), shot noise (*red*) and the sum of the shot noise and the radiation pressure shot noise (*blue*) are shown. The *dotted magenta*and *red* represent the case of 10-times higher power than the above. If the sum of the quantum back-action and the shot noise is minimized with respect to the input power, the minimum noise is equal to the (free-mass) SQL.

has a frequency dependence of f^{-2} beyond a resonant frequency (furthermore, the quantum radiation pressure fluctuation does not have any frequency-dependence within the cavity linewidth; see also in Sect. 2.3.1). If these two types of noise are *not* correlated, they will induce a lower bound on the detector sensitivity independent of the optical power, which leads to the SQL [65, 67], as shown in Fig. 1.2.

Another part of the SQL derived from the quantization of an oscillator is understandable as described below. The oscillator consists of various types of normal modes, and its energy is delivered in discrete packets, called phonon. Let us focus on the specific normal mode, and naturally assume that the other modes are sufficiently sparse, such that there is no spectral overlap with each other. For a specific mechanical mode being sufficiently cooled [e.g., by laser cooling and direct cooling], which is a good approximation to the ground state and has zero-point energy, the oscillator

undergoes inevitable fluctuation. This fluctuation, which is called the "zero-point fluctuation", also limits the sensitivity as force noise.

So far, no experiment has yet reached the free-mass SQL, since the thermal fluctuating force induced by a thermal bath is usually far above the free-mass SQL. In general, reaching the free-mass SQL requires that (i) the force noise be dominated by quantum back-action, (ii) the readout noise be dominated by shot noise, and (iii) the readout laser power be optimized such that their sum is minimized. Therefore, our development of the macroscopic oscillator driven by quantum back-action larger than thermal fluctuating force is the first step toward the free mass SQL. On the other hand, reaching the SQL on the resonance represents the ground-state cooling, because the (approximate) phonon occupation number $k_{\mathrm{B}}T/\hbar\omega_{\mathrm{m}}$ represents the ratio of the thermal fluctuating force to the SQL (See Eq. 7.1). On the macroscopic scale, ground-state cooling via (cavity-assisted) passive cooling is very difficult, because the cavity condition is usually *bad* (see also in Sect. 2.3.1) due to the low resonant frequency of the oscillator. This results in an increase of the quantum back-action, even if the thermal excitation can be removed. The dilution techniques (see also in Sect. 2.2.2) and a *back-action evasion* method (see also in Sect. 3.1.1) might enable the macroscopic mirror to reach its ground state.

1.2 Observation of Quantum Back-Action

Lastly in this chapter, we provide a short history about the observation of quantum back-action.

The first measurement of quantum back-action was performed using cold atoms by Stamper-Kurn et al. in 2008 [68]. Using copper wires embedded in an atom chip, they magnetically trapped and loaded an ultracold ensemble of Rb 87 (the number of atoms is 10^5) into the cavity. They then transferred the ensemble into a laser trap (wavelength of 850 nm), a very far detuned longitudinal mode of the cavity. The probe light (wavelength of 780 nm) was coupled to another longitudinal mode, which drives the ensemble through the optical dipole force. Its transmission was recorded while exiting the ensemble, because the ensemble behaves similarly to that of a dispersive piece of glass, changing the effective length of the cavity (i.e., "dispersive" optomechanical coupling). By blue-detuning the probe laser, such that it deposited phonons into the ensemble, the quantum back-action could be observed as a heating of the ensemble. As a result, they were able to measure the cavity-light-induced heating of the intracavity atomic ensemble. After this measurement, they also measured the ponderomotive squeezing in 2012 [42].

The second measurement was performed using a photonic crystal nanobeam by Safavi-Naeini et al. in 2012 [69]. At first, they reported their experiment as being an observation of the quantum motion of a nanomechanical resonator. Khalili et al. [65] showed that the results of this experiment not only characterized the quantum motion, but also demonstrated the existence of quantum back-action noise, just as in 2012.

In their experiment, they used a patterned silicon nanobeam, which formed an optomechanical crystal capable of localizing both optical and acoustic waves. An optical fiber taper was used to couple light evanescently into the breathing mechanical mode of the silicon optomechanical device (effective mass of 311 fg). The cavity was designed to have two optical resonances, one for cooling (wavelength is 1460 nm) and one for readout of mechanical motion (wavelength is 1545 nm). In this case, the cooling had the key to characterize the zero-point motion. After this measurement, they also measured ponderomotive squeezing in 2013 [43].

The third measurement was performed using a SiN membrane (effective mass of 7 ng) by Purdy et al. in 2013 [13]. The membrane motion could be coupled to a cavity through the dispersive interaction. This interaction imprinted phase and amplitude modulations onto transmitted laser light, thus allowing for readout of the membrane motion. In addition, the laser applied an optical gradient force to the membrane, while pushing it toward higher optical intensity. They used one laser source (wavelength of 1064 nm) being split into two components by an acousto-optical modulator (AOM): one for cooling and the other for readout of the mechanical motion. In this case, the cooling was used for reducing the technical difficulties (e.g., parametric instability), not for enhancing the ratio of the quantum back-action to thermal noise (see also in Sect. 2.2.2). After this measurement, they also measured the ponderomotive squeezing in 2013 [14].

In our experiment, we developed a suspended 5 mg mirror driven by (classical) back-action, whose quantum component was estimated to be larger than thermal fluctuating force by a factor of 1.4 ± 0.2 at 325 Hz [16]. Concerning the macroscopic mass scale, there have been intensive studies at MIT, NAOJ, etc. [70–72] since the mid-2000s. The MIT group used a 1 g suspended mirror, and they reported the usefulness of the double optical spring [21]. The NAOJ group (currently, ICRR group) used a 22 mg suspended mirror, and they reported the measurement of an anti-torsional spring effect [26] in a linear optical cavity. Our development are based on their findings. The details will be described after this chapter.

References

1. Kepler, J.: De Cometis (1619)
2. Bartoli, A.G.: Sopra i movimenti prodotti dalla luce e dal calore (1876)
3. Lebedew, P.: Untersuchungen über die Druckkräfte des Lichtes. Ann. Phys. **311**, 433 (1901)
4. Nichols, E.F., Hull, G.F.: The pressure due to radiation. Astrophys. J. **17**(5), 315–351 (1903)
5. Einstein, A.: Entwicklung unserer Anschauungen über das Wesen und die Konstitution der Strahlung. Phys. Z. **10**, 817–825 (1909)
6. Hirakawa, H., Hiramatsu, S., Ogawa, Y.: Damping of Brownian motion by cold load. Phys Lett. **63**, 3 (1977)
7. Ashkin, A.: Trapping of atoms by resonance radiation pressure. Phys. Rev. Lett. **40**, 12 (1978)
8. Ashkin, A., Dziedzic, J.M., Yamane, T.: Optical trapping and manipulation of single cells using infrared laser beams. Nature **330**, 769–771 (1987)
9. Tongcang, L., Kheifets, S., Medellin, D., Raizen, M.G.: Measurement of the instantaneous velocity of a Brownian particle. Science **328**, 1673 (2010)

10. O'Connell, A.D., et al.: Quantum ground state and single-phonon control of a mechanical resonator. Nature **464**, 697–703 (2010)
11. Teufel, J.D., et al.: Sideband cooling of micromechanical motion to the quantum ground state. Nature **475**, 359–363 (2011)
12. Chan, J., et al.: Laser cooling of a nanomechanical oscillator into its quantum ground state. Nature **478**, 89–92 (2011)
13. Purdy, T.P., Peterson, R.W., Regal, C.A.: Observation of radiation pressure shot noise on a macroscopic object. Science **339**, 801 (2013)
14. Purdy, T.P., Yu, P.-L., Peterson, R.W., Kampel, N.S., Regal, C.A.: Strong optomechanical squeezing of light. Phys. Rev. X. **3**, 031012 (2013)
15. Matsumoto, N., Michimura, Y., Aso, Y., Tsubono, K.: Optically trapped mirror for reaching the standard quantum limit. Opt. Express **22**, 12915 (2014)
16. Matsumoto, N., Komori, K., Michimura, Y., Hayase, G., Aso, Y., Tsubono, K.: 5-mg suspended mirror driven by measurement-induced backaction. Phys. Rev. A **92**, 033825 (2015)
17. Braginsky, V.B., Manukin, A.: Ponderomotive effects of electromagnetic radiation. Sov. Phys. JETP **25**, 653 (1967)
18. Braginsky, V.B., Gorodetsky, M.L., Khalili, F.Y.: Optical bars in gravitational wave antennas. Phys. Lett. A. **232**, 340 (1997)
19. Braginsky, V.B., Khalili, F.Y.: Low noise rigidity in quantum measurements. Phys. Lett. A. **257**, 241 (1999)
20. Sheard, B.S., Gray, M.B., Mow-Lowry, C.M., McClelland, D.E.: Observation and characterization of an optical spring. Phys. Rev. A. **69**, 051801(R) (2004)
21. Corbitt, T., et al.: An all-optical trap for a gram-scale mirror. Phys. Rev. Lett. **98**, 150802 (2007)
22. Dorsel, A., McCullen, J.D., Meystre, P., Vignes, E., Walther, H.: Optical bistability and mirror confinement induced by radiation pressure. Phys. Rev. Lett. **51**, 17 (1983)
23. Braginsky, V.B., Vyatchanin, S.P.: Parametric oscillatory instability in Fabry-Perot interferometer. Phys. Lett. A. **287**, 331–338 (2001)
24. Carmon, T., Rokhsari, H., Yang, L., Kippenberg, J., Vahala, J.: Temporal behavior of radiation-pressure-induced vibrations of an optical microcavity phonon mode. Phys. Rev. Lett. **94**, 223902 (2005)
25. Sidles, J.A., Sigg, D.: Optical torques in suspended Fabry-perot interferometers. Phys. Lett. A. **354**, 167–172 (2006)
26. Sakata, S., Miyakawa, O., Nishizawa, A., Ishizaki, H., Kawamura, S.: Measurement of angular antispring effect in optical cavity by radiation pressure. Phys. Rev. D. **81**, 064023 (2010)
27. Heisenberg, W.: Über den anschaulichen Inhalt der quantentheoretischen Kinematik und Mechanik. Z. Phys. **43**, 172–198 (1927)
28. Braginsky, V.B., Khalili, T.Y.: Quantum Measurement. Cambridge University Press, Cambridge (1992)
29. Braginsky, V.B., Khalili, F.Y.: Quantum Measurements. Cambridge University Press, Cambridge (1995)
30. Caves, C.M.: Quantum-mechanical noise in an interferometer. Phys. Rev. D. **23**, 8 (1981)
31. Kimble, H.J., Levin, Y., Matsko, A.B., Thorne, K.S., Vyatchanin, S.P.: Conversion of conventional gravitational-wave interferometers into quantum nondemolition interferometers by modifying their input and/or output optics. Phys. Rev. D. **65**, 022002 (2001)
32. Goda, K., et al.: A quantum-enhanced prototype gravitational-wave detector. Nature Phys. **4**, 472–476 (2008)
33. Buonanno, A., Chen, Y.: Optical noise correlations and beating the standard quantum limit in advanced gravitational-wave detectors. Class. Quant. Grav. **18**, L95–L101 (2001)
34. Buonanno, A., Chen, Y.: Quantum noise in second generation, signal-recycled laser interferometric gravitational-wave detectors. Phys. Rev. D. **64**, 042006 (2001)
35. Buonanno, A., Chen, Y.: Signal recycled laser-interferometer gravitational-wave detectors as optical springs. Phys. Rev. D. **65**, 042001 (2002)
36. Braginsky, V.B., Vorontsov, Y.I., Thorne, K.S.: Quantum nondemolition measurements. Science **209**, 4456 (1980)

37. Purdue, P., Chen, Y.: Practical speed meter designs for quantum nondemolition gravitational-wave interferometers. Phys. Rev. D. **66**, 122004 (2002)
38. Chen, Y., Danilishin, S.L., Khalili, F.Y., Müller-Ebhardt, H.: QND measurements for future gravitational-wave detectors. Gen. Relativ. Gravit. **43**, 671–694 (2011)
39. Müller-Ebhardt, H., Rehbein, H., Schnabel, R., Danzmann, K., Chen, Y.: Entanglement of macroscopic test masses and the standard quantum limit in laser interferometry. Phys. Rev. Lett. **100**, 013601 (2008)
40. Mancini, S., Tombesi, P.: Quantum noise reduction by radiation pressure. Phys. Rev. A. **49**, 5 (1994)
41. Fabre, C., et al.: Quantum-noise reduction using a cavity with a movable mirror. Phys. Rev. A. **49**, 2 (1994)
42. Brooks, D.W.C., et al.: Non classical light generated by quantum-noise-driven cavity optomechanics. Nature **488**, 476–480 (2012)
43. Safavi-Naeini, A.H., et al.: Squeezed light from a Silicon micromechanical resonator. Nature **500**, 185–189 (2013)
44. Mancini, S., Giovannetti, V., Vitali, D., Tombesi, P.: Entangling macroscopic oscillators exploiting radiation pressure. Phys. Rev. Lett. **88**, 12 (2002)
45. Pinard, M., et al.: Entangling movable mirrors in a double-cavity system. Europhys. **72**, 747–753 (2005)
46. Mazzola, L., Paternostro, M.: Distributing fully optomechanical quantum correlations. Phys. Rev. A. **83**, 062335 (2011)
47. Vitali, D., et al.: Optomechanical entanglement between a movable mirror and a cavity field. Phys. Rev. Lett. **98**, 030405 (2007)
48. Paternostro, M., et al.: Creating and probing multipartite macroscopic entanglement with light. Phys. Rev. Lett. **99**, 250401 (2007)
49. Joshi, C., Larson, J., Jonson, M., Andersson, E., Öhberg, P.: Entanglement of distant optomechanical systems. Phys. Rev. A. **85**, 033805 (2012)
50. Mial, H., Danilishin, S., Chen, Y.: Universal quantum entanglement between an oscillator and continuous fields. Phys. Rev. Lett. **81**, 052307 (2010)
51. Korneev, L.K., Tssander, F.A.: Problems of flight by jet propulsion interplanetary flights (1961)
52. Cole, G.D., Aspelmeyer, M.: Cavity optomechanics mechanical memory sees the light. Nat. Nanotechnol. **6**, 690–691 (2011)
53. Wang, Y.-D., Clerk, A.: A using interference for high fidelity quantum state transfer in optomechanics. Phys. Rev. Lett. **108**, 153603 (2012)
54. Stannigel, K., Rabl, P., Sørensen, A.S., Zoller, P., Lukin, M.D.: Optomechanical transducers for long-distance quantum communication. Phys. Rev. Lett. **105**, 220501 (2010)
55. Weis, S., et al.: Optomechanically induced transparency. Science **330**, 1520 (2010)
56. Zhang, J., Peng, K., Braunstein, L.: Quantum-state transfer from light to macroscopic oscillators. Phys. Rev. Lett. **68**, 013808 (2003)
57. Palomaki, T.A., Harlow, J.W., Teuful, J.D., Simmonds, R.W., Lehnert, K.W.: Coherent state transfer between itinerant microwave fields and a mechanical oscillator. Nature **495**, 14 (2013)
58. Tsuda, Y., et al.: Achievement of IKAROS—Japanese deep space solar sail demonstration mission. Acta Astronaut. **82**, 183–188 (2013)
59. Harry, G.M., et al.: Advanced LIGO: the next generation of gravitational wave detectors. Class. Quant. Gravity **27**, 084006 (2010)
60. Somiya, K.: Detector configuration of KAGRA-the Japanese cryogenic gravitational-wave detector. Class. Quant. Grav. **29**, 12 (2012). (Aso, Y. et al. Interferometer design of the KAGRA gravitational wave detector. Phys. Rev. D. **88**, 043007 (2013)). http://gwcenter.icrr.u-tokyo.ac.jp/en/. Accessed 9 Mar 2015
61. http://www.geo600.uni-hannover.de. Accessed 9 Mar 2015
62. http://wwwcascina.virgo.infn.it. Accessed 9 Mar 2015
63. Giessibl, F.J.: Advances in atomic force microscopy. Rev. Mod. Phys. **75**, 949–983 (2003)
64. Westphal, T., et al.: Interferometer readout noise below the standard quantum limit of a membrane. Phys. Rev. A. **85**, 063806 (2012)

65. Khalili, F.Y., et al.: Quantum back-action in measurements of zero-point mechanical oscillations. Phys. Rev. A. **86**, 033840 (2012)
66. Braginsky, V.B., et al.: Noise in gravitational-wave detectors and other classical-force measurements is not influenced by test-mass quantization. Phys. Rev. D. **67**, 082001 (2003)
67. Braginsky, V.B., Khalili, F.Y.: Quantum nondemolition measurements: the route from toys to tools. Rev. Mod. Phys. **68**, 1–11 (1996)
68. Murch, K.W., Moore, K.L., Gupta, S., Stamper-Kurn, D.-M.: Observation of quantum-measurement backaction with an ultracold atomic gas. Nat. Phys. **4**, 561–564 (2008). http://ultracold.physics.berkeley.edu/pmwiki/Main/E3. Accessed 9 Mar 2015
69. Safavi-Naeini, A.H., et al.: Observation of quantum motion of a nanomechanical resonator. Phys. Rev. Lett. **108**, 033602 (2012)
70. Okutomi, A., Yamamoto, K., Miyoki, S., Ohashi, M., Kuroda, K.: Development of a radiation pressure noise interferometer. J. Phys.: Conf. Ser. **32**, 327–332 (2006)
71. Mow-Lowry, C.M., et al.: Towards the SQL: status of the direct thermal-noise measurements at the ANU. J. Phys.: Conf. Ser. **32**, 362–367 (2006)
72. Verlot, P., et al.: Towards the experimental demonstration of quantum radiation pressure noise. C. R. Phys. **12**, 826–836 (2011)

Chapter 2
Theory of Optomechanics

Abstract In this chapter, we describe the basic aspects of optical cavities, mechanical resonators, and cavity optomechanical systems, e.g. optical response of the cavity, mechanical dissipation (thermal decoherence), dilution technique, the (double) optical spring, quantum back-action, phase-induce back-action noise, and Raman decoherence. Especially, the dilution technique due to the gravitational and optical potential is explained in detail, because it is one of the most important technical features in our experiment. This chapter also presents the basic concepts and mathematical tools for understanding later chapters.

Keywords Gravitaional dilution · Optical dilution · Cavity optomechanics · Quantum back-action · Bad cavity condition

2.1 Optical System

There are two equally important aspects in the physical theory: the mathematical formalism of the theory, and its intuitive interpretation. In this section, we describe the mathematical formalism for the quantization of light and the result. Also, we present intuitive interpretations of classical/quantum fluctuation, which is so-called the *ball-on-stick* picture.

2.1.1 The Quantized Electromagnetic Field

In 1927, Paul Dirac proposed quantization of the electromagnetic field in order to solve the problem of the wave-particle duality. In this quantum theory, each mode of a radiation field is identified by a quantized simple harmonic oscillator.f The properties of the quantized field are introduced in the context of an optical cavity mode with angular frequency of $\omega_{\boldsymbol{k}}$. The positive and negative components of the electric field can be written in terms of the boson creation and annihilation operators, $\hat{a}_{\boldsymbol{k}}^{\dagger}$ and $\hat{a}_{\boldsymbol{k}}$, and the spatial mode function, $\boldsymbol{u}(\boldsymbol{r})$:

N. Matsumoto, *Classical Pendulum Feels Quantum Back-Action*,
Springer Theses, DOI 10.1007/978-4-431-55882-8_2

$$\boldsymbol{E}^{(+)}(\boldsymbol{r},t) = i\sum_{\boldsymbol{k}}\left(\frac{\hbar\omega_{\boldsymbol{k}}}{2\varepsilon_0}\right)^{1/2}\hat{a}_{\boldsymbol{k}}\boldsymbol{u}(\boldsymbol{r})\exp(-i\omega_{\boldsymbol{k}}t), \tag{2.1}$$

$$\boldsymbol{E}^{(-)}(\boldsymbol{r},t) = -i\sum_{\boldsymbol{k}}\left(\frac{\hbar\omega_{\boldsymbol{k}}}{2\varepsilon_0}\right)^{1/2}\hat{a}^{\dagger}_{\boldsymbol{k}}\boldsymbol{u}(\boldsymbol{r})^{*}\exp(i\omega_{\boldsymbol{k}}t). \tag{2.2}$$

Here, $\hbar$ is the Dirac constant and ε_0 is the permittivity of free space. The sum of the positive and negative components gives the whole electric field given by

$$\boldsymbol{E}(t) = i\sum_{\boldsymbol{k}}\left(\frac{\hbar\omega_{\boldsymbol{k}}}{2\varepsilon_0}\right)^{1/2}\left[\hat{a}_{\boldsymbol{k}}\boldsymbol{u}(\boldsymbol{r})\exp(-i\omega_{\boldsymbol{k}}t) - \hat{a}^{\dagger}_{\boldsymbol{k}}\boldsymbol{u}(\boldsymbol{r})^{*}\exp(i\omega_{\boldsymbol{k}}t)\right]. \tag{2.3}$$

The creation and annihilation operators are dimensionless, and satisfy the boson commutation relations,

$$[\hat{a}_{\boldsymbol{k}},\hat{a}_{\boldsymbol{k}'}] = [\hat{a}^{\dagger}_{\boldsymbol{k}},\hat{a}^{\dagger}_{\boldsymbol{k}'}] = 0,\ [\hat{a}_{\boldsymbol{k}},\hat{a}^{\dagger}_{\boldsymbol{k}'}] = \delta_{\boldsymbol{k}\boldsymbol{k}'}. \tag{2.4}$$

These commutation relations can allow us to distinct between classical and quantum optics. In classical optics, an equivalent of Eq. (2.3) can be found by replacing the annihilation and creation operators with complex field amplitudes. The amplitudes in classical optics commute, and thus they are not limited by the Heisenberg uncertainty relation and its consequences. In quantum mechanics, however, the operators must be Hermitian in order to represent observable quantities. The annihilation and creation operators are not Hermitian, and are thus not observables. They can be written in terms of a Hermitian operator pair for the amplitude quadrature, $\hat{X}_1$, and the phase quadrature, $\hat{X}_2$:

$$\hat{a} = \frac{1}{2}(\hat{X}_1 + i\hat{X}_2), \tag{2.5}$$

$$\hat{a}^{\dagger} = \frac{1}{2}(\hat{X}_1 - i\hat{X}_2), \tag{2.6}$$

The quadrature operators for the amplitude and phase are:

$$\hat{X}_1 = \hat{a} + \hat{a}^{\dagger}, \tag{2.7}$$

$$\hat{X}_2 = -i(\hat{a} - \hat{a}^{\dagger}). \tag{2.8}$$

The amplitude and phase quadratures represent non-commuting observable parameters. The operator for an arbitrary quadrature, ξ, can be defined using a linear combination of $\hat{X}_1$ and $\hat{X}_2$,

$$\hat{X}_{\xi} = \hat{X}_1\cos(\xi) + \hat{X}_2\sin(\xi). \tag{2.9}$$

2.1.2 The Heisenberg Uncertainty Principle

The Heisenberg uncertainty principle (HUP) [1] quantifies the ultimate precision of continuous measurement of non-commuting observable parameters, as described in Chap. 1. HUP tells us that if any two observable parameters, $\hat{O}_1$ and $\hat{O}_2$, satisfy the commutation relation,

$$[\hat{O}_1, \hat{O}_2] = \xi, \tag{2.10}$$

they are bounded by HUP,

$$\Delta\hat{O}_1 \Delta\hat{O}_2 \geq \frac{|\xi|}{2}, \tag{2.11}$$

where $\Delta\hat{O}$ is the standard deviation of the operator $\hat{O}$. The standard deviation is defined by

$$\Delta\hat{O} = \sqrt{\langle\hat{O}^2\rangle - \langle\hat{O}\rangle^2}. \tag{2.12}$$

The variance of the operator is the square of the standard deviation,

$$V = (\Delta\hat{O})^2. \tag{2.13}$$

The commutator relation of the amplitude and the phase quadratures of the electromagnetic field is

$$[\hat{X}_1, \hat{X}_2] = 2i, \tag{2.14}$$

and thus HUP is

$$\Delta\hat{X}_1 \Delta\hat{X}_2 \geq 1. \tag{2.15}$$

This relation shows that the trade-off between the fluctuation of the amplitude quadrature and that of the phase quadrature. Therefore, this also shows the trade-off between the shot noise and the radiation pressure shot noise for the force measurement.

2.1.3 States of Light

Here, several common states (a coherent state, a vacuum state, a squeezed state of light, and a classically noisy state) are described and shown in *ball-on-stick* pictures. In the ball-on-stick pictures, the classical steady-state coherent amplitude of the field is represented as a stick, while the fluctuation of light is represented as a ball on the

stick, which is analogous to the phasor diagram used in classical physics where the orthogonal axes are the real and imaginary parts of an electromagnetic field. Various states of light can be visually understood by this.

- **The coherent state**
  A coherent state is a minimum-uncertainty state with equal uncertainties in the two quadrature components, so that

$$\Delta\hat{X}_1 = \Delta\hat{X}_2 = 1. \tag{2.16}$$

  The quadrature fluctuations of the coherent state have no frequency dependence, and obey Poissonian statistics. For the coherent state, the sidebands are randomly distributed in phase, and thus there is no special phase. Although the coherent state is realized by the laser, the laser light has excess noise below the MHz region, whereas we measured a pendulum motion. Thus, stabilization of the laser intensity fluctuation is necessary for measurement of the quantum back-action. In our case, the quantum back-action was now estimated by measurement of the classical behaver, see also in Fig. 6.5a.
- **The vacuum state**
  A vacuum state is also a minimum-uncertainty state with equal uncertainties in the two quadrature components, but it has no coherent amplitude ($\bar{a} = \langle\hat{a}(t)\rangle = 0$). It always occupies all frequency, spatial, and polarization modes. The vacuum state is important in quantum-optical experiments, since it enters optical systems in any unfilled ports of the beam splitters, cavities, and partially transmissive mirrors. In our case, the vacuum state prevents stabilization of the laser intensity noise from achieving the minimum uncertainty level, see in Sect. 5.1 and Appendix.
- **The squeezed state**
  A squeezed state is a non-classical state in which fluctuation is reduced below the symmetric quantum limit in one quadrature component. In order to satisfy HUP, the standard deviation of the orthogonal quadrature must be greater than the quantum noise limit and the product of the two quadratures greater than or equal to unity. If the amplitude quadrature is reduced, it is called the amplitude squeezed state, and vice versa. Thus, the minimum uncertainty amplitude squeezed state, for example, has

$$\Delta\hat{X}_1 = 1/z, \tag{2.17}$$

$$\Delta\hat{X}_2 = z, \tag{2.18}$$

  where z is a real and a positive number. The amplitude-squeezed state is shown in Fig. 2.1.
- **Classically noisy states**
  In general, lasers produce non-minimum-uncertainty states, which have excess noise of classical origin at sideband frequencies below the MHz region. The classical noise of a laser is often many times greater than the quantum noise in both quadratures,

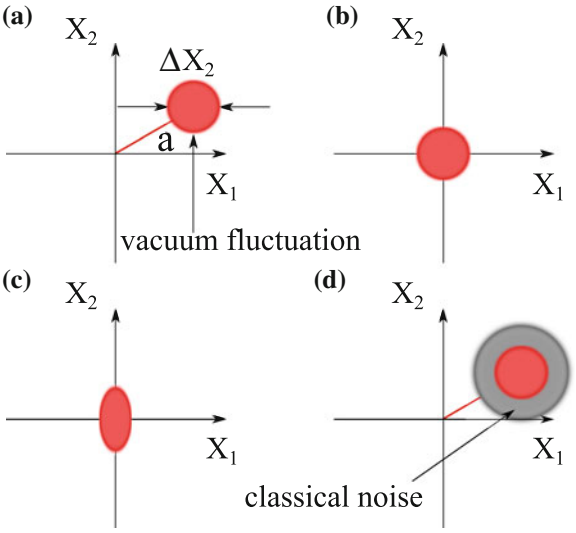

Fig. 2.1 Ball-and-stick pictures for states of light. **a** Coherent state is represented. **b** Vacuum state is represented. **c** Amplitude squeezed state is represented. **d** Classically noisy state is represented

$$\Delta\hat{X}_1 \geq 1, \ \Delta\hat{X}_2 \geq 1. \tag{2.19}$$

The classical noise can be reduced via: passive noise suppression using an optical cavity [2]; active feedback control ; or both. The noisy state is characterized by comparing with the shot noise level in units of dB (so-called the relative to the shot-noise level) and its coherent laser power in units of $1/\mathrm{Hz}^{1/2}$ (so-called relative intensity noise). The former is an useful index for quantum measurements, such as observation of the quantum back-action and generation of the squeezed state. The latter is an useful index for force measurement, such as that used in gravitational-wave detectors.

2.1.4 Optical Cavity

Fabry-Perot interferometers, often referred to as (optical) cavities, consist of two or more partially transmissive mirrors in order to make the light resonate inside it. In this section, the equation of motion for a cavity mode is introduced; we then obtain the reflected and transmitted fields using this equation.

2.1.4.1 Equation of Motion

Consider the empty cavity shown in Fig. 2.2. It is made of three partially transmissive optics labeled, in, out, and l, referring to the input coupler, the output coupler, and

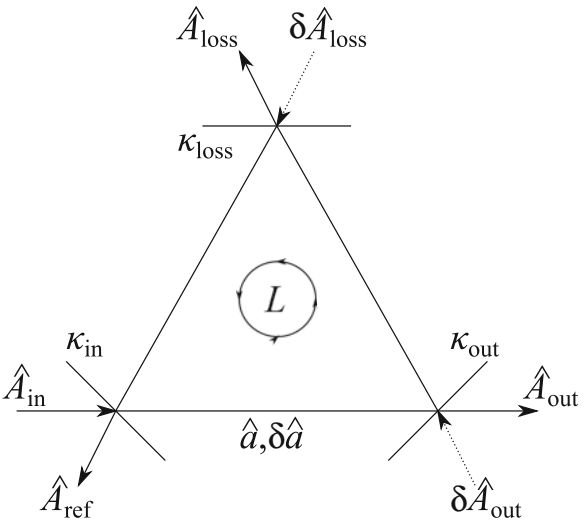

Fig. 2.2 Layout of the optical cavity. Consider a cavity composed of two mirrors: an input coupler, with a decay rate of κ_{in}; an output coupler, with a decay rate of κ_{out}; a mirror to represent intracavity loss, with a decay rate of κ_{loss}; and the roundtrip length of the cavity, L. The cavity mode is labeled $\hat{a}$. The extracavity fields are: $\hat{A}_{\text{in}}$, $\hat{A}_{\text{out}}$, $\hat{A}_{\text{ref}}$, $\hat{A}_{\text{loss}}$, $\delta\hat{A}_{\text{out}}$ and $\delta\hat{A}_{\text{loss}}$

the partially transmissive mirror used to simulate losses, respectively. The equation of motion for cavity mode $\hat{a}$ in units of $\sqrt{\text{photon}}$ is [3]

$$\dot{\hat{a}} = -(i\omega_{\text{c}} + \kappa)\hat{a} + \sqrt{2\kappa_{\text{in}}}\hat{A}_{\text{in}}e^{-i\omega_A t} + \sqrt{2\kappa_{\text{out}}}\hat{A}_{\text{out}} + \sqrt{2\kappa_{\text{loss}}}\hat{A}_{\text{loss}}, \tag{2.20}$$

where the driving field, A_{in}, in units of $\sqrt{\text{photon}/\text{s}}$ has a coherent amplitude at frequency ω_{A}; the other fields, A_{out} and A_{loss}, are assumed to be in the vacuum state. The cavity mode has a resonant frequency of ω_c.

The equation of motion can be written in the rotating frame of reference by setting

$$\hat{a} \rightarrow \hat{a}e^{-i\omega_A t}, \tag{2.21}$$

$$\hat{A}_{\text{in}} \rightarrow \hat{A}_{\text{in}}e^{-i\omega_A t}, \tag{2.22}$$

and thus

$$\dot{\hat{a}} = (i\triangle - \kappa)\hat{a} + \sqrt{2\kappa_{\text{in}}}\hat{A}_{\text{in}} + \sqrt{2\kappa_{\text{out}}}\hat{A}_{\text{out}} + \sqrt{2\kappa_{\text{loss}}}\hat{A}_{\text{loss}}, \tag{2.23}$$

where $\Delta = \omega_A - \omega_c$ is the cavity detuning [i.e., the positive (negative) detuning means the blue-detuning (red-detuning)]. In the mean-field approximation [4, 5], the amplitude decay rates for each mirror are given by the amplitude transmissivity divided by the round trip time, $\tau = L/c$, where L is the roundtrip of the cavity. That is,

$$\kappa_{\text{in}} = \frac{\sqrt{T_{\text{in}}}}{\tau} \simeq \frac{T_{\text{j}}}{2\tau}$$
$$\kappa_{\text{out}} \simeq \frac{T_{\text{out}}}{2\tau}$$
$$\kappa_{\text{loss}} \simeq \frac{1 - \mathscr{L}_c}{2\tau}, \tag{2.24}$$

where $\mathscr{L}_{\text{c}}$ is the cavity round-trip loss. The total decay rate is given by

$$\kappa = \kappa_{\text{in}} + \kappa_{\text{out}} + \kappa_{\text{loss}}. \tag{2.25}$$

In the steady state, the cavity mode can be found by setting $\dot{\hat{a}} = 0$ and considering the time-independent component $\bar{a}$. Given that the steady state amplitudes of the fields $\bar{A}_{\text{out}} = \bar{A}_{\text{loss}} = 0$, the steady state cavity mode is given by

$$\bar{a} = \frac{\sqrt{2\kappa_{\text{in}}}}{\kappa - i\triangle} \bar{A}_{\text{in}}. \tag{2.26}$$

This equation enables us to obtain the reflected and transmitted fields as a function of detuning in the following was. We are also interested in the Fourier components of the cavity mode. These can be found by Fourier transforms of the operators,

$$Q(\omega) = \int_{-\infty}^{\infty} Q(t) \exp(-i\omega t) dt, \tag{2.27}$$

for $Q = \hat{a}$, $\hat{A}_{\text{in}}$, $\hat{A}_{\text{out}}$, and $\hat{A}_{\text{loss}}$. The equation of motion in the frequency domain is

$$-i\omega\delta\hat{a} = (i\triangle - \kappa)\delta\hat{a} + \sqrt{2\kappa_{\text{in}}}\delta\hat{A}_{\text{in}} + \sqrt{2\kappa_{\text{in}}}\delta\hat{A}_{\text{out}} + \sqrt{2\kappa_{\text{loss}}}\delta\hat{A}_{\text{loss}}, \tag{2.28}$$

where ω is the sideband frequency. Simply put, this fluctuating term induces the quantum back-action force (details are described in Sect. 2.3).

2.1.4.2 Reflected and Transmitted Fields

Using the cavity input-output relations [3], the reflected field, A_{ref} and transmitted field, A_{trans}, can be determined:

$$A_{\text{trans}} = \sqrt{2\kappa_{\text{out}}}a - A_{\text{out}},$$
$$A_{\text{ref}} = \sqrt{2\kappa_{\text{in}}}a - A_{\text{in}}, \tag{2.29}$$

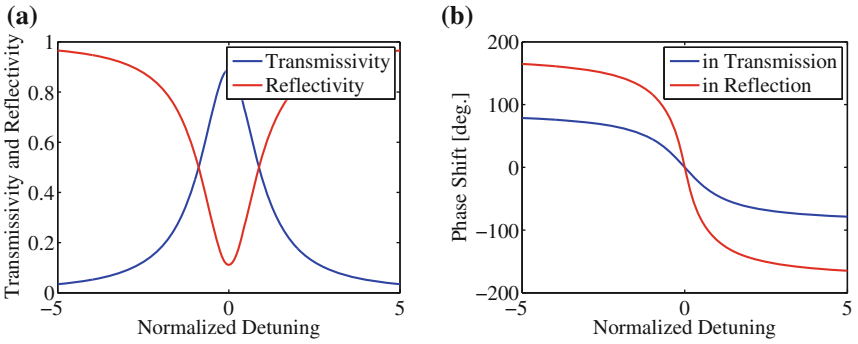

Fig. 2.3 Optical cavity. These show the reflected and transmitted fields as a function of detuning normalized by the cavity decay rate. **a** The (power) reflectivity and transmissivity are shown. **b** The phase shifts in reflection and transmission are shown

which give

$$\bar{A}_{\mathrm{trans}} = \frac{2\sqrt{\kappa_{\mathrm{in}}\kappa_{\mathrm{out}}}}{\kappa - i\triangle}\bar{A}_{\mathrm{in}}, \tag{2.30}$$

$$\bar{A}_{\mathrm{ref}} = \frac{2\kappa_{\mathrm{in}} - \kappa + i\triangle}{\kappa - i\triangle}\bar{A}_{\mathrm{in}}. \tag{2.31}$$

The amplitude transmissivity and reflectivity of the cavity are respectively given by

$$t(\triangle) = \frac{\bar{A}_{\mathrm{trans}}}{\bar{A}_{\mathrm{in}}} = \frac{2\sqrt{\kappa_{\mathrm{in}}\kappa_{\mathrm{out}}}}{\kappa - i\triangle}, \tag{2.32}$$

$$r(\triangle) = \frac{\bar{A}_{\mathrm{ref}}}{\bar{A}_{\mathrm{in}}} = \frac{2\kappa_{\mathrm{in}} - \kappa + i\triangle}{\kappa - i\triangle}, \tag{2.33}$$

and both of them are shown in Fig. 2.3. By using these equations, one can experimentally estimate important parameters, i.e., κ, κ_{in} and κ_{out}, see in Sects. 6.1 and 6.3.

2.2 Mechanical Oscillator

In this section, we describe the mechanical oscillator, especially concerning mechanical dissipation. Mechanical dissipation is one of the most important parameters, because the Fluctuation-Dissipation Theorem (FDT) [6] connects the spectrum of the thermal fluctuating force to the mechanical dissipation in the system, which is given by

$$S^{(2)}_{\mathrm{FF,th}} = \frac{2k_{\mathrm{B}}T_{\mathrm{th}}}{\omega}\mathrm{Im}\chi_{\mathrm{m}} = 4k_{\mathrm{B}}T_{\mathrm{th}}\gamma_{\mathrm{m}}m. \tag{2.34}$$

Here, k_{B} is the Boltzmann constant, T_{th} is the temperature of the thermal bath, χ_{m} is the mechanical susceptibility derived below, ω is the sideband frequency, γ_{m} is the mechanical damping rate (i.e., it represents the dissipation) and m is the mass of the mechanical oscillator. This equation represents that the reduction of the thermal noise requires a low mechanical dissipation and a low bath temperature. To reduce the dissipation, we used gravitational *dilution* technique. Details are described below.

2.2.1 Mechanical Normal Modes

Let us consider a suspended mirror (i.e., pendulum) having a resonant frequency of ω_m, naturally assuming that the mode spectrum is sufficiently sparse such that there is no spectral overlap with other mechanical modes, such as a rocking mode and a violin mode. This condition can be easily satisfied by choosing appropriate parameters [7]. The equation of motion for the position of the mirror, $x(t)$, can be described by

$$m\ddot{x} + 2m\gamma_{\mathrm{m}}\dot{x} + m\omega_{\mathrm{m}}^2 x = F_{\mathrm{ext}}. \tag{2.35}$$

Here, m is the mass of the pendulum, γ_{m} is the amplitude damping rate (i.e., the mechanical quality factor is $Q_{\mathrm{m}} = \omega_{\mathrm{m}}/2\gamma_{\mathrm{m}}$), ω_{m} i the resonant frequency of the oscillator, and $F_{\mathrm{ext}}(t)$ is the external force acting on the mirror. Even if there is no external force, it is given by the thermal fluctuating force.

To solve this equation, we again introduce the Fourier transform via $x(\omega) = \int_{-\infty}^{\infty} dt\, \exp(-i\omega t)x(t)$. Then, the mechanical susceptibility $\chi_{\mathrm{m}}(\omega)$ connecting the external force to the displacement of the oscillator is given by

$$\chi_{\mathrm{m}}(\omega) \equiv \frac{x(\omega)}{F_{\mathrm{ext}}(\omega)} = \frac{1}{m}\frac{1}{\omega_{\mathrm{m}}^2 - \omega^2 + 2i\omega\gamma}. \tag{2.36}$$

The stationary response is given by $\chi_{\mathrm{m}}(0) = (m\omega_{\mathrm{m}}^2)^{-1} = 1/k_{\mathrm{m}}$, where k_{m} is the spring constant.

A quantum-mechanical treatment of the mechanical harmonic oscillator leads to the Hamiltonian

$$\hat{H} = \hbar\omega_{\mathrm{m}}\hat{c}^{\dagger}\hat{c} + \frac{1}{2}\hbar\omega_{\mathrm{m}}. \tag{2.37}$$

Here, the phonon creation, $\hat{c}^\dagger$, and annihilation, $\hat{c}$, operators have been introduced similarly to Eqs. (2.7), (2.8), with

$$\hat{x} = x_{\mathrm{zpf}}(\hat{c} + \hat{c}^\dagger), \tag{2.38}$$

$$\hat{p} = -im\omega_{\mathrm{m}} x_{\mathrm{zpf}}(\hat{c} - \hat{c}^\dagger), \tag{2.39}$$

where

$$x_{\mathrm{zpf}} = \sqrt{\frac{\hbar}{2m\omega_{\mathrm{m}}}} \tag{2.40}$$

is the zero-point fluctuation (root-meas-square) amplitude of the mechanical oscillator. The quantity $\hat{c}^\dagger\hat{c}$ is the phonon number operator, whose average is denoted by $\bar{n} = \langle \hat{c}^\dagger \hat{c} \rangle$. In general, the mechanical oscillator is coupled to a high-temperature bath, and thus the average phonon number will evolve according to the expression [8]

$$\frac{d}{dt}\langle n \rangle = -2\gamma_{\mathrm{m}} \left(\langle n \rangle - \bar{n}_{\mathrm{th}} \right). \tag{2.41}$$

For an oscillator that is initially in the ground state, the time dependence of the occupation is given by

$$\frac{d}{dt}\langle n \rangle_{t=0} = 2\bar{n}_{\mathrm{th}}\gamma_{\mathrm{m}} \simeq \frac{k_{\mathrm{B}} T_{\mathrm{th}}}{\hbar Q_{\mathrm{m}}}, \tag{2.42}$$

where $\bar{n}_{\mathrm{th}}$ is the average phonon number of the thermal bath, T_{th} is the temperature of the thermal bath, and here we suppose the mechanical decay rate γ_{m} has *no* dependence on frequency for the sake of simplicity. Equation (2.42) represents the thermal decoherence rate having the unit of Hz, because it gives the inverse time of the absorption of a phonon from the environment. This expression shows that in order to attain a low thermal decoherence, a high mechanical quality factor, Q_{m}, and a low temperature bath are important. In addition, from this equation, the number of coherent oscillations in the presence of thermal decoherence n_{osc} is given by,

$$n_{\mathrm{osc}} = \omega_{\mathrm{m}} \times \frac{\hbar Q_{\mathrm{m}}}{k_{\mathrm{B}} T_{\mathrm{th}}} = Q_{\mathrm{m}} \cdot f_{\mathrm{m}} \times \frac{h}{k_{\mathrm{B}} T_{\mathrm{th}}}. \tag{2.43}$$

Thus, the "$Q_{\mathrm{m}} \cdot f_{\mathrm{m}}$" product quantifies the decoupling of the mechanical resonator from a thermal environment. Note that full coherence over one mechanical period is obtained for $Q_{\mathrm{m}} \cdot f_{\mathrm{m}} > k_{\mathrm{B}} T_{\mathrm{th}}/\hbar$, i.e., $Q_{\mathrm{m}} \cdot f_{\mathrm{m}} > 6 \times 10^{12}$ Hz is a minimum requirement for room-temperature quantum optomechanics. One might consider that satisfying the criteria is impossible on the macroscopic scale; however, the *dilution* techniques described below will enable us to realize it.

2.2.2 Mechanical Dissipation & Dilution Techniques

The energy loss of mechanical oscillations is quantified by the (amplitude) mechanical dissipation rate, $\gamma_m = \omega_m/2Q_m$. Here, we introduce the loss mechanisms:

- Viscous damping is mainly caused by interactions with the surrounding gas atoms. A resistance force proportional to the velocity is applied to the oscillator, which is given by $\gamma_{gas} = SP\sqrt{m_{mol}}/(2C\sqrt{k_B T m})$, where C is a dimensionless constant of order unity that depends on the shape of the oscillator, S is the cross-sectional area, P the pressure, m_{mol} the mass of a residual molecule of the gas, and m the mass of a mechanical oscillator [9]. In our case, the gas damping will become an issue in future, see in Chap. 7.
- Clamping losses are due to radiation of elastic waves into the substrate through the supports of the oscillator. In our case, a thin tungsten wire is clamped between two aluminum plates at the top, while a mirror is attached to the wire using an epoxy glue at the bottom. Although this lossy configuration has sufficient quality factor for observing the quantum back-action, it will not be sufficient for future experiments. Therefore, we must change it to other relatively lossless materials, such as stainless steels (See Chap. 7).
- A thermoelastic damping is a fundamental anharmonic effect, which is caused by heat flow along the temperature gradients. This effect often causes problems, such as a mirror thermal noise, because the temperature gradients often occur at around the laser beam spot on the mirror. In our case, the mirror thermal noise has been negligible until now; however, it will also become an issue in the future (See Chaps. 5 and 7).
- An intrinsic loss of a material is caused by the relaxation of intrinsic defect states in the bulk or surface of the material. In general, intrinsic loss could not be measured directly because of the loss coming from the support for the measurement. To solve this problem, a nodal support system, which in principle does not introduce any external loss to the sample by supporting it at their nodal points, was proposed by Kenji Numata in 2000 [10]. Since then, this technique has been used [11, 12]. In our case, it was estimated using a torsional mode (See Chap. 6), similarly to that described in Ref. [13].

The various dissipation processes contribute independently to the overall mechanical losses, and hence add up incoherently. The resulting mechanical quality factor, Q_{total}, is given by $1/Q_{total} = \sum_i 1/Q_i$, where i labels the different loss mechanisms.

Since the loss of the energy is only associated with the elastic part of the stored energy, the mechanical dissipation can be mitigated by storing most of the mechanical energy in a nearly lossless gravitational or optical potential, thereby strongly diluting the effect of the dissipation.

- **Gravitational dilution:** The total mechanical loss of an oscillator is diluted with gravity by a factor of k_{grav}/k_{el}, where k_{grav} and k_{el} are the gravitational and elastic spring constants [14]. The mechanical quality factor thus becomes about k_{grav}/k_{el}-times larger. This effect can be given by using loss angle ϕ, as below

$$k_{\rm el}(1+i\phi)+k_{\rm g}=\left(1+\frac{k_{\rm g}}{k_{\rm el}}\right)k_{\rm el}\left[1+\frac{i\phi}{1+\frac{k_{\rm g}}{k_{\rm el}}}\right]\simeq k_{\rm g}\left[1+\frac{i\phi}{1+\frac{k_{\rm g}}{k_{\rm el}}}\right]. \quad (2.44)$$

The loss angle is given by using the quality factor, Q, as follows

$$Q=\frac{1}{\phi}\left(\text{structure damping, i.e., } \gamma=\frac{\omega_{\rm g}^2}{2Q\omega}\right), \text{ or} \quad (2.45)$$

$$=\frac{1}{\phi}\frac{\omega}{\omega_{\rm g}}\left(\text{viscous damping, i.e., } \gamma=\frac{\omega_{\rm g}}{2Q}\right). \quad (2.46)$$

Thus, the quality factor is enhanced by the gravitational dilution by a factor of $Q_{\rm en}$, which is given by

$$Q_{\rm en}=\left(1+\frac{k_{\rm g}}{k_{\rm el}}\right). \quad (2.47)$$

In practice, only $k_{\rm el}$ is variable, and thus thermal fluctuating force is also diluted as below,

$$S^{\prime(2)}_{\rm FF,th}=4k_{\rm B}T\frac{\omega_{\rm g}}{2Q'}\simeq S^{(2)}_{\rm FF,th}\frac{k_{\rm el}}{k_{\rm g}} \quad (2.48)$$

Here, $S^{(2)}_{\rm FF,th}$ is thermal noise with the small gravitational dilution, while the parameters with prime indicates the similar but with the large gravitational dilution. In our case, an ultimate thin wire (the radius is 1.5 μm) assures that the amount of energy stored in the pendulum is dominated by the gravitational potential over the elastic bending energy of the wire. More concretely, the mechanical dissipation is about 600-times diluted (See Chaps. 5 and 6).

- **Optical dilution:** Mechanical energy is stored in the lossless potential provided by the optical restoring forces, which dilutes the effects of internal material dissipation. The mechanical quality factor thus becomes about $k_{\rm opt}/k_{\rm el}$-times and $\omega_{\rm opt}/\omega_{\rm el}$-times larger for the structure damping case and the viscous damping case, respectively. Here, $f_{\rm eff}$ is the effective resonant frequency of the mechanical oscillator trapped by the optical spring. In the case of the *soft* suspension, such as the suspended mirror, this effect is relatively increased, and thereby it is often used with pendulums [15–17]. This effect can be given by using loss angle ϕ, as below

$$k_{\rm el}(1+i\phi)+k_{\rm opt}=\left(1+\frac{k_{\rm opt}}{k_{\rm el}}\right)k_{\rm el}\left[1+\frac{i\phi}{1+\frac{k_{\rm opt}}{k_{\rm el}}}\right]. \quad (2.49)$$

The loss angle is given by using the quality factor, Q, as follows

$$Q = \frac{1}{\phi}\left(\text{structure damping, i.e., } \gamma = \frac{\omega_{\rm el}^2}{2Q\omega}\right), \text{ or} \tag{2.50}$$

$$= \frac{1}{\phi}\frac{\omega}{\omega_{\rm el}}\left(\text{viscous damping, i.e., } \gamma = \frac{\omega_{\rm el}}{2Q}\right). \tag{2.51}$$

Thus, the quality factor is enhanced by the optical dilution by a factor of $Q_{\rm en}$, which is given by

$$Q_{\rm en} = \left(1 + \frac{k_{\rm opt}}{k_{\rm el}}\right)(\text{structure damping}), \text{ or} \tag{2.52}$$

$$\simeq \left(\frac{\omega_{\rm el}}{\omega_{\rm opt}} + \frac{\omega_{\rm opt}}{\omega_{\rm el}}\right) \simeq \frac{\omega_{\rm opt}}{\omega_{\rm el}}(\text{viscous damping}). \tag{2.53}$$

In practice, $k_{\rm opt}$ is variable, and thus thermal fluctuating force is *not* diluted as below,

$$S_{\rm FF,th}^{\prime(2)} = 4k_{\rm B}T\frac{\omega_{\rm opt}}{2Q'} = 4k_{\rm B}T\frac{\omega_{\rm el}}{2Q} = S_{\rm FF,th}^{(2)} \tag{2.54}$$

Here, $S_{\rm FF,th}^{(2)}$ is thermal noise with the small gravitational dilution, while the parameters with prime indicates the similar but with the large gravitational dilution. In our case, the effective frequency of the pendulum is enhanced from 2 to 400 Hz (See Chap. 6).

We note that the only gravitational dilution can reduce thermal fluctuating force from Eqs. (2.48) and (2.54), since we naturally suppose that the gravitational dilution is changed without changing the gravitational potential, while the optical dilution is changed by changing the optical potential. The dilution techniques mentioned above have a key to experimentally investigate the macroscopic quantum mechanics because any macroscopic object is strongly affected by thermal decoherence as just it is. When the oscillator is trapped and damped by the nearly lossless field, the Eq. (2.41) is given by

$$\frac{d}{dt}\langle n\rangle = -2\gamma_{\rm m}\left(\langle n\rangle - \bar{n}_{\rm th}\right) - 2\gamma_{\rm eff}\left(\langle n\rangle - \bar{n}_{\rm th,eff}\right), \tag{2.55}$$

where $\gamma_{\rm eff}$ is the effective mechanical decay rate, $\bar{n}_{\rm th,eff}$ (becomes zero for lossless fields) is the effective thermal occupation number of the effective bath, and here we also suppose the mechanical decay rate and effective decay rate have *no* dependence on frequency (i.e., viscous damping model is supposed). Here, the number of coherent oscillations in the presence of thermal decoherence is given by

$$n_{\mathrm{osc}} = \frac{\hbar}{2k_{\mathrm{B}}T_{\mathrm{th}}} \times \frac{\omega_{\mathrm{eff}}^2}{\gamma_{\mathrm{m}}}, \\ = Q_{\mathrm{m}} \cdot f_{\mathrm{m}} \times \frac{h}{k_{\mathrm{B}}T_{\mathrm{th}}} \times \left(\frac{\omega_{\mathrm{eff}}}{\omega_{\mathrm{m}}}\right)^2. \tag{2.56}$$

Thus, the requirement for room-temperature quantum optomechanics is mitigated by a factor of $(\omega_{\mathrm{eff}}/\omega_{\mathrm{m}})^2$. In our case, the original $Q_{\mathrm{m}} \cdot f_{\mathrm{m}}$ is about 1×10^6 Hz, which is about 6×10^6-times lower than the original requirement, even though the gravitational potential increases the mechanical quality factor. The optical spring further reduces the difference to $6 \times 10^6 \cdot (2/400)^2 = 150$ at the least. In practically, since our measurement determined the dissipation model as structure damping, the requirement ought to be further mitigated (but it is not calculated now). Also, the effective phonon number of the mechanical oscillator is given by

$$n_{\mathrm{eff}} = \frac{k_{\mathrm{B}}T_{\mathrm{th}}}{\hbar\omega_{\mathrm{m}}} \times \left(\frac{\omega_{\mathrm{m}}}{\omega_{\mathrm{eff}}}\right)^2 \times \frac{Q_{\mathrm{eff}}}{Q_{\mathrm{m}}}, \\ = \frac{Q_{\mathrm{eff}}}{n_{\mathrm{osc}}}. \tag{2.57}$$

Thus, if the requirement for $f \cdot Q$ product is satisfied, n_{eff} can be reduced under one with Q_{eff} over one.

2.3 Optomechanical System

2.3.1 Theoretical Derivation of Quantum Back-Action

Here, we calculate the quantum back-action in the optomechanical system shown in Fig. 2.4. We again start from Newton's law to describe the mechanical response,

$$m\ddot{x} + 2m\gamma_{\mathrm{m}}\dot{x} + k_{\mathrm{m}}x = F, \tag{2.58}$$

where m is the mass of the movable mirror (mechanical oscillator), ω_{m} is the mechanical resonant frequency, γ_{m} is the mechanical amplitude decay rate, k_{m} is the mechanical spring constant, and x is the position for the mirror. To derive the mechanical susceptibility, we Fourier transform Eq. (2.58) according to the following conventions: $f(\omega) \equiv \int_{-\infty}^{\infty} dt f(t) \exp(-i\omega t)$,

$$\chi_{\mathrm{m}} \equiv \frac{x}{F} = \frac{1}{m(\omega_{\mathrm{m}}^2 - \omega^2 + i2\omega\gamma_{\mathrm{m}})}. \tag{2.59}$$

Let us next calculate the response of an optomechanical system to two independent laser driving fields. We consider the two beams in order to explain so-called "double optical spring" [18]. The Hamiltonian describing the optomechanical coupling [19] can be written and linearized in the form

$$\begin{aligned}\hat{\mathscr{H}} &= \hbar\omega_{\mathrm{c}}(x)\hat{a}^{\dagger}\hat{a} + \hbar\omega_{\mathrm{c}}(x)\hat{b}^{\dagger}\hat{b} + \hat{\mathscr{H}}_{\kappa} \\ &\simeq \hbar\omega_{\mathrm{c}}\hat{a}^{\dagger}\hat{a} + \hbar\omega_{\mathrm{c}}\hat{b}^{\dagger}\hat{b} + \hbar g\hat{a}^{\dagger}\hat{a}x + \hbar g\hat{b}^{\dagger}\hat{b}x + \hat{\mathscr{H}}_{\kappa},\end{aligned} \tag{2.60}$$

where $g = 2\omega_{\mathrm{c}}\cos\beta/L$ is the optomechanical coupling constant[1] (the coupling constant will be given in Chap. 5, Sect. 5.2.4), ω_{c} is the cavity resonance frequency, β is the incident angle on the movable mirror, L is the round-trip length and $\hat{\mathscr{H}}_{\kappa}$ represents the optical input and output coupling; and $\hat{a}$ and $\hat{b}$ are the annihilation operators (cavity modes) for two counterpropagating directions in the triangular cavity, respectively. The Heisenberg Langevin equations of motion for the cavity modes are:

$$\dot{\hat{a}} = -(\kappa + i\omega_{\mathrm{c}})\hat{a} - ig_{\mathrm{a}}x\hat{a} + \sum_{\mathrm{l}}\sqrt{2\kappa_{\mathrm{l}}}\hat{A}_{\mathrm{l}}, \tag{2.61}$$

$$\dot{\hat{b}} = -(\kappa + i\omega_{\mathrm{c}})\hat{b} - ig_{\mathrm{b}}x\hat{b} + \sum_{\mathrm{l}}\sqrt{2\kappa_{\mathrm{l}}}\hat{B}_{\mathrm{l}}, \tag{2.62}$$

where the κ_{in1}, κ_{in2}, κ_{in3} are the cavity amplitude decay rates for each mirror, κ_{in4} is the decay rate for the cavity round-trip loss and κ is the total decay rate; $\hat{A}_{\mathrm{l}}$ and $\hat{B}_{\mathrm{l}}$ are the input optical fields. The equation of motion can be written in a rotating frame of reference by setting $\hat{a} = \exp(-i\omega_{\mathrm{a}}t)\hat{a}$ and linearized in the following form:

$$\dot{\delta\hat{a}} = -(\kappa - i\Delta_{\mathrm{a}})(\bar{\mathrm{a}} + \delta\hat{a}) - iG_{\mathrm{a}}\delta x + \sqrt{2\kappa_{\mathrm{in1}}}\bar{A}_{\mathrm{in1}} + \sum_{\mathrm{l}}\sqrt{2\kappa_{\mathrm{l}}}\delta\hat{A}_{\mathrm{l}}, \tag{2.63}$$

$$\dot{\delta\hat{b}} = -(\kappa - i\Delta_{\mathrm{b}})(\bar{b} + \delta\hat{b}) - iG_{\mathrm{b}}\delta x + \sqrt{2\kappa_{\mathrm{in2}}}\bar{B}_{\mathrm{in2}} + \sum_{\mathrm{l}}\sqrt{2\kappa_{\mathrm{l}}}\delta\hat{B}_{\mathrm{l}}, \tag{2.64}$$

where $\Delta_{\mathrm{a}} = \omega_{\mathrm{a}} - \omega_{\mathrm{c}} - G_{\mathrm{a}}\bar{x}$ and $\Delta_{\mathrm{b}} = \omega_{\mathrm{b}} - \omega_{\mathrm{c}} - G_{\mathrm{b}}\bar{x}$ are the cavity detuning; $G_{\mathrm{a}} = \bar{a}g$ and $G_{\mathrm{b}} = \bar{b}g$ are the light-enhanced optomechanical couplings for the linearized regime; $\bar{a}$ and $\bar{b}$ are the average parts for each cavity mode; $\delta\hat{a}$ and $\delta\hat{b}$ are the fluctuating parts for each cavity mode; $\bar{A}_{\mathrm{in1}}$ and $\bar{B}_{\mathrm{in2}}$ are the real valued coherent amplitudes for input lasers; $\delta\hat{A}_{\mathrm{l}}$ and $\delta\hat{B}_{\mathrm{l}}$, for $\mathrm{l} = \mathrm{in1}, \mathrm{in2}, \mathrm{in3}, \mathrm{in4}$ are the vacuum fluctuation entering from each port.

The average intracavity field amplitudes are described by Eqs. (2.63) and (2.64):

$$\bar{a} = \frac{\sqrt{2\kappa_{\mathrm{in1}}}}{\kappa - i\Delta_{\mathrm{a}}}\bar{A}_{\mathrm{in1}}, \tag{2.65}$$

[1] optomechanical single-photon coupling strength g_0 (e.g. in Ref. [8, 20]), which gives $\hat{\mathscr{H}} = \hbar g_0\hat{a}^{\dagger}\hat{a}(\hat{b} + \hat{b}^{\dagger})$, is x_{zpf}-times lager than g.

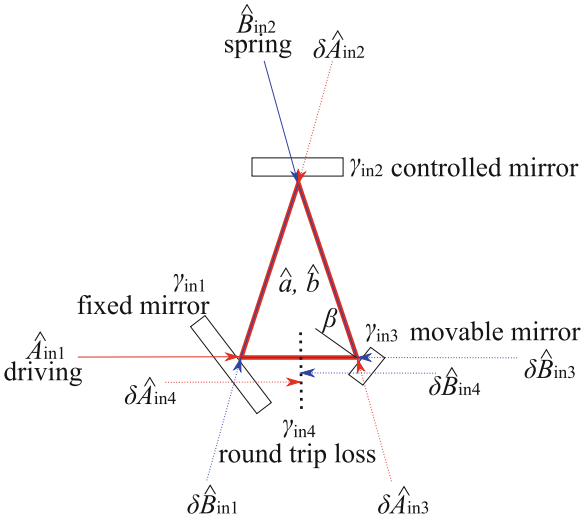

Fig. 2.4 Layout of the triangular cavity. The cavity consists of three mirrors: the input coupler for the driving beam, with a decay rate of κ_{in1}; the input coupler for the spring beam, with a decay rate of κ_{in2}; the movable mirror, with a decay rate of κ_{in3}; and a mirror to represent intracavity loss, with a decay rate of κ_{in4}. The cavity mode is labeled $\hat{a}$ and $\hat{b}$. The extracavity fields are: $\hat{A}_{in1}$, $\delta\hat{A}_{in2}$, $\delta\hat{A}_{in3}$, $\delta\hat{A}_{in4}$, $\delta\hat{B}_{in1}$, $\hat{B}_{in2}$, $\delta\hat{B}_{in3}$, and $\delta\hat{B}_{in4}$

$$\bar{b} = \frac{\sqrt{2\kappa_{in2}}}{\kappa - i\Delta_b}\bar{B}_{in2}. \tag{2.66}$$

From these equations, the intracavity power is given by

$$\begin{aligned}\bar{P}_{circ} &= \frac{\hbar\omega_c|a|^2}{\tau} + \frac{\hbar\omega_c|b|^2}{\tau} \\ &= \frac{2\kappa_{in1}}{\tau(\kappa^2+\Delta_a^2)}\bar{P}_{in1} + \frac{2\kappa_{in2}}{\tau(\kappa^2+\Delta_b^2)}\bar{P}_{in2}, \\ &= \bar{P}_{in1,circ} + \bar{P}_{in2,circ}\end{aligned} \tag{2.67}$$

where τ is the cavity round-trip time.

The fluctuation components of Eqs. (2.63) and (2.64) are similarly at given by

$$\dot{\delta\hat{a}} = -(\kappa - i\Delta_a)\delta\hat{a} - iG_a\delta x + \sum_l \sqrt{2\kappa_l}\delta\hat{A}_l, \tag{2.68}$$

$$\dot{\delta\hat{b}} = -(\kappa - i\Delta_b)\delta\hat{b} - iG_b\delta x + \sum_l \sqrt{2\kappa_l}\delta\hat{B}_l. \tag{2.69}$$

In terms of the frequency components, these can be rewritten by

$$\delta\hat{a} = \chi_a(-iG_a\delta x + \sum_l \sqrt{2\kappa_l}\delta\hat{A}_l), \tag{2.70}$$

$$\delta\hat{b} = \chi_b(-iG_b\delta x + \sum_l \sqrt{2\kappa_l}\delta\hat{B}_l). \tag{2.71}$$

Here, $\chi_a = (\kappa + i(\omega - \Delta_a))^{-1}$ and $\chi_b = (\kappa + i(\omega - \Delta_b))^{-1}$ are the cavity susceptibilities for the two modes. These lead to forces induced by the cavity modes, being applied to the movable mirror, which are given by:

$$\bar{F}_{BA} = -\frac{(g_a + g_b)\tau}{\omega_c}\bar{P}_{circ}, \tag{2.72}$$

$$\delta F_{BA} = i\hbar|G_a|^2\delta x(\chi_a(\omega) - \chi_a^*(-\omega)) + i\hbar|G_b|^2\delta x(\chi_b(\omega) - \chi_b^*(-\omega)), \tag{2.73}$$

$$\begin{aligned}\delta\hat{F}_{BA} = &-\hbar G_a^*\chi_a(\omega)\sum_l \sqrt{2\kappa_l}\delta\hat{A}_l - \hbar G_a\chi_a^*(-\omega)\sum_l \sqrt{2\kappa_l}\delta\hat{A}_l^\dagger \\ &- \hbar G_b^*\chi_b(\omega)\sum_l \sqrt{2\kappa_l}\delta\hat{B}_l - \hbar G_b\chi_b^*(-\omega)\sum_l \sqrt{2\kappa_l}\delta\hat{B}_l^\dagger,\end{aligned} \tag{2.74}$$

where $\bar{F}_{BA}$ is the average back-action force, δF_{BA} is the dynamic back-action, which influences the dynamics of the harmonically bound mirror, and $\delta\hat{F}_{BA}$ is the quantum back-action force.

From the dynamic back-action, the optical spring effect is given by

$$\begin{aligned}K(\omega) = -\frac{\delta F_{BA}}{\delta x} &= 2\hbar|G_a|^2\frac{\Delta_a}{(\kappa + i\omega)^2 + \Delta_a^2} + 2\hbar|G_b|^2\frac{\Delta_b}{(\kappa + i\omega)^2 + \Delta_b^2} \\ &= \frac{8P_{in1,circ}\omega_c}{Lc}\frac{\Delta_a\cos^2(\beta)}{(\kappa + i\omega)^2 + \Delta_a^2} + \frac{8P_{in2,circ}\omega_c}{Lc}\frac{\Delta_b\cos^2(\beta)}{(\kappa + i\omega)^2 + \Delta_b^2}.\end{aligned} \tag{2.75}$$

The experiment is performed under the "slowly varying" condition, $\omega \ll \sqrt{\Delta_a^2 + \kappa^2}$; then, the spring effect can be written by

$$\begin{aligned}K &= 2\hbar|G_a|^2\left[\frac{\Delta_a}{\kappa^2 + \Delta_a^2} - \frac{2i\kappa\Delta_a}{(\kappa^2 + \Delta_a^2)^2}\omega\right] + 2\hbar|G_b|^2\left[\frac{\Delta_b}{\kappa^2 + \Delta_b^2} - \frac{2i\kappa\Delta_b}{(\kappa^2 + \Delta_b^2)^2}\omega\right] \\ &\equiv K_{opt} + i\omega\Gamma_{opt}.\end{aligned} \tag{2.76}$$

This condition is also called the "bad" cavity condition because of the weakness of the cooling effect due to the delay of light itself. Under this condition, the intracavity optical power is largely increased as an effect of the laser cooling being increased, and thereby the back-action is also increased. If the light-enhanced optomechanical coupling constant, G, is larger than $\sqrt{m\kappa\gamma_m\omega_m}/\hbar$, the back-action becomes larger than the SQL on resonance of the mechanical oscillator. Thus, in general, this condition is not appropriate for the laser (passive) cooling of the object for achieving its ground state (this condition is suitable for feed-back cooling [21]). On the other hand, in the resolved sideband regime, defined as $\omega_m \gg \kappa$, one can reduce the occupation number to $(\kappa/2\omega_m)^2$ [22, 23]. Therefore, this condition is called the "good" cavity condition.

This spring modifies the dynamics of the mirror as

$$\omega_{\rm eff}^2 = \omega_{\rm m}^2 + \frac{K_{\rm opt}}{m}, \tag{2.77}$$

$$\gamma_{\rm eff} = \gamma_{\rm m} + \frac{\Gamma_{\rm opt}}{2m}, \tag{2.78}$$

which indicates that the positive (negative) rigidity is always accompanied by negative (positive) damping. In either case, the system is unstable if we use a single optical spring. To stabilize the system, one can use a feedback control; however, it is difficult to control if we use a tiny oscillator. An appropriate alternative is to implement the idea of the double optical spring [18], by inputting two lasers to the cavity at different frequencies. One laser with a small detuning provides a large positive damping, while the other higher input-power beam with a large detuning provides a strong restoring force. The resulting system is self-stabilized with both positive rigidity and positive damping, as shown in Fig. 2.5. In addition, unlike mechanical springs, the optical spring effect does not change the thermal excitation spectrum of the mirror, since the optical field is almost in its ground state (in our case, the infrared optical field has an effective temperature of 15,000 K). We can measure the quantum back-action force fluctuation as a displacement fluctuation via the effective susceptibility, $\chi_{\rm eff}$.

The double-sided force spectrum, $S_{FF,q}^{(2)}$, is written as

$$\begin{aligned} S_{\rm FF,q}^{(2)} &= \langle \delta \hat{F}_{\rm BA}(-\omega) \delta \hat{F}_{\rm BA}(\omega) \rangle \\ &= 2\hbar^2 \kappa |G_{\rm a}|^2 |\chi_{\rm a}(-\omega)|^2 + 2\hbar^2 \kappa |G_{\rm b}|^2 |\chi_{\rm b}(-\omega)|^2 \\ &= 2N_{\rm in1,circ} \frac{\hbar^2 g^2}{\kappa} \left(1 + \left(\frac{\omega + \Delta_{\rm a}}{\kappa} \right)^2 \right)^{-1} + 2N_{\rm in2,circ} \frac{\hbar^2 g^2}{\kappa} \left(1 + \left(\frac{\omega + \Delta_{\rm b}}{\kappa} \right)^2 \right)^{-1}. \end{aligned} \tag{2.79}$$

Therefore, the quantum back-action is given by $|\chi_{\rm eff}|^2 S_{\rm FF,q}^{(2)}$ as displacement fluctuations (in the unit of m^2/Hz). The ratio of the quantum back-action to thermal fluctuating force is then given by

$$\frac{S_{\rm FF,q}^{(2)}}{S_{\rm FF,th}^{(2)}} = \frac{1}{n_{\rm th}} \frac{N_{\rm circ} g^2}{\kappa \gamma_{\rm m}}. \tag{2.80}$$

Here, $N_{\rm circ}$ is the intracavity photon number of the single laser, which dominates the quantum back-action, and we suppose the bad cavity condition.

In practice, a laser has a classical intensity fluctuation generating the "classical" back-action force. This effect is given by

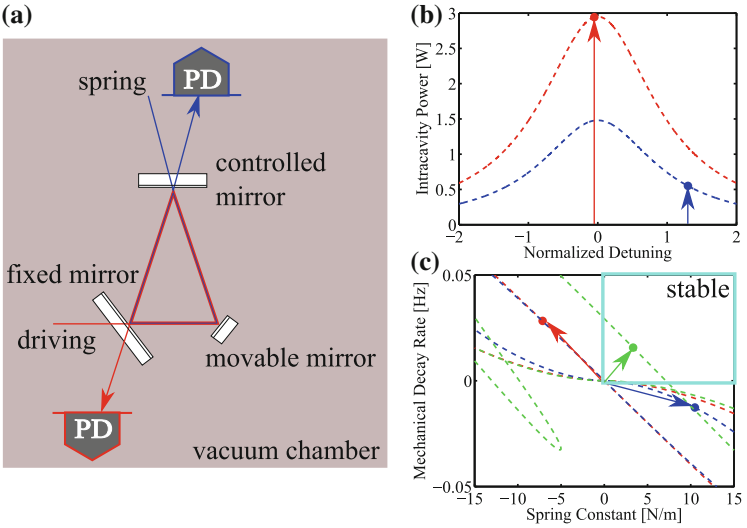

Fig. 2.5 The double optical spring effect. a The beams illustrated as the *red* and the *blue lines* incident on the fixed and controlled mirrors, respectively. **b** The intracavity power and detuning for each beam. The *red* and *blue* points show both laser-cavity detuning and the intracavity power. The *dashed red* and *blue curves* show the optical power as a function of the cavity detuning for each beam. The driving beam dominates the quantum back-action due to the higher intracavity power than the spring beam. **c** The optical spring effect. The *red* point represents the beam illustrated as the *red line* at $\Delta_a/\kappa = -0.05$, the *blue* point represents the beam illustrated as the *blue line* at $\Delta_b/\kappa = +1.3$, and the *dashed green* represents their sum. The *dashed red* and *blue curves* show parametric plots of the optical spring as a function of the detuning for each beam, and the *dashed green curve* is their sum. Inside the cyan flame, both the spring and the mechanical decay rates have a positive values, and thus the mirror is stably trapped

$$S^{(2)}_{\mathrm{FF,c}} = 2(B_{\mathrm{in1}} - 1)\hbar^2\kappa_{\mathrm{in1}}|G_a|^2\left(|\chi_a(\omega) + \chi_a(-\omega)|^2\right) + 2(B_{\mathrm{in2}} - 1)\hbar^2\kappa_{\mathrm{in2}}|G_b|^2\left(|\chi_b(\omega) + \chi_b(-\omega)|^2\right), \tag{2.81}$$

where B_{in1} and B_{in2} are the relative shot noise levels for each beam.

2.3.2 Phase-Induced Radiation Pressure

Here, we present phase-induced radiation pressure noise [24]. Phase fluctuations of the laser induce force fluctuations imposed on the mirror similar to that of intensity fluctuations, if the cavity is *detuned* from the resonance. The detuned cavity generates phase difference between the input laser and the intracavity field, and thus phase fluctuations of the input laser contributes to intensity fluctuations inside the cavity. To present a detailed expression of the phase-induced radiation pressure, we consider an intracavity field $a(t)$, which is input to the small phase-modulated beam

($d\varphi \ll 1$). The intracavity field is expanded to the first order of the Bessel-functions as below [25]

$$a(t) \propto \frac{1}{\kappa + i\Delta} + \frac{e^{i\Omega_{\mathrm{m}}t}/2}{\kappa + i(\Delta + \Omega_{\mathrm{m}})}d\varphi - \frac{e^{-i\Omega_{\mathrm{m}}t}/2}{\kappa + i(\Delta - \Omega_{\mathrm{m}})}d\varphi, \tag{2.82}$$

where Ω_{m} is a modulation frequency, and $d\varphi$ is the phase fluctuations. We respectively define e^{+} and e^{-} as $e^{i\Omega_{\mathrm{m}}t}$ and $e^{-i\Omega_{\mathrm{m}}t}$ for simplicity, and then the intracavity intensity is calculated as below,

$$\begin{aligned}
|a(t)|^2 &\propto \left[\frac{1}{\kappa + i\Delta} + \frac{e^{+}/2}{\kappa + i(\Delta + \Omega_{\mathrm{m}})}d\varphi - \frac{e^{-}/2}{\kappa + i(\Delta - \Omega_{\mathrm{m}})}d\varphi\right] \\
&\times \left[\frac{1}{\kappa - i\Delta} + \frac{e^{-}/2}{\kappa - i(\Delta + \Omega_{\mathrm{m}})}d\varphi - \frac{e^{+}/2}{\kappa - i(\Delta - \Omega_{\mathrm{m}})}d\varphi\right], \\
&\simeq \frac{1}{\kappa^2 + \Delta^2} \\
&+ \frac{[\kappa - i(\Delta - \Omega_{\mathrm{m}})]e^{-}/2 - [\kappa - i(\Delta + \Omega_{\mathrm{m}})]e^{+}/2}{[\kappa - i(\Delta + \Omega_{\mathrm{m}})][\kappa - i(\Delta - \Omega_{\mathrm{m}})]}\frac{d\varphi}{\kappa + i\Delta} \\
&+ \frac{[\kappa + i(\Delta - \Omega_{\mathrm{m}})]e^{+}/2 - [\kappa + i(\Delta + \Omega_{\mathrm{m}})]e^{-}/2}{[\kappa + i(\Delta + \Omega_{\mathrm{m}})][\kappa + i(\Delta - \Omega_{\mathrm{m}})]}\frac{d\varphi}{\kappa - i\Delta}, \\
&\simeq \frac{1}{\kappa^2 + \Delta^2} \\
&+ \frac{-i(\kappa - i\Delta)\sin\Omega_{\mathrm{m}}t + i\Omega_{\mathrm{m}}\cos\Omega_{\mathrm{m}}t}{(\kappa - i\Delta)^2}\frac{d\varphi}{\kappa + i\Delta} \\
&+ \frac{i(\kappa + i\Delta)\sin\Omega_{\mathrm{m}}t - i\Omega_{\mathrm{m}}\cos\Omega_{\mathrm{m}}t}{(\kappa + i\Delta)^2}\frac{d\varphi}{\kappa - i\Delta}, \\
&= \frac{1}{\kappa^2 + \Delta^2} \\
&+ \frac{[-(i\kappa + \Delta)\sin\Omega_{\mathrm{m}}t + i\Omega_{\mathrm{m}}\cos\Omega_{\mathrm{m}}t](\kappa + i\Delta)}{(\kappa^2 + \Delta^2)^2}d\varphi \\
&+ \frac{[(i\kappa - \Delta)\sin\Omega_{\mathrm{m}}t - i\Omega_{\mathrm{m}}\cos\Omega_{\mathrm{m}}t](\kappa - i\Delta)}{(\kappa^2 + \Delta^2)^2}d\varphi, \\
&= \frac{1}{\kappa^2 + \Delta^2} \\
&+ \frac{-2\kappa\Delta\sin\Omega_{\mathrm{m}}t + 2i\Delta(-i\kappa\sin\Omega_{\mathrm{m}}t + i\Omega_{\mathrm{m}}\cos\Omega_{\mathrm{m}}t)}{(\kappa^2 + \Delta^2)^2}d\varphi, \\
&= \frac{1}{\kappa^2 + \Delta^2} - \frac{2\Delta\Omega_{\mathrm{m}}\cos\Omega_{\mathrm{m}}t}{(\kappa^2 + \Delta^2)^2}d\varphi,
\end{aligned} \tag{2.83}$$

where, we suppose the condition of $\kappa \gg \Omega_{\mathrm{m}}$. Thus, the radio of radiation pressure fluctuations (zeroth-order term) to phase-induced radiation pressure fluctuations (first-order term) is given by,

$$\frac{S_{\text{phase}}}{S_{\text{rad}}} = -\frac{2\Delta\Omega_{\text{m}}\cos\Omega_{\text{m}}t}{\kappa^2+\Delta^2}d\varphi, \\ = -\frac{2\Omega_{\text{m}}\cos\Omega_{\text{m}}t}{\kappa}\frac{\delta}{1+\delta^2}d\varphi, \tag{2.84}$$

where $\delta \equiv \Delta/\kappa$ is the normalized detuning. From this equation, phase-induced radiation pressure noise is negligible small if the bad cavity condition is valid. In our measurements shown in Chap. 6, roughly only 0.3 % of the force fluctuation is due to the phase noise.

2.3.3 Photo-Thermal Shot Noise

Here, we present photo-thermal shot noise [26, 27], which is caused by optical power fluctuations absorbed in dielectrical reflective layers. The fluctuated power absorption makes the fluctuation of the mirror's surface through the thermal expansion coefficient. The photo-thermal shot noise $S^{(2)}_{\text{FF,photo-thermal}}$ is given by

$$S^{(2)}_{\text{FF,photo-thermal}} = \frac{2\alpha^2(1+\sigma)^2\hbar\omega_{\text{c}}T_{\text{abs}}P_{\text{circ}}m\omega^2}{(\rho C\pi r_0^2)^2}. \tag{2.85}$$

Here, α is thermal expansion coefficient, σ is the Poisson coefficient, T_{abs} is the absorption coefficient of the 5-mg mirror, P_{circ} is intra-cavity power, ρ is density of the mirror, C is specific heat capacity of the mirror, r_0 is the spot size on the mirror. In our measurements, it is maximumly only 0.2 % of the quantum back-action.

2.3.4 Raman Decoherence

Here, we present Raman decoherence [28], which is induced by Raman scattering of the optical pump field. To make the point clarify, the effect of the optical spring given by Eq. (2.75) is divided into following two terms as,

$$\frac{1}{(\kappa+i\omega)^2+\Delta^2} = \frac{\kappa^2+\Delta^2-\omega^2-2i\kappa\omega}{(\kappa^2+(\Delta-\omega)^2)(\kappa^2+(\Delta+\omega)^2)} \\ = \frac{\kappa^2+\Delta^2-\omega^2-2i\kappa\omega}{4\Delta\omega}\left[\frac{1}{(\kappa^2+(\Delta-\omega)^2)}-\frac{1}{(\kappa^2+(\Delta+\omega)^2)}\right]. \tag{2.86}$$

Thus, the optical damping effect (imaginary part of the optical spring) is given by

$$\gamma_{\text{opt}} = A_+ - A_- \tag{2.87}$$

$$A_{\pm} = \frac{\hbar\kappa|G|^2}{2m\omega(\kappa^2 + (\Delta \pm \omega)^2)}. \tag{2.88}$$

This equation is interpreted as the difference between anti-Stokes (A_+) and Stokes (A_-) scattering rates, because $A_{\pm}$ define the rates at which laser photons are scattered by the moving oscillator simultaneously with the absorption or emission of the oscillator vibrational phonons [21]. Note that the Raman scattering destroy quantum coherence of the carrier light, which is given by the sum of the anti-Stokes and Stokes scattering rates, although two Raman scattering events has no net effect in terms of energy. Now, let us focus on only the beam that leads to stiffening in relevant regime of large detuning $\Delta \gg \omega$, in order to obtain the effective quality factor under the Raman decoherence. This is given by

$$Q_{\mathrm{Raman}} \equiv \frac{\omega_{\mathrm{eff}}}{2\gamma_{\mathrm{Raman}}} \simeq \frac{\Delta}{\kappa}\frac{\omega}{g}\sqrt{\frac{m\omega_{\mathrm{c}}\Delta^3}{\kappa P_{\mathrm{in}}}} \simeq \frac{\Delta}{\kappa}, \tag{2.89}$$

where γ_{Raman} is defined as $A_+ + A_-$. From this equation, one can find that the large input power and the large detuning are necessary in order to increase the resonant frequency of the mechanical oscillator, with reducing the Raman decoherece at the same time.

References

1. Heisenberg, W.: Über den anschaulichen Inhalt der quantentheoretischen Kinematik und Mechanik. Z. Phys. **43**, 172–198 (1927)
2. Rüdiger, A., et al.: A mode selector to suppress fluctuations in laser beam geometry. Optica Acta **28**, 641 (1981)
3. Walls, D.F., Milburn, G.J.: Quantum Optics. Springer, New York (1994)
4. White, A.G.: Classical and quantum dynamics of optical frequency conversion. Ph.D. thesis, Physics Department, The Australian National University, Canberra, Australia (1995)
5. McKenzie, K.: Squeezing in the audio gravitational wave detection band, Ph.D. thesis, Physics Department, The Australian National University, Canberra, Australia (2008)
6. Callen, H.B., Welton, T.A.: Irreversibility and generalized noise. Phys. Rev. **83**, 34 (1951)
7. Gonzalez, G.I., Saulson, P.R.: Brownian motion of a mass suspended by an anelastic wire. J. Acoust. Soc. Am. **96**, 1 (1994)
8. Aspelmeyer, M., Kippenberg, T.J., Marquardt, F.: Cavity optomechanics. Rev. Mod. Phys. **86**, 1391 (2014)
9. Saulson, P.R.: Fundamentals of Interferometric Gravitational Wave Detectors. World Scientific, Singapore (1994)
10. Numata, K., et al.: Measurement of the intrinsic mechanical loss of low-loss samples using a nodal support. Phys. Rev. A. **276**, 37 (2000)
11. Numata, K., et al.: Measurement of the mechanical loss of crystalline samples using a nodal support. Phys. Rev. A. **284**, 162 (2001)
12. Cole, G.D., Wilson-Rae, I., Werbach, K., Vanner, M.R., Aspelmeyer, M.: Phonon-tunnelling dissipation in mechanical resonators. Nat. Commun. **2**, 231 (2011)
13. Gonzalez, G., Saulson, P.R.: Brownian motion of a torsion pendulum with internal friction. Phys. Rev. A. **201**, 1 (1995)

14. Saulson, P.R.: Thermal noise in mechanical experiments. Phys. Rev. D. **42**, 8 (1990)
15. Corbitt, T., et al.: Optical dilution and feedback cooling of a Gram-Scale Oscillator to 6.9 mK. Phys. Rev. Lett. **99**, 160801 (2007)
16. Chang, D.E., Ni, K.-K., Painter, O., Kimble, H.J.: Ultrahigh-Q mechanical oscillators through optical trapping. New J. of Phys. **14**, 045002 (2012)
17. Ni, K.-K., et al.: Enhancement of mechanical Q factors by optical trapping. Phys. Rev. Lett. **108**, 214302 (2012)
18. Corbitt, T., et al.: An all-optical trap for a gram-scale mirror. Phys. Rev. Lett. **98**, 150802 (2007)
19. Law, C.K.: Interaction between a moving mirror and radiation pressure: a Hamiltonian formulation. Phys. Rev. A. **51**, 3 (1995)
20. Purdy, T.P., Peterson, R.W., Regal, C.A.: Observation of radiation pressure shot noise on a macroscopic object. Science **339**, 801 (2013)
21. Genes, C., Vitali, D., Gigan, S., Aspelmeyer, M.: Ground-state cooling of a micromechanical oscillator: comparing cold damping and cavity-assisted cooling schemes. Phys. Rev. A. **77**, 033804 (2008)
22. Wilson-Rae, L., Nooshi, N., Zwerger, W., Kippenberg, T.J.: Theory of ground state cooling of a mechanical Oscillator using dynamical back-action. Phys. Rev. Lett. **99**, 093901 (2007)
23. Marquardt, F., Chen, J.P., Clerk, A.A., Girvin, S.M.: Quantum theory of cavity-assisted sideband cooling of mechanical motion. Phys. Rev. Lett. **99**, 093902 (2007)
24. Rabl, P., Genes, C., Hammerer, K., Aspelmeyer, M.: Phase-noise induced limitations on cooling and coherent evolution in optomechanical systems. Phys. Rev. A. **80**, 063819 (2009)
25. Schliesser, A., Rivière, R., Anetsberger, G., Arcizet, O., Kippenberg, T.J.: Resolved sideband cooling of a micromechanical Oscillator. Nat. Phys. **4**, 415–419 (2008)
26. Braginsky, V.B., Gorodetsky, M.L., Vyatchanin, S.P.: Thermodynamical fluctuations and photo-thermal shot noise in gravitational wave antennae. Phys. Lett. A **264**, 1–10 (1999)
27. Restrepo, J., Gabelli, J., Ciuti, C., Favero, I.: Classical and quantum theory of photothermal cavity cooling of a mechanical oscillator. Comptes Rendus Physique **12**, 860–870 (2011)
28. Chang, C.E., Ni, K.-K., Painter, O., Kimble, H.J.: Ultrahigh-Qmechanical oscillators through optical trapping. New J. Phys. **14**, 045002 (2012)

Chapter 3
Application of Optomechanics

Abstract In this chapter, we describe how an observation of the quantum back-action is related to the gravitational-wave (GW) detectors and test of quantum mechanics in macroscopic domain. As for force measurements such as the GW detectors, in which the mechanical oscillator is used as a probe of external force, its sensitivity has almost been limited by the standard quantum limit (SQL). Also, theoretical analysis has proven to be a connection between reaching the SQL imposed on the free mass (so-called free-mas SQL) and the generation of entanglement states, even between massive mechanical oscillators, such as suspended mirrors. Because of the massiveness (and the long relaxation time of the oscillator), such states might have a key to solve the quantum measurement problem. Thus, optomechanics is not only useful as sensitive probes for the weak force, but also leads to possibilities of testing fundamental problems. Although there are some motivations for using optomechanical system in the field of quantum information, let us focus on the above two topics.

Keywords Gravitational-wave detectors · Back-action evasion · Macroscopic quantum mechanics · Planck mass · Measurement problem

3.1 Towards Gravitational Wave Astronomy

Gravitational waves are ripples of space-time curvature that propagate across the universe at the speed of light. They were theoretically predicted from the Einstein equation in the General Theory of Relativity [1]. Their existence was indirectly proved by an observation of a binary pulsar, PSR1913+16 [2]. The observed decrease in the period of its revolution agrees with the theoretical expectation of the orbital decay due to gravitational radiation. There is no doubt that gravitational waves exist. However, gravitational waves have not been directly detected yet, because of the weakness of the gravitational interaction. On the other hand, due to the weakness, these waves enable us to view the dark ages of the universe through direct measurements. Their direct observation requires modern laser technology and highly sensitive measurements at almost the standard quantum limit (SQL). Furthermore,

N. Matsumoto, *Classical Pendulum Feels Quantum Back-Action*,
Springer Theses, DOI 10.1007/978-4-431-55882-8_3

for gravitational-wave astronomy, the GW detection rate should be increased through ultimate sensitive measurements beyond the (free-mass) SQL.

In the past two decades, an international array of ground-based, kilometer-scale Michelson interferometers composed of quasi-freely suspended mirrors (shown in Fig. 3.1), has been set up aiming at the first direct observation. The Michelson interferometer makes it possible to naturally decompose the optical fields and the corresponding motion of the suspended mirrors into common and differential modes. Since the Michelson interferometer is usually operated on a dark fringe (i.e., the beam splitter can be regarded as having a perfect reflectivity for the carrier light), ideally only optical signals induced by the differential motion of the suspended mirrors exit the unused port shown in Fig. 3.1. This signal enables us to measure the gravitational waves because one can consider the gravitational waves as being tidal force imposed on the suspended mirror [3].

These interferometric GW detectors have been operating all over the world. GEO600 in Germany [4] is currently the only large detector taking data, while the two LIGO observatories in the US [5] and the Virgo detectors in Italy [6] are being upgraded to their advanced state, and KAGRA in Japan [7] is under construction. These ground-based GW detectors target signals at audio frequencies in a band of 10 Hz to 10 kHz above the resonant frequency of the suspended mirror. At higher frequencies, their sensitivity will be limited by the shot noise. The shot-noise arises from the vacuum fluctuation of light, which enters the interferometer through the unused port. At lower frequencies, the quantum noise will be dominated by the

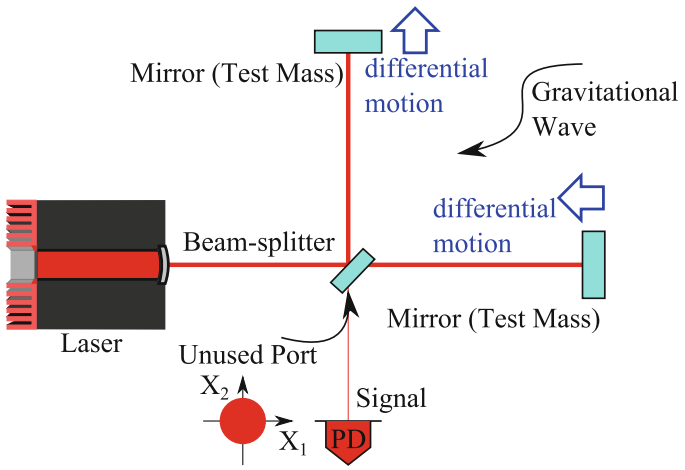

Fig. 3.1 Schematic of the gravitational-wave detector. A classic Michelson interferometer as a GW detector consists of a laser, a 50/50 beamsplitter (BS), two suspended test mass mirrors and a photodetector (PD). The gravitational wave can be considered to be a tidal force imposed on the mirrors, thereby shortening the length of one arm while expanding the length of the other. The vacuum fluctuation entering from the unused port masks the GW signal because the detector is operated at the dark fringe

quantum back-action (radiation pressure shot noise, RPSN) from the same vacuum fluctuation giving shot noise, but at the orthogonal quadrature phase. At any given frequency, the spectral density of the quantum noise is the sum of those of the shot noise, the RPSN, and a term arising from their correlation. Note that the zero-point fluctuation of the mirror does not affect the sensitivity because the GW detectors only pay attention to the sideband frequency above the resonant frequency of the suspended mirror, in which the mirror can be considered to be a free mass. The standard quantum limit (SQL) on the force measurement arises when the two noise sources are uncorrelated [8, 9]. Therefore, the correlation between the shot noise and the RPSN becomes a key to overcome the SQL.

3.1.1 Background of This Section

One of the most important features of future GW detectors is that they will operate at sufficiently high laser powers such that the quantum back-action acting on the suspended mirrors will become a dominant force at a lower frequency band (typically below 100 Hz). The effects of the radiation pressure will be manifested mainly in two ways in terms of the *fluctuation* of the pressure or the *stationary* pressure; the vacuum fluctuation will drive the mirror and the light is squeezed (called ponderomotive squeezing) through the self-phase modulation, which increases the phase noise of the measurement; also, the optical spring effects will alter the mechanical dynamics of the mirrors. Although the latter has been sufficiently studied [10–12], the former has not been observed yet on the macroscopic scale. Our result concerning the observation of quantum back-action changed the situation, and will provide the field of the GW detectors with a suitable platform to experimentally investigate a *back-action evasion* method in order to overcome the free-mass SQL.

3.1.2 Back-Action Evasion Method

In order to overcome the free-mass SQL, there are primarily three types of techniques: (i) creating correlations between the shot noise and the back-action noise [13, 14]; (ii) measuring the conserved dynamical quantity of the mechanical oscillator, e.g., momentum [15, 16]; (iii) an *effective* modification of the mechanical dynamics, e.g., using the optical spring effect created by the detuning of a signal recycling (SR) cavity in the GW detectors (unlike our case, it creates *frequency-dependent* rigidity called ponderomotive rigidity) [17–19]; and a variety of other techniques [20, 21]. Although these QND techniques have been theoretically developed, almost all of them have not been implemented in the quantum regime because the preparation of a platform, whose sensitivity must be limited by the quantum back-action, is very difficult.

Here, we introduce the first technique of creating correlations between the shot noise and the RPSN for the QND measurement, because our setup will be suitable to investigate this technique. It includes: (i-i) modifying the input optics called input (frequency-dependent) squeezing; (i-ii) modifying the output optics, called (frequency-dependent) homodyne measurement. This technique evades the quantum back-action and achieves a sensitivity limited only by the shot noise.

- **Input-squeezing**
  Since both the shot noise and the RPSN can be attributed to the same vacuum fluctuation entering the detector from the unused port, injecting a squeezed vacuum into this port can improve the sensitivity of the interferometer. In practice, this technique was experimentally implemented so as to reduce the shot noise using the phase-squeezed vacuum [22]. For overcoming the free-mass SQL, however, the required squeezed vacuum is very different, because a nearly phase-squeezed vacuum is required for higher frequencies, at which the shot noise dominates. However, a nearly amplitude-squeezed vacuum is required for lower frequencies, at which the radiation pressure noise dominates. To meet the demand, the squeezing angle should have an appropriate frequency-dependence, thereby creating the correlation between the shot noise and the RPSN (i.e., it includes not only back-action evasion, but also reduces the readout noise). Frequency-dependent squeezing can be created using the optical cavity, which was demonstrated at around 10 MHz [23]. At around the more suitable frequency for GW detectors, it is being prepared at MIT [24].

- **Utilization of ponderomotive squeezing**
  Unlike input-squeezing, ponderomotive squeezing has a superb feature, i.e., it does not need an external squeezed vacuum generator (squeezer), such as an OPO (optical parametric oscillator). However, similarly to input-squeezing, the *frequency-dependence* is ideally necessary not for the squeezer, but for the readout of the optical signal. In the conventional interferometer, shown in Fig. 3.1, the displacement signal is measured in the phase quadrature, and then the anti-squeezing limits the sensitivity. To utilize the correlation created by the ponderomotive squeezing, the output signal should be appropriately read out in a frequency-dependent quadrature, because the ponderomotive squeezing also has a frequency dependence. This is because the quantum radiation pressure fluctuation in Eq. (2.79) has no frequency dependence inside the cavity linewidth; however, the mechanical susceptibility in Eq. (2.36) has a dependence above the resonant frequency.

3.2 Test of Quantum Mechanics

Although quantum mechanics has proven to be highly successful in explaining physics below the microscopic scale, its validity at the macroscopic scale is still being debated. Recent advances in technology have gradually enabled experimental

tests of quantum mechanics at scales close to the macroscopic scale of our everyday life [20, 25, 26]. However, the superposition of positions of macroscopic objects beyond the Planck mass has not been observed, even though quantum mechanics predicts it. This is at the heart of the so-called "quantum measurement problem". Until now, intense theoretical and experimental studies have revealed that the environment, such as a thermal bath, plays an important role in the decoherence—the loss of quantum interference [27–30]. Under the many-world interpretation [31], this decoherence effect makes us understand the problem without any inconsistency [32]. From a positivistic point of view; however, it is not a fundamental solution, because linear quantum mechanics *cannot* destroy superposition.

According to alternative approaches, on the other hand, quantum theory must be modified in order to fundamentally solve the quantum measurement problem. The models of such modifications, e.g., the particular gravity-related (or DP) model [33, 34] and the continuous spontaneous localization (CSL) model [32], are designed to induce a wave-function collapse above a critical mass scale of a given quantum system. The CSL model introduces a nonlinear stochastic addition to the Schrödinger equation such that the new dynamic naturally breaks the superposition principle at the macroscopic level and naturally explain the probabilistic evolution, whose random outcomes obey the Born probability rule. "In many respects, the CSL model can be regarded as the prime example of a broad generic class of macrorealist modifications; it is compatible with all experimental observations to date and with most of the symmetry principles underlying both quantum and classical mechanics" (S. Nimmrichter et al. *PRL* **113**, 020405-1 2014 [35]). In the CSL model, all microscopic particles are continuously monitored with a rate λ_{CSL} and a spatial accuracy (correlation length) r_{CSL}. Another important model called the DP model explains the effect by gravitational interaction. According to their models [33, 34], dimensional analysis suggests that the quantum superpositions vanish within a timescale of $\tau = \hbar/\Delta E$, where ΔE is the spread of the mutual gravitational energy among components of the quantum superposition or the self-energy of the mass-distribution-difference, respectively.

To test the effect of the collapse models, the utilization of optomechanical oscillators combined with light, such as a levitated micro-sphere (e.g., satellite mission MAQRO [36]) and suspended mirrors (e.g., gravitational-wave detectors such as LIGO [5, 37]) have been proposed. The former system enables us to test the effect directly via demonstration of the quantum coherence, because the cooled micro sphere behaves like an electron in the *double slit* experiment. The latter system also enables us to test the effect, because the mirror is expected to be entangled with the laser field, and the resulting entanglement causes the position of the oscillator to be superposed [37]. If we prepare a massive object sufficiently isolated from the environment so that the superposition state is expected to be prepared from the viewpoint of the quantum mechanics, we can test the unknown collapse models. Especially the massive suspended mirror attracts considerable attention, since these models predict that the violation of the quantum superposition principle grows with growing mass. In following subsections, we present how we can test the models and estimate the each requirements.

3.2.1 Direct Test of Interference of a Massive Pendulum Via Single-Photon Coupling

The simplest way to test of quantum mechanics in the macroscopic domain is demonstration of interference of macroscopic objects (e.g., see in Ref. [36]). However, it is practically impossible performing the double slit experiment using a suspended mirror in order to demonstrate the quantum coherence of the superposition state, since the wave packet ($\propto \sqrt{1/m}$) is too small. The single-photon coupling, on the other hand, might create macroscopic superpositions, similarly to that presented by Schrödinger. The basic idea used by Schrödinger for generating macroscopic superpositions was entangling the states of a microscopic and a macroscopic system. Because it is easy to put the state of a microscopic system into a superposed states, by interacting with a macroscopic and microscopic system, the superposed states of the macroscopic system can be created. In Schrödinger's case, the microscopic system was a radioactive atom, while the macroscopic system was a cat. In the case proposed in Ref. [38], the microscopic system was a single photon, while the macroscopic system was a mechanical oscillator such as a suspended mirror. Here, we present the requirement if our suspended mirror is applied to the method proposed in Refs. [38, 39].

The requirement

This experiment requires; (i) the momentum imparted by the single photon has to be larger than the initial quantum uncertainty of the mirror's momentum such that the interference can be observed; (ii) the mechanical oscillator has to be decoupled from the known decoherence [here, let us consider the thermal (see Eq. (2.56)) and the Raman decoherence (see Eq. (2.89))] over one period of oscillation; (iii) the initial condition of the oscillator is better to be cooled down to its ground state; and (iv) long life-time of the optical cavity for storing the single photon is necessary such that the photon can be detected after one mechanical period. There requirements are respectively written by

$$\Lambda \equiv \frac{g x_{\rm zrf}}{\omega_{\rm eff}} \geq 1, \tag{3.1}$$

$$Q_{\rm eff} > 1, \tag{3.2}$$

$$n_{\rm eff}(t=0) < 1, \tag{3.3}$$

$$\frac{1}{\kappa} \sim \frac{1}{\omega_{\rm eff}}, \tag{3.4}$$

where g is the optomechanical coupling constant; $x_{\rm zpf}$ is the zero-point fluctuation of the mechanical oscillator; $\omega_{\rm eff}$ is the effective resonant frequency of the optically trapped mechanical oscillator; $Q_{\rm eff}$ is the effective quality factor of the optically trapped mirror; $n_{\rm eff}$ is the effective phonon number of the oscillator; and κ is the total cavity decay rate for storing the single photon. In practice, above requirements can be met individually, but they are extremely difficult to meet simultaneously. Here, let us focus on the weak coupling regime ($\Lambda < 1$), and we consider the use of

postselection technique proposed by Brian Pepper et al. [39]. In this technique, the interferometer is locked at the dark port such that the photon can be detected only when the suspended mirror interacts with single photon. In this case, a (maximum) detection rate per second is given by

$$\alpha = \frac{\Lambda^2}{4} \times \exp\left(-\frac{2\kappa}{f_{\rm eff}}\right) \times f_{\rm eff}, \tag{3.5}$$

where the first term is the rate of the postselecting succeeding, the second term is the rate of the photon remaining after a full mechanical period for the assumed optical loss characterized by κ, and the last term is an inverse of the full mechanical period. The rate is reduced by a factor of $\Lambda^2/4$ than the case of strong coupling regime ($\Lambda > 1$) since the many of events are eliminated by the postselection. Note that there are two parameters making the trade-off between the increase of Λ and the increase of the remaining photon number after a full period: (i) length of the cavity for storing single photon, given by L, is contributed to the detection rate via change of the coupling constant g ($\alpha \propto 1/L^2$) and the change of the cavity decay rate ($\alpha \propto \exp(-1/L)$); and (ii) the effective resonant frequency of the mirror is contributed to the detection rate via change of Λ ($\alpha \propto 1/\omega_{\rm eff}^3$) and the change of the period of the oscillation ($\alpha \propto \omega_{\rm eff} \exp(-1/\omega_{\rm eff})$). Because we can tune these parameters, maximum value of the rate does not depend on the these values, and thus parameters except for L and $\omega_{\rm eff}$, e.g., mass of the mirror given by m and the finesse of the optical cavity for storing the single photon given by $\mathscr{F}$ ($\simeq \pi/(\tau\kappa)$, where τ is roundtrip time) are especially important to increase the detection rate.

- **Towards the ground-state of the suspended mirror**. Let us focus on the feedback cooling (cold damping), since the bad cavity condition is generally satisfied if a suspended mirror is used as an optomechanical device. Because the feedback cooling is based on the measurement-feedback system (i.e., the oscillator position is measured, and then it is fed back to the oscillator by applying a force whose intensity is proportional to the oscillator's velocity), the noise level of the measurement must be limited by the SQL [40]. In our case of using the 5-mg mirror, displacement sensitivity of $2 \times 10^{-18}\,{\rm m}/\sqrt{\rm Hz}$ at 1 kHz is required.
- **Triangular optical cavity for creating the optical spring**. To increase the resonant frequency of the oscillator without additional thermal noise, a triangular optical cavity with the wavelength of 1064 nm is used such that the suspended mirror with the large gravitational dilution can be used with large intracavity power, see also in Chap. 4. The cavity parameters are as follows: finesse is 4,000; cavity round-trip length is 10 cm; input laser power is 0.1 W; cavity detuning Δ is 6κ; resulting intracavity power is 7 W; and the resulting effective frequency is 1 kHz.
- **Linear optical cavity for storing the single photon**. In order to increase the interaction time between photon and the suspended mirror, let us consider the ultra high finesse (6×10^7 is supposed) and the relatively short optical linear cavity (the detection rate has peak around the cavity length of 1 cm). Let us consider

the wavelength of the single photon as 532 nm, in order to increase the coupling constant. Also similarly to that described in Ref. [38], on average 0.1 photons go into the linear cavity such that the two-photon contribution causing noise in interferometer has to be kept low.

- **Decoherece**. To decouple the suspended mirror from the thermal decoherence, the mirror is trapped by the optical spring from 1 Hz to 1 kHz. Thus, natural quality factor Q_{m} has to be larger than $6 \times 10^{12} \times 10^{-6} = 6 \times 10^{6}$. To decouple the single photon from the Raman decoherence, the linear optical cavity is tuned on resonance (in the limit of $\Delta \to 0$, γ_{Raman} becomes zero).
- **Vacuum condition**. In order to reduce the gas damping enough, the experimental setup including the suspended mirror is set inside the vacuum tank, whose pressure has to be under 10^{-4} Pa.
- **Possible detection rate**. By using above parameters, the detection rate becomes three. Our assumption is now very optimistic about the finesse [41]. If it is reduced by a factor of 10, the rate is reduced by a factor of 100, and it becomes extremely difficult to observe the interference. Thus, the suspended mirror has to be changed to the mirror with smaller mass in order to increase the detection rate, if the finesse is smaller than the expected value.

3.2.2 Test of Gravity-Induced Decoherece Models by Linear Continuous Measurement

Next approach to test the quantum mechanics in macroscopic domain is to prepare/probe a conditional quantum state of the mechanical oscillator via continuous displacement measurement [42, 43]. Conditional state is a state into which continuously measured oscillator is projected, and the quantum dynamics of the oscillator can be probed by: (i) the (freely swinging) suspended mirror is continuously monitored by laser (e.g., by locking an optical cavity), whose sensitivity must be limited by the SQL; (ii) After the steady-state is reached, the conditional state is determined by the noise budget using Wienar filtering; (iii) the oscillator again freely evolves by turning off the laser such that the oscillator will be diffused both by well-known noise source like thermal noise, and if it exists, by unknown decoherence effect like gravitational decoherence; and (iv) after the free evolution, the growing variance is verified by the back-action evasion method, e.g., by adopting an optimal time-dependent homodyne detection such that the conditional quantum state can be characterized freely from the measurement-induced back-action. The back-action evasion method allows us to characterize the conditional quantum state below the SQL, and thus it also allows us to test whether Gaussian entangle states between two macroscopic masses can indeed be established [37].

With increase of the free-evolution time, the thermal decoherence will increase the variance and eventually the entanglement vanishes, which indicates how long the quantum entanglement can survive. If there are any additional decoherence effect,

the variance would grow faster than the case with the well-known decoherence, and the entanglement would vanish faster. Thus, measurement of the life-time of the quantum entanglement can help us to understand whether there is any additional decoherence effect, such as the models of the gravity decoherence [33, 34]. These models respectively give the life-time as follows [44]

$$\tau_{\mathrm{D}} \sim \frac{\sqrt{\hbar\Omega_{\mathrm{q}}}L^2}{Gm^{3/2}}, \tag{3.6}$$

$$\tau_{\mathrm{P}} \sim \frac{\Omega_{\mathrm{q}}}{G\rho}, \tag{3.7}$$

where τ_{D} is the life-time for the Diósi's model, τ_{P} is the life-time for the Penrose's model, L is the distance between two oscillators, G is the gravitational constant, ρ is the density of the oscillator, m is the mass of the oscillator, and $\Omega_{\mathrm{q}}/(2\pi)$ is the frequencies at which the quantum back-action noise intersect the (free mass) SQL. In Ref. [44], $\tau_{\mathrm{D}} = 1 \times 10^{-5}$ s, $\tau_{\mathrm{P}} = 4.3 \times 10^{9}$ s, which were obtained for GW detectors. In our case shown in Fig. 7.2, we estimate τ_{D} and τ_{P} to be 0.07 s and 2×10^{10} s, respectively [$\rho = 2.2\,\mathrm{kg/m^3}$, $L = 1$ cm, $\Omega_{\mathrm{q}}/(2\pi) = 2.6 \times 10^{3}$ Hz and $m = 5$ mg are used]. Our table-top system might be possible to test the Diósi's model similarly to GW detectors [43]. To distinguish these models (furthermore, there are many other models, e.g., to see [32, 36]), it should be tested for various mass scales such that a specific mass-dependent loss of the life-time is observed.

The requirement

The generation of the entanglement requires that the sensitivity must be limited by the free-mass SQL, shot noise, and quantum back-action in the wide bandwidth. The area under the free-mass SQL, which is reachable through the QND technique, is called the sub-SQL window. We have to realize a low Ω_{F} and a high Ω_{x}, where Ω_{F}, and Ω_{x} are the frequencies at which the classical force noise (e.g., the suspension thermal noise), and the classical sensing noise (e.g., the mirror thermal noise) intersect the free-mass SQL, respectively. For $\Omega_{\mathrm{x}}/\Omega_{\mathrm{F}} > 2$, there is a nonzero frequency band between Ω_{F} and Ω_{x}, in which the classical noise is completely below the free-mass SQL. Thus, our next goal is to prepare a cavity that satisfies this condition. In Refs. [37, 42, 44], the *logarithmic negativity* [45], which characterizes the degree of entanglement of the quantum state, is also calculated as a function of $\Omega_{\mathrm{x}}/\Omega_{\mathrm{F}}$.

3.2.3 *Test of Spontaneous Wave-Function Collapse Models Using a Classical Pendulum*

Above approaches for testing quantum mechanics requires the preparation of macroscopic superpositions such that mass-dependent loss of visibility in interference can be directly observed. This is extremely difficult. Quite recently, Bahrami et al. [46] suggested a different approach, which allows classical non-interferometric tests.

They demonstrated that the random localization process predicted by the CSL (and the DP) model inherently implies the back-action (classical momentum diffusion), which is the testable effect. Nimmrichter et al. [35] identified the generic sensitivity requirements for detecting the predicted the back-action caused by collapse models, in the optomechanical setup like the GW detector (i.e., the force fluctuation acting on the oscillator is continuously measured in the free-mass limit). They found that the power spectral density of the spontaneous momentum diffusion caused by the CSL can be given by (in Ref. [35], spectral density for the DP model is also calculated)

$$S^{(2)}_{\mathrm{FF,CSL}} = \lambda_{\mathrm{CSL}} \left(\frac{\hbar}{r_{\mathrm{CSL}}} \right)^2 \alpha \equiv D_{\mathrm{CSL}}, \tag{3.8}$$

where α is a mass-dependent geometry factor [35], $\tilde{\varrho}(\boldsymbol{k})$ is the Fourier transform of the mass density normalized to the total mass given by $\tilde{\varrho}(\mathbf{0}) = m$. For the perpendicular momentum diffusion of a disk, whose thickness d and radius are much larger than r_{CSL}, D_{CSL} is given by [47]

$$D_{\mathrm{CSL}} = \lambda_{\mathrm{CSL}} \frac{\hbar^2}{m_0^2} 4\pi r_{\mathrm{CSL}}^2 \frac{\varrho m}{d}, \tag{3.9}$$

where m_0 is the standard atomic unit. Lajos [47] further elucidate and simplify these considerations, and he found that a certain spontaneous increase ΔT_{CSL} (the spontaneous heating effect) of the equilibrium temperature, which is produced by the classical momentum diffusion caused by the CSL models, is given by (in Ref. [47], the heating effect for the DP model is also calculated)

$$\Delta T_{\mathrm{CSL}} = \frac{D_{\mathrm{CSL}}}{m k_{\mathrm{B}}} \tau, \tag{3.10}$$

where $\tau = 2/\gamma_{\mathrm{m}}$ is the (energy) relaxation time of the mechanical oscillator. From this equation, the heating effect proportional to the relaxation (ring-down) time and independent of the mass.

The requirement

To measure the diffusion given by Eq. (3.8), the SQL must be smaller than the predicted diffusion, whose condition gives

$$\Lambda_{\mathrm{SQL}} \equiv \frac{r_{\mathrm{CSL}}^2 \omega^2}{\hbar} \frac{m}{\alpha} < \lambda_{\mathrm{CSL}}. \tag{3.11}$$

Here, the measurement frequency ω is supposed to be larger than the effective resonant frequency of the mechanical oscillator (i.e., we consider the SQL as the free-mass SQL). From this equation, one can estimate that the reachable bound on the collapse rate λ_{CSL}, and the detailed reachable bound, if our system is used, is given in Ref. [35].

To measure the heating effect given by Eq. (3.10), the accuracy of measuring the effective temperature of the mechanical oscillator has to be better than the heating effect. The thermal noise floor level for the high-Q oscillator is given by $\sqrt{2\pi k_B T_{th}/(m\omega_m^3)}$ having the unit of $m/\sqrt{Hz}$, since the root mean square of the thermal motion is given by $k_B T_{th}/(2k_m)$. The floor level is $5 \times 10^{-9}\,m/\sqrt{Hz}$ if the condition with $m = 5$ mg, $f_m = 1$ Hz, and $T = 300$ K are considered. In this case, relatively large heating compared with the value used in Ref. [47] [τ is $(6 \times 10^{-6})^{-1}$ for our suspended disc] is predicted because the relaxation time of the mechanical oscillator can be increased by increasing the gravitational dilution (i.e., increasing the length of the suspension wire); however, the accuracy of measurement is extremely demanding because the noise floor is extremely lower than the back-ground seismic motion typically given by factor of $10^{-7}\,m/\sqrt{Hz}$ at 1 Hz. Furthermore, passive seismic isolation system is also difficult at the resonant frequency of 1 Hz. Active control can in principle reduce the back-ground seismic motion under the thermal floor level. The floor level is $1 \times 10^{-10}\,m/\sqrt{Hz}$ if the condition with $m = 5$ mg, $f_m = 10$ Hz, and $T = 300$ K are considered. In this case, relatively small heating compared with the value used in Ref. [47] [τ is $(6 \times 10^{-6})^{-1}$ for our suspended disc] is predicted because the relaxation time of the mechanical oscillator is reduced by reducing the gravitational dilution (i.e., decreasing the length of the suspension wire); however, the accuracy of measurement can be easily increased because passive seismic isolation system can greatly reduce the seismic motion at 10 Hz, even if the noise floor is lower than the back-ground seismic motion typically given by factor of $10^{-9}\,m/\sqrt{Hz}$ at 10 Hz.

References

1. Einstein, A.: Näherungsweise Integration der Feldgleichungen der Gravitation. Sitzungsbericht Preuss. Akad. Wiss. **688** (1916)
2. Taylor, J.H., Weisberg, J.M.: Further experimental tests of relativistic gravity using the binary pulsar PSR 1913+ 16. Astrophys. J. **345**, 434 (1989)
3. Saulson, P.R.: If light waves are stretched by gravitational waves, how can we use light as a ruler to detect gravitational waves? Am. J. Phys. **65**, 6 (1997)
4. http://www.geo600.uni-hannover.de (2015). Accessed 9 Mar 2015
5. Harry, G.M., et al.: Advanced LIGO: the next generation of gravitational wave detectors. Class. Quantum Gravity **27**, 084006 (2010)
6. http://wwwcascina.virgo.infn.it (2015). Accessed 9 Mar 2015
7. Somiya, K.: Detector configuration of KAGRA-the Japanese cryogenic gravitational-wave detector. Class. Quantum Gravity **29**, 12 (2012). Aso, Y. et al.: Interferometer design of the KAGRA gravitational wave detector. Phys. Rev. D. **88**, 043007 (2013). http://gwcenter.icrr.u-tokyo.ac.jp/en/ (2015). Accessed 9 Mar 2015
8. Braginsky, V.B., Ya, K.F.: Quantum Measurement. Cambridge University Press, Cambridge (1992)
9. Braginsky, V.B., Ya, K.F.: Quantum nondemolition measurements. Rev. Mod. Phys. **68**, 1–11 (1996)
10. Corbitt, T., et al.: An all-optical trap for a gram-scale mirror. Phys. Rev. Lett. **98**, 150802 (2007)
11. Sakata, S., Miyakawa, O., Nishizawa, A., Ishizaki, H., Kawamura, S.: Measurement of angular antispring effect in optical cavity by radiation pressure. Phys. Rev. D. **81**, 064023 (2010)

12. Chen, Y., Danilishin, S.L., Ya, K.F., Müller-Ebhardt, H.: QND measurements for future gravitational-wave detectors. Gen. Relativ. Gravit. **43**, 671–694 (2011)
13. Caves, C.M.: Quantum-mechanical noise in an interferometer. Phys. Rev. D. **23**, 8 (1981)
14. Kimble, H.J., Levin, Y., Matsko, A.B., Thorne, K.S., Vyatchanin, S.P.: Conversion of conventional gravitational-wave interferometers into quantum nondemolition interferometers by modifying their input and/or output optics. Phys. Rev. D. **65**, 022002 (2001)
15. Braginsky, V.B., Vorontsov, Y.I., Thorne, K.S.: Quantum nondemolition measurements. Science **209**, 4456 (1980)
16. Purdue, P., Chen, Y.: Practical speed meter designs for quantum nondemolition gravitational-wave interferometers. Phys. Rev. D. **66**, 122004 (2002)
17. Buonanno, A., Chen, Y.: Optical noise correlations and beating the standard quantum limit in advanced gravitational-wave detectors. Class. Quantum Gravity **18**, L95–L101 (2001)
18. Buonanno, A., Chen, Y.: Quantum noise in second generation, signal-recycled laser interferometric gravitational-wave detectors. Phys. Rev. D. **64**, 042006 (2001)
19. Buonanno, A., Chen, Y.: Signal recycled laser-interferometer gravitational-wave detectors as optical springs. Phys. Rev. D. **65**, 042001 (2002)
20. Purdy, T.P., Peterson, R.W., Regal, C.A.: Observation of radiation pressure shot noise on a macroscopic object. Science **339**, 801 (2013)
21. Heidmann, A., Hadjar, Y., Pinard, M.: Quantum nondemolition measurement by optomechanical coupling. Appl. Phys. **64**, 173–180 (1997)
22. Goda, K., et al.: A quantum-enhanced prototype gravitational-wave detector. Nat. Phys. **4**, 472–476 (2008)
23. Chelkowski, S., et al.: Experimental characterization of frequency-dependent squeezed light. Phys. Rev. A. **71**, 013806 (2005)
24. Isogai, T.: (personal communication)
25. Arndt, M., et al.: Wave-particle duality of C_{60} molecules. Nature **401**, 680–682 (1999)
26. Gerlich, S., et al.: Quantum interference of large organic molecules. Nat. Commun. **2**, 263 (2011)
27. Joos, E., Zeh, H.D.: The emergence of classical properties through interaction with the environment. Z. Phys. B—Condens. Matter. **59**, 223–243 (1985)
28. Zurek, W.H.: Decoherence, einselection, and the quantum origins of the classical. Rev. Mod. Phys. **75**, 3 (2003)
29. Hackermüller, L., Hornberger, K., Brezger, B., Zeilinger, A., Arndt, M.: Decoherence of matter waves by thermal emission of radiation. Nature **427**, 19 (2004)
30. Pikovski, I., Zych, M., Costa, F., Brukner, C.: Universal decoherence due to gravitational time dilation (2013). arXiv:1311.1095v1
31. Everett III, H.: Relative State formulation of quantum mechanics. Rev. Mod. Phys. **29**, 454 (1957)
32. Bassi, A., Lochan, K., Satin, S., Singh, T.P., Ulbricht, H.: Models of wave-function collapse, underlying theories, and experimental tests. Rev. Mod. Phys. **85**, 471 (2013)
33. Diósi, L. Models for universal reduction of macroscopic quantum fluctuations. *Phys. Rev. A*. **40**, 3 (1989)
34. Penrose, R.: On gravity's role in quantum state reduction. Gen. Relativ. Gravit. **28**, 5 (1996)
35. Nimmrichter, S., Hornberger, K., Hammerer, K.: Optomechanical sensing of spontaneous wave-function collapse. Phys. Rev. Lett. **113**, 020405 (2014)
36. Kaltenbaek, R., et al.: Macroscopic quantum resonators (MAQRO). Exp. Astron. **34**, 123–164 (2012)
37. Müller-Ebhardt, H., Rehbein, H., Schnabel, R., Danzmann, K., Chen, Y.: Entanglement of macroscopic test masses and the standard quantum limit in laser interferometry. Phys. Rev. Lett. **100**, 013601 (2008)
38. Marshall, W., Simon, C., Penrose, R., Bouwmeester, D.: Towards quantum superpositions of a mirror. Phys. Rev. Lett. **91**, 13 (2003)
39. Pepper, B., Ghobadi, R., Jeffrey, E., Simon, C., Bouwmeester, D.: Optomechanical superpositions via nested interferometry. Phys. Rev. Lett. **109**, 023601 (2012)

40. Abbott, B., et al.: Observation of a kilogram-scale oscillator near its quantum ground state. New J. Phys. **11**, 073032 (2009)
41. Valle, F.D., et al.: Extremely long decay time optical cavity. Opt. Express **22**, 11570–11577 (2014)
42. Müller-Ebhardt, H., et al.: Quantum-state preparation and macroscopic entanglement in gravitational-wave detectors. Phys. Rev. A. **80**, 043802 (2009)
43. Miao, H., et al.: Probing macroscopic quantum states with a sub-Heisenberg accuracy. Phys. Rev. A. **81**, 012114 (2010)
44. Miao, H.: Exploring macroscopic quantum mechanics in optomechanical devices. Ph.D. thesis, Physics Department, The University of Western Australia, Australia (2010)
45. Aurelian, I.: Entanglement dynamics in open systems. Romanian Rep. Phys. **61**, 4 (2009)
46. Bahrami, M., Paternostro, M., Bassi, A., Ulbricht, H.: Proposal for a noninterferometric test of collapse models in optomechanical systems. Phys. Rev. Lett. **112**, 210404 (2014)
47. Diósi, L. Testing spontaneous wave-function collapse models on classical mechanical oscillators. *Phys. Rev. Lett.***114**, 050403 (2015)

Chapter 4
Optical Torsional Spring

Abstract One of the key milestones toward the SQL is the development of the mechanical oscillator driven by the quantum back-action. However, the quantum back-action acting on the massive objects beyond the Planck mass ($\sim$22 μg) had not yet been observed because strong thermal fluctuating forces induced by the environment usually dominate measurements. To reduce the environmental noise, making the pendulum is suitable for allowing the mirror to be isolated from the environment. Although this isolation can largely reduce the noise, a stationary radiation pressure of the light exposes the free mass to instability if a *linear* optical cavity is used. This technical limitation had been a significant issue since there is a fundamental compromise between the technical limitation and the sensitivity; sufficient tolerance with firm suspension makes the mass differ from the free mass, which results in an increase of the thermal fluctuating force. In this chapter, we present how by using a *triangular* optical cavity it is possible to overcome this limitation. The relevant publication is Opt. Express **22** 12915 (2014) (Matsumoto, Michimura and Aso, Opt. Express 22:12915, 2014, [1]).

Keywords Triangular optical cavity · Positive torsional optical spring · Siddles-Sigg instability · Gravitational dilution

4.1 Trade-Off Relationship

The *positive* torsional spring effect is the key effect in our experiment because it enables us to use the large gravitational dilution effect (See Chaps. 5 and 6). This effect was independently discovered by Sigg [2] and myself. Unlike a linear cavity, light experiences *odd* numbers of reflections on mirrors inside a triangular cavity. This results in a *positive* torsional spring effect. Figure 4.1 enables us to intuitively and visually understand the difference between the linear and triangular optical cavities. Although one can calculate the optical positive torsional effect using the result described in Ref. [3], we use the result described in Ref. [2] for simplicity. Also, we describe an experimental demonstration of the effect.

N. Matsumoto, *Classical Pendulum Feels Quantum Back-Action*,
Springer Theses, DOI 10.1007/978-4-431-55882-8_4

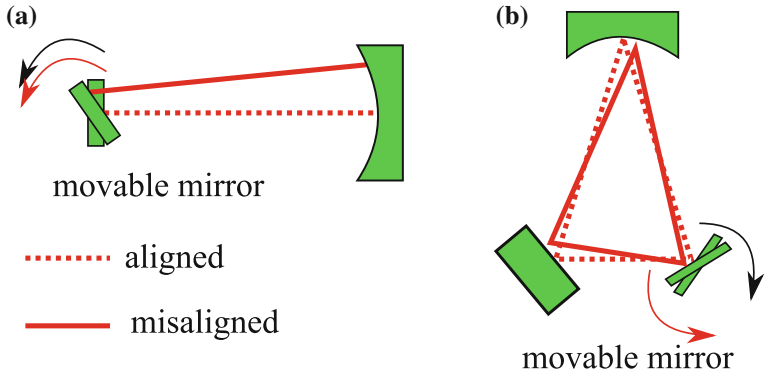

Fig. 4.1 Schematic of optical torsional effects. The schematic responses of the optical axes to the angular motion of the movable mirror are shown. The detailed response for the triangular cavity is given in Ref. [3]. An optical torque occurs through the stationary radiation pressure. **a** In the case of the linear optical cavity, the optical torque occurs in the same direction as the angular motion. This results in an anti-restoring force. **b** In the case of the triangular optical cavity, the optical torque occurs in the opposite direction as the angular motion. This results in a restoring force

Firstly, we explain the trade-off relationship between the stability and the sensitivity, which is generated if an optical linear cavity, which consists of the mirror suspended by a single wire, is used. In order to reach the SQL, the force noise must be dominated by the quantum back-action; however, measurements are usually dominated by strong thermal fluctuating force, whose power spectrum is given by

$$S^{(2)}_{\mathrm{FF,th}} = 4k_{\mathrm{B}}T\gamma_{\mathrm{m}}m. \tag{4.1}$$

Here, k_{B} is the Boltzmann constant and T is the temperature. Thus, reaching the SQL needs the condition:

$$R_{\mathrm{s}} = \frac{S^{(2)}_{\mathrm{FF,q}}}{S^{(2)}_{\mathrm{FF,th}}} = \frac{|G_{\mathrm{opt}}|^2}{(n_{\mathrm{th}}\kappa\gamma_{\mathrm{m}})} > 1, \tag{4.2}$$

where nth is the phonon occupation number. To reduce the thermal noise, one can freely suspend a massive mirror in order to allow the mirror to be isolated from the environment. The pendulum motion of the suspended mirror is dominantly trapped by the gravitational potential, and thus the dissipation of the pendulum is gravitationally diluted by a factor of $k_{\mathrm{grav}}/k_{\mathrm{el}} = 4l\sqrt{mg/\pi Y}/r^2$ (in this paper, we call it "Q enhancement factor") [4], where k_{grav} and k_{el} are respectively the gravitational and elastic spring constants of the pendulum, m is the mass of the mirror, l is the length of the wire, r is the radius of the wire, Y is the Young's module of the wire, and g is the gravitational acceleration. From Eq. (4.1), any reduction of the dissipation results in a reduction of the thermal fluctuation force, which also drives the mechanical motion similarly to the quantum back-action, by a factor of $k_{\mathrm{grav}}/k_{\mathrm{el}}$.

This isolation largely reduces the suspension thermal noise; however, a stationary radiation force of the light exposes the free mass to instability through an optical torsional anti-spring effect as shown in Fig. 4.1a, which is given by $\kappa_{\rm opt} = -P_{\rm circ} L_{\rm round}/c$, in conventional experiments utilizing a linear optical cavity [5, 6] (we suppose that the g-parameter closes to zero, which results in the smallest anti-restoring force). Here, $P_{\rm circ}$ is the intra-cavity power, $L_{\rm round}$ the round-trip length of the cavity, and c the speed of light. The stable condition concerning both the mechanical restoring force of the wire $\kappa_{\rm wire}$ and the optical anti-restoring force $\kappa_{\rm opt}$ is given by

$$\kappa_{\rm wire} + \kappa_{\rm opt} > 0. \tag{4.3}$$

Thus, $\pi G c/(2 l L_{\rm round}) > P_{\rm circ}/r^4$ must be satisfied in the case of using a single wire to suspend, where G is the modulus of rigidity of the wire. Thus, the enhancement of $R_{\rm s}$ due to the gravitational dilution is limited by

$$Q_{\rm en} < \sqrt{\frac{G}{Y} 8 l m g \frac{1}{\tau P_{\rm circ}}} = \sqrt{\frac{2 l m g}{(1+\sigma)} \frac{\kappa}{P_{\rm in}}}. \tag{4.4}$$

Here, $Q_{\rm en}$ is the Q enhancement factor, and τ is the round-trip time, σ is the Poisson's ratio, and $P_{\rm in}$ is the input laser power. The ratio of $R_{\rm s}$ in the case of using the linear cavity is plotted as a function both of the input laser power and the Q enhancement factor in Fig. 4.2a.

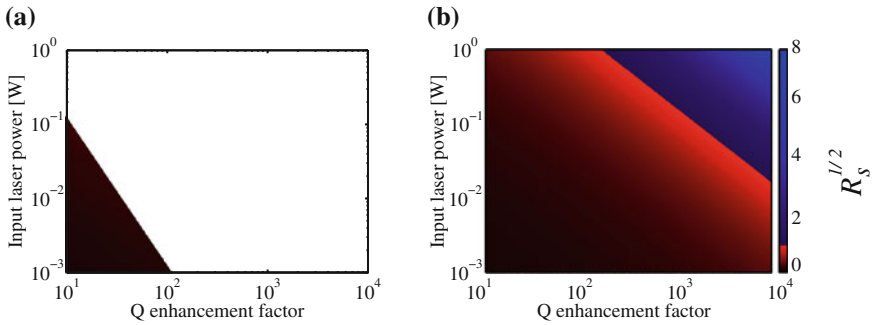

Fig. 4.2 The square root of the ratio of the quantum back-action to the thermal fluctuating force. **a** Trade-off relationship between the sensitivity and the stability is generated, in the case of using a linear cavity. A white domain represents the area, where $\kappa_{\rm wire} + \kappa_{\rm opt} < 0$. Parameters: $l = 0.02\,{\rm m}$, $m = 14.7\,{\rm mg}$, $\sigma = 0.28$, $T = 300\,{\rm K}$, and $\kappa/(2\pi) = 1.39\,{\rm MHz}$. Here, we suppose that each dissipation mechanisms are due to viscous friction (frequency dependent friction), for simplicity. In addition, we suppose that the intrinsic quality factor of the wire of $Q_{\rm in}$ is 3,800 (i.e., $Q_{\rm m} = Q_{\rm en} \times Q_{\rm in}$), and it has no dependence of the radius of the wire. **b** As for a triangular cavity, the square root of the ratio is plotted. The ratio of $R_{\rm s}$ becomes one at the boundary of blue and red domains. In the blue domain, there is a possibility to reach the SQL. The same parameters as in Fig. 4.2a are used, but there is no unstable domain. In addition, the incident angle of β is supposed to be 0.64 rad

4.2 Model of a Triangular Optical Cavity

Here, we present the torsional spring effect around the suspension axis (yaw) due to the radiation-pressure torque in a triangular cavity. We use Sigg's result [2], and begin by considering a two-dimensional triangular cavity formed by two flat mirrors, labeled M_a and M_c, and a curved mirror, labeled M_b, as shown in Fig. 4.3. We decompose the rotations of the two flat mirrors into two basis modes: the common-mode (same the rotation direction, the same amount) and the differential-mode (opposite rotation direction, the same amount). Any misalignment state of the two mirrors can be expressed as a linear combination of these two basis modes. In this picture, the relationship between the misalignment angle, $\Delta\alpha$, of the basis modes and the change in beam position on each of the mirror, Δx, is given by [2]

$$\Delta x = L K_h \Delta\alpha \tag{4.5}$$

with

$$K_h = \frac{1}{L(d+L-R)} \begin{pmatrix} \frac{-2d(L-R)}{\cos\beta} & 0 & \frac{-\sqrt{2}dR}{\cos\beta} \\ 0 & \frac{-2L(d+L-R)}{\cos\beta} & 0 \\ -\sqrt{2}dR & 0 & (d+L)R \end{pmatrix}. \tag{4.6}$$

Here, L is the distance between the curved mirror and the flat mirror, d is half the distance between the two flat mirrors, R is the radius of curvature of mirror M_b, and β is the incident angle on the flat mirror. The torque, N_{rad}, on each mirror induced by the radiation pressure is given by

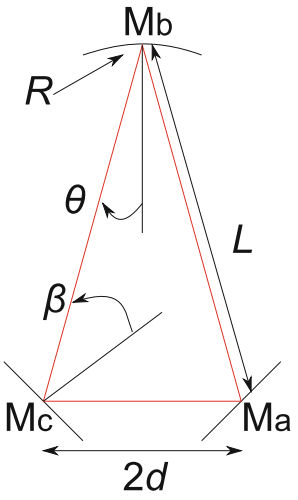

Fig. 4.3 Schematic of the triangular cavity. This figure represents the layout of the triangular cavity. The triangular cavity formed by two flat mirrors, labeled M_a and M_c (the movable mirror), and a curved mirror, labeled M_b. L, represents the distance between the curved mirror and the flat mirror; d is half the distance between the two flat mirrors, R is the radius of curvature of mirror M_b, θ is the incident angle on the curved mirror, and β is the incident angle on the flat mirror

$$N_{\mathrm{rad}} = \frac{2P_{\mathrm{circ}}}{c} L T K_{\mathrm{h}} \tag{4.7}$$

with

$$T = \begin{pmatrix} \cos\beta & 0 & 0 \\ 0 & \cos\beta & 0 \\ 0 & 0 & \cos\theta \end{pmatrix}, \tag{4.8}$$

where c is the speed of light in a vacuum, P_{circ} is the circulating power in the triangular cavity, θ is the incident angle on the curved mirror, and β is the incident angle on the flat mirror. When the acute-angled isosceles triangular optical cavity with a positive g-factor is considered, the optical spring constant is always positive, because all eigenvalues of Eq. (4.7) become negative [2]. This suggests that the triangular cavity is intrinsically stable in the yaw direction.

For simplicity, let us consider the situation where only the mirror $\mathrm{M_a}$ is movable and others are fixed. In this case, the equations of motion are given by

$$I_{\mathrm{a}} \ddot{\alpha}_{\mathrm{a}} = -(k_{\mathrm{t,opt}} + k_{\mathrm{t,m}})\alpha_{\mathrm{a}}, \tag{4.9}$$

$$\begin{aligned} k_{\mathrm{t,opt}} &\equiv -\frac{P_{\mathrm{circ}}}{c} l \cos\beta \left(K_{\mathrm{h}}(1,1) + K_{\mathrm{h}}(2,2)\right), \\ &= -\frac{2P_{\mathrm{circ}}L}{c} \frac{(d+L)[R-(L+dL/(d+L))]}{L(d+L-R)}, \end{aligned} \tag{4.10}$$

where I_{a} is the moment of inertia about the wire axis of mirror $\mathrm{M_a}$, $k_{\mathrm{t,opt}}$ is the angular spring constant of mirror $\mathrm{M_a}$ induced by the radiation pressure, and $k_{\mathrm{t,m}}$ is the mechanical torsional spring constant of mirror $\mathrm{M_a}$ in yaw. Under the self-consistent condition of the cavity, which is given by $0 < d + L < R\cos(\theta)$, Eq. (4.10) is always positive. Therefore, this configuration has intrinsic stability in the yaw direction.

From this equation, we can derive the resonant frequency of the yaw motion as

$$f_{\mathrm{a}} = \frac{1}{2\pi} \sqrt{\frac{k_{\mathrm{t,opt}} + k_{\mathrm{t,m}}}{I_{\mathrm{a}}}}. \tag{4.11}$$

From Eqs. (4.10) and (4.11) it is found that the angular resonant frequency is increased with increased circulating power.

4.3 Experimental Setup

In order to quantitatively verify the model described in the previous section, we measured the angular resonant frequency of a mirror, which is a part of a triangular optical cavity. By varying the incident laser power, thus varying $k_{\mathrm{t,opt}}$, we expect the resonant frequency to vary according to Eq. (4.11).

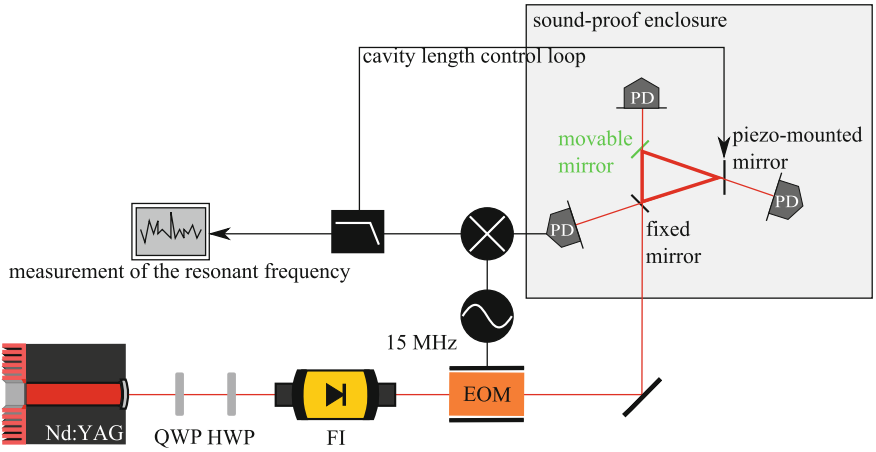

Fig. 4.4 Detailed experimental setup for observing the optical torsional spring effect. The laser beam (*red line*) was fed into the triangular cavity. An electro-optic modulator (EOM) was used to apply frequency sidebands for a Pound-Drever-Hall (PDH) method. Light was detected at various points using photodetectors (PD). HWP, Half-Wave Plate; QWP, Quarter-Wave Plate; FI, Faraday Isolator

Fig. 4.5 Photograph of the experiment for observing the optical torsional spring effect

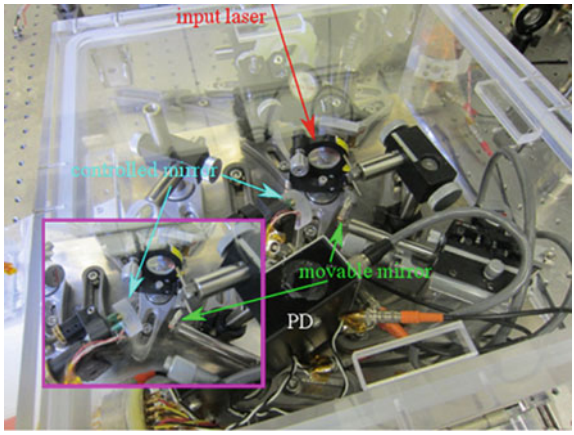

A schematic of the experimental setup is shown in Fig. 4.4, and its photograph is shown in Fig. 4.5. The laser source was a monolithic non-planar Nd:YAG ring laser with a 2 W continuous-wave single-mode output power at 1064 nm (Coherent Inc., Mephisto). We used an electro-optic modulator (EOM) as a phase modulator at 15 MHz (Newport Inc., model 4003) to lock the triangular cavity using a Pound-Drever-Hall (PDH) locking method. (The EOM is made up of a LiNbO3 crystal and a tank circuit tuned at 15 MHz, and was driven by a commercial oscillator at 15.000 MHz.) The triangular optical cavity with a finesse of 223 and a round-trip length of 100 mm was composed of two flat mirrors and a fixed curved mirror with

a radius of curvature of 75 mm. A part of two flat mirrors was a half-inch fused silica mirror suspended by a tungsten wire of 40 mm in length and 20 μm in diameter. The suspended mirror was attached to an oxigen-free copper cylinder of 3 mm in diameter and 3 mm in thickness, which was damped by an eddy-current by a doughnut-shaped magnet. Because of its shape, the magnet can in principle damp only the pendulum motion without decreasing the mechanical quality factor of the yaw motion. The (natural) resonant frequency of the yaw motion was measured to be 369 mHz, by optical shadow sensing. The curved mirror was fixed, and was mounted on a piezoelectric transducer (PZT; NEC Tokin, AE0505D08F), which was used as an actuator to keep the cavity in resonance with the laser. The triangular optical cavity and photo-detectors (HAMAMATSU, G10899-01K, InGaAs photodiode) were placed in a vacuum desiccator (ASONE, 1-070-01) for acoustic shielding.

The reflected light was detected by a photo-detector, and its output signal was demodulated at the modulation frequency. This signal was low-pass filtered with a cutoff frequency of 1 Hz, and fed back to the PZT actuator. The unity gain frequency for the length-control was about 1 kHz. We used this signal to stabilize the cavity length, and also to measure the angular (yaw) resonant frequency. The yaw motion of the suspended mirror generated the PDH signal, since there was a slight miscentering of the beam position on the suspended mirror. The transmitted light was also received in order to measure the intra-cavity power. The incident laser power into the cavity was changed from 60 mW to 1 W, in order to measure the change in the angular resonant frequency.

4.4 Experimental Results & Discussions

Figure 4.6a shows the observed spectra of the feedback signal with the intra-cavity power at 4, 32, 46 and 68 W. The peaks at around 0.4 Hz are the yaw resonances. The angular resonant frequency increases with increasing circulating power. The measured angular resonant frequencies are plotted against the intra-cavity power in Fig. 4.6b. The blue circles are the measured values and the horizontal lines are the statistical errors. The dashed red curves are the theoretical predictions, obtained from Eqs. (4.10) and (4.11) with $l = (4.4 \pm 0.1) \times 10$ mm, $d = (1.0 \pm 0.1) \times 10$ mm, $\beta = 0.7 \pm 0.1$ rad, $k_{\mathrm{t,opt}} = (3.9 \pm 0.2) \times 10^{-10} \times P_{\mathrm{circ}}$ Nm/rad, $I_{\mathrm{a}} = 6.6 \times 10^{-9}$ kgm^2, and $k_{\mathrm{t,m}} = 6.0 \times 10^{-8}$ Nm/rad. The theoretically calculated values show good agreement with the experimental results, which suggests that Eq. (4.10) is suitable for modeling the torsional spring effect caused by the optical restoring force.

Until now, we have only paid attention to the yaw. Note that this is a sufficient discussion in order to consider the stability of our triangular cavity. Because the suspended mirror can easily have sufficient mechanical positive torsional spring constants for a pitch without increasing the suspension thermal noise, even though the anti-torsional spring effect occurs for the pitch. This is due to the fact that the stiffness of the pitch does not depend on the radius of the wire, which mainly determines the dilution factor, but depends on the radius of the mirror.

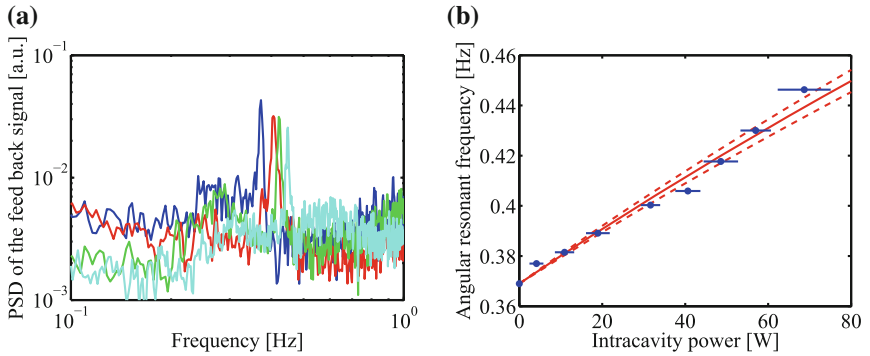

Fig. 4.6 Optical torsional spring response for various power levels. **a** Observed spectra of the feedback signal. The peaks correspond to the yaw resonance of the suspended mirror with the intra-cavity power (4 W(*blue*), 32 W(*red*), 46 W(*green*) and 68 W(*cyan*)). **b** Angular resonant frequency of the mirror suspension against the intra-cavity power. The *blue* circles are the measurement data and the *blue* horizontal lines are the statistical errors. The *solid red curve* is the theoretical prediction obtained from Eqs. (4.10) and (4.11) and the *dashed red curve* shows the systematic error

From this result and the following consideration, the advantage of the triangular cavity is verified. If the linear cavity is used, the instability can be mitigated, e.g., by: (i) decreasing the optical power; (ii) shortening the cavity length; (iii) using a thick wire for suspension; (iv) using multiple wires for suspension; (v) active control; and (vi) using a linear optical cavity that consists of fixed and suspended mirrors under the *negative*-g condition (i.e., both focal points are inside the cavity; in other words, both mirrors have a concaved structure). However, those respectively induce: (i) decrease of the quantum back-action; (ii) no issue; however, in practice it is insufficient only by it; (iii) decrease of the gravitational dilution (i.e., increase of the suspension thermal noise); (iv) introducing an unexpected thermal noise through the unexpected normal mode generated by the complicated suspension system [7]; (v) the necessity of using a more lager mirror to be attached along with the actuator, which would result in decrease of the quantum back-action (i.e., relatively increases all technical noise), and also might introduce some other dissipation through the actuator [to avoid these issues, using the lossless control system via radiation pressure without attached actuators was proposed [8]]; and (vi) the necessary of using a sufficiently concaved and small mirror to make the cavity length shorten (as a supplemental explanation, the linear cavity demands the condition given by $0 \leq (1 - L/R_1)(1 - L/R_2) \leq 1$, where L is the cavity length, R_1 is the curvature of the one mirror and R_2 is the curvature of the other mirror) and avoid the same issue of (v). (If an appropriate mirror can be manufactured, this method has no issue. We have been trying, but it is still challenging.) On the other hand, the triangular cavity has an *intrinsic* stability for yaw motion. Thus, one can conclude that the triangular cavity overcomes the fundamental compromise between the sensitivity and the instability for the linear optical cavity.

References

1. Matsumoto, N., Michimura, Y., Aso, Y., Tsubono, K.: Optically trapped mirror for reaching the standard quantum limit. Opt. Express **22**, 12915 (2014)
2. Sigg, D.: Angular stability in a triangular fabry-perot cavity. LIGO-T030275-00. www.ligo.caltech.edu/docs/T/T030275-00.pdf (2003)
3. Kawazoe, F., Schilling, R., Lück, H.: Eigenmode changes in a misaligned triangular optical cavity. J. Opt. **13**, 055504 (2011)
4. Saulson, P.R.: Thermal noise in mechanical experiments. Phys. Rev. D. **42**, 8 (1990)
5. Sidles, J.A., Sigg, D.: Optical torques in suspended Fabry-perot interferometers. Phys. Lett. A. **354**, 167–172 (2006)
6. Sakata, S., Miyakawa, O., Nishizawa, A., Ishizaki, H., Kawamura, S.: Measurement of angular antispring effect in optical cavity by radiation pressure. Phys. Rev. D. **81**, 064023 (2010)
7. Neben, A.R., et al.: Structural thermal noise in gram-scale mirror oscillators. New J. Phys. **14**, 115008 (2012)
8. Kawamura, S.: (personal communication)

Chapter 5
Experimental Setup

Abstract In this chapter, we describe an experimental setup, e.g., the 5-mg suspended mirror, geometry of the optical cavity, vibration isolation system, laser source, calibration method, detection and vacuum system. Figure 5.1 shows the displacement noise due to the quantum back-action that sets our goal of sensitivity in displacement measurement. At the resonant frequency of the pendulum (130 Hz is supposed), the displacement noise is approximately 1×10^{-12} m/$\sqrt{\text{Hz}}$. Every component has to be specially designed to achieve the sensitivity needed to detect the quantum back-action. Especially, we explain how to measure the back-action using the optically coupled oscillator in detail because it is the special case where the feedback force for length control is transferred to the 5-mg suspended mirror via the optical spring effect. The relevant publication is Phys. Rev. A **92**, 033825 (2015) [1].

Keywords 5-mg massive pendulum · Seismic isolation system · Calibration of the optically coupled oscillator

5.1 All Aspects of the Experiment

In this section, we describe all aspects of the experiment: both the experimental setup and the technical features.

Experimental Setup

The schematic of the experimental setup is shown in Fig. 5.2, and its photograph is shown in Fig. 5.3. Our optical cavity had a triangular configuration constructed from one movable mirror (mass, 5 mg; shown in Fig. 5.4), one half-inch fixed mirror, and one half-inch suspended mirror with a coil-magnet actuator attached onto its aluminum mirror holder for cavity length control (mass, 1×10^2 g; radius of curvature, 2×10^2 mm) (Figs. 2.5a and 5.2). The 5-mg mirror was suspended by a tungsten wire of 5 cm in length with 3 μm in diameter, attached to the mirror with epoxy resin. On the top of the wire, a picomotor-actuated stage for yaw alignment was attached. The fixed mirror and the controlled mirror had picomotors for both pitch and yaw alignment. Also, there were two picomotor-actuated folding mirrors for aligning each incident beam. These adjustment mechanisms allow us to align the optics inside the

N. Matsumoto, *Classical Pendulum Feels Quantum Back-Action*,
Springer Theses, DOI 10.1007/978-4-431-55882-8_5

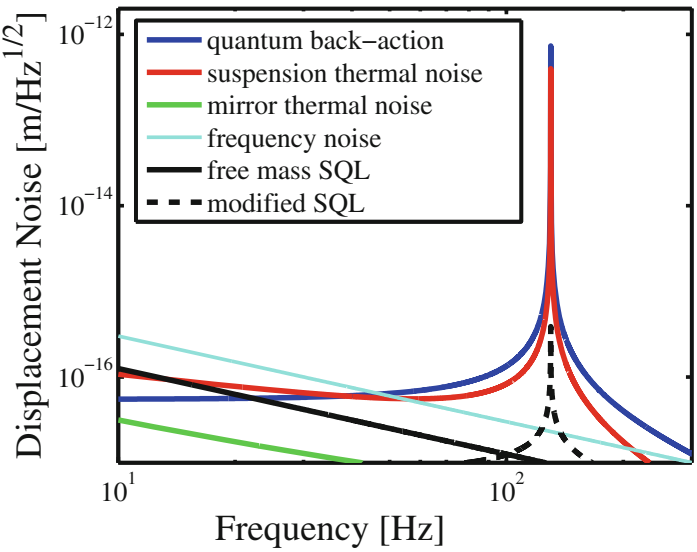

Fig. 5.1 Goal sensitivity for observing the quantum back-action. The quantum back-action (*blue*), the suspension thermal noise (*red*), the mirror thermal noise (*green*), the laser frequency noise (*cyan*), the SQL for the free mass (*dotted black*) and the SQL for the modified mirror (*black line*) are shown

vacuum chamber remotely. The triangular cavity, which was suspended by a double pendulum on a double-stage pre-isolation stack, was installed in a vacuum chamber (1×10^{-3} Pa) in order to sufficiently reduce any seismic motion, acoustic vibration, gas damping and so on.

The shape of the optical path of the cavity was an isosceles triangle, which had round-trip length of $L = 8.7 \pm 0.2$ cm. The incident angle to the movable mirror, β, was estimated to be $\cos\beta = 0.75 \pm 0.04$. The (amplitude) optical total decay rate was $\kappa/(2\pi) = (1.181 \pm 0.003) \times 10^6$ Hz, i.e., finesse of the cavity was $(1.47 \pm 0.03) \times 10^3$, and (amplitude) decay rate for the fixed mirror and the controlled mirror were $\kappa_{\mathrm{in1}}/(2\pi) = (8.7 \pm 0.3) \times 10^5$ Hz, and $\kappa_{\mathrm{in2}}/(2\pi) = (0.44 \pm 0.05) \times 10^5$ Hz. The optomechanical coupling constant was $g/(2\pi) = (2.8 \pm 0.2)\omega_{\mathrm{c}}$/m, where ω_{c} is the cavity resonant frequency.

The Nd:YAG laser source at the operational wavelength of 1064 nm was used, and the whole input optics system was covered by a sound-proof acryl box so as to reduce any jitter of the input beams. Two beams split from the same laser source were injected into the cavity in the same spatial mode, but in opposite directions. One of the two beams was injected from the controlled mirror in a clockwise direction (illustrated as the blue line in Fig. 5.2), and the other one was injected from the fixed mirror in a counterclockwise direction (illustrated as the red line in Fig. 5.2). The beam illustrated as the red was frequency shifted by 80 ± 3 MHz with an AOM and phase modulated in 15 MHz with an EOM, while the beam illustrated as the blue was frequency shifted by 80 MHz with the other AOM in the double pass

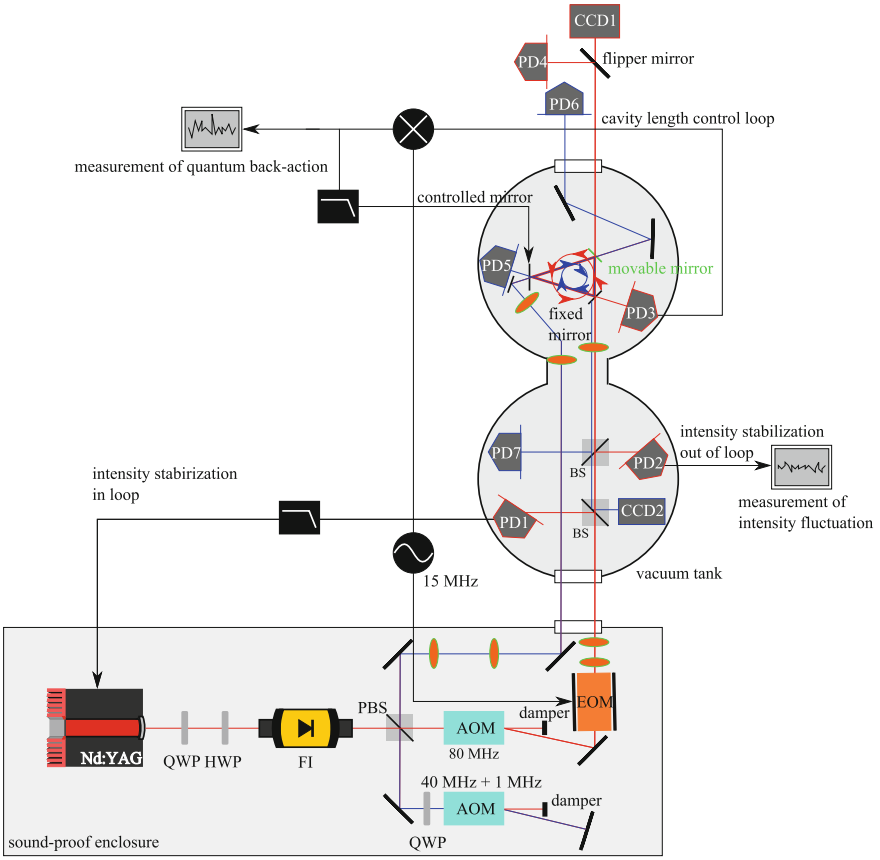

Fig. 5.2 Detailed experimental setup for observing the quantum back-action. The beam illustrated as red line and the beam illustrated as blue line were fed into the triangular cavity in the same spatial mode, but in different directions. Acousto-optic modulators (AOM) were used to shift the laser frequency. An electro-optic modulator (EOM) was used to apply frequency sidebands for the PDH method. Light was detected at various points using photodetectors (PD). HWP, Half-Wave Plate; QWP, Quarter-Wave Plate; FI, Faraday Isolator

configuration. The beam illustrated as the blue was injected into the cavity when the cavity linewidth (decay rate) was measured by sweeping the laser frequency across the optical resonance. A portion of the beam illustrated as the red was picked-off and detected by a photo-detector with a high quantum efficiency (Perkin Elmer, C30632, InGaAs photo-diode) to monitor intensity fluctuations of the laser.

The beam illustrated as the red was injected into the cavity, and the cavity reflected beam was detected with the fast-responding PD (PD3; HAMAMATSU, G10899-01K, InGaAs photo-diode). The output of this PD was demodulated with a 15 MHz RF signal to obtain the cavity length signal. We used this signal for cavity length control, and also to extract a quantum back-action signal. One of the transmitted

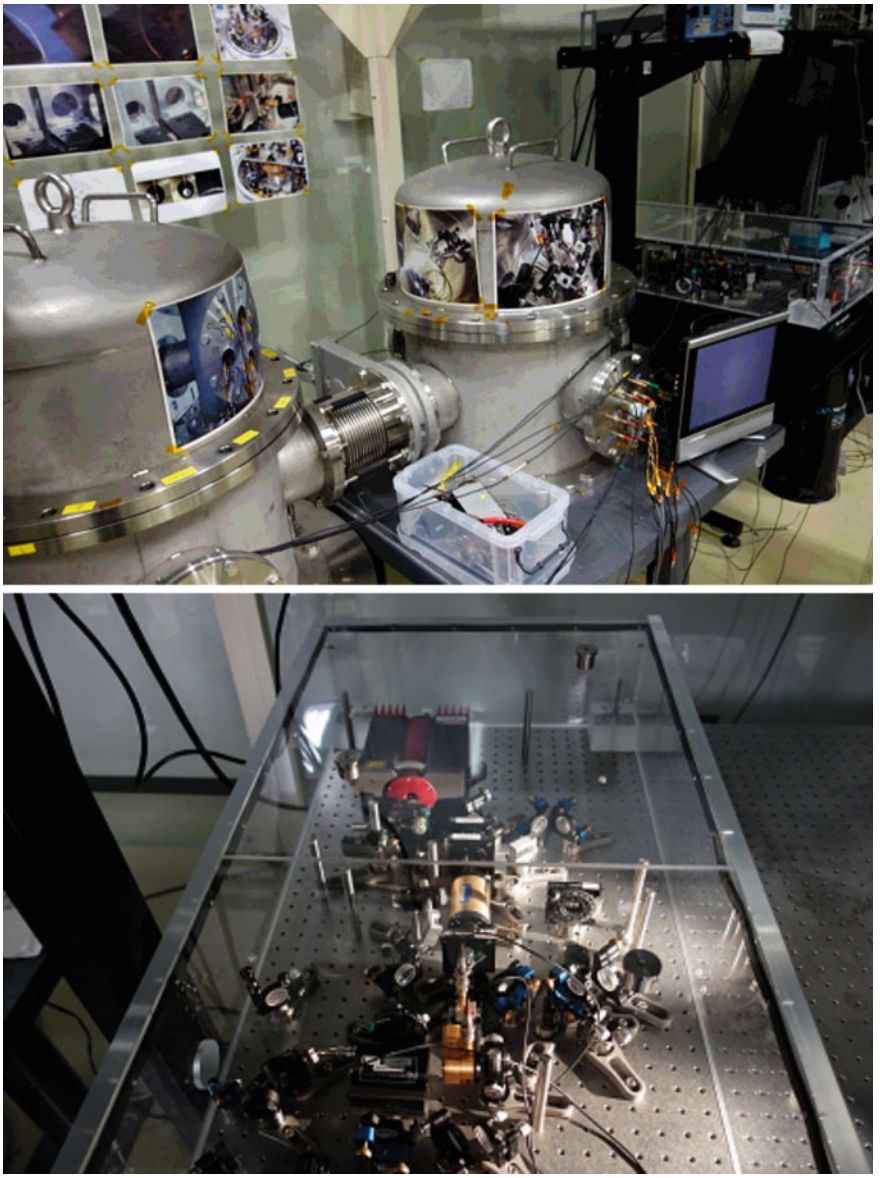

Fig. 5.3 Photographs of the experiment for observing the quantum back-action

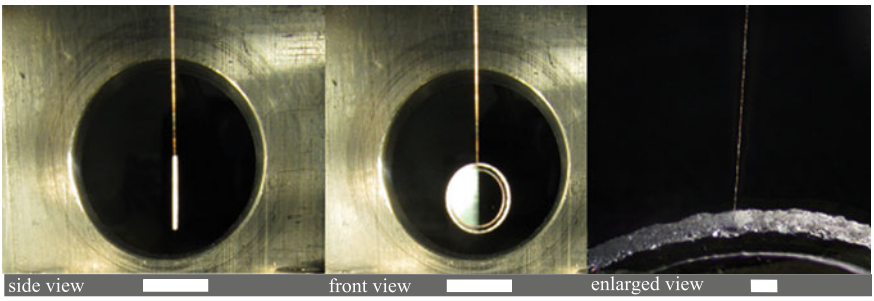

Fig. 5.4 Mechanical oscillator. The mirror was manufactured by SIGMA KOKI. It has a radius of 2 mm, a thickness of 0.2 mm, and a mass of 5 mg. A tungsten wire of 3 μm diameter and 50 mm length was attached to the mirror with epoxy resin. In both side and front views, it appears to be much larger than the real size of the tungsten wire because of an overexposure of the camera. The enlarged view photographed by a stereoscopic microscope (Olympus, SZ61) shows the interface between the wire and the mirror. Scale bars, 4 mm in both side and front views, and 0.2 mm in an enlarged view. Reprinted with permission from Ref. [1]. Copyright 2015 by American Physical Society

beams from the cavity was monitored by CCD1 or PD4 (flipped by a flipped mirror), and the other one was eventually rejected at the Faraday isolator.

In order to stabilize the intensity of the laser beam, we have to take into account the vacuum fluctuation, $\delta\hat{a}_1$ and $\delta\hat{a}_2$, inevitably injected from the open ports of BS1 and B2, respectively. Because the vacuum fluctuation, $\delta\hat{a}_1$, has an anti-correlation between an in-loop (PD1) and an out-of-loop (PD2), a correlation between the laser intensity fluctuation and the vacuum $\delta\hat{a}_1$ will be generated in the out-of-loop after stabilization (See Appendix). This results in increasing the noise level in out-of-loop, which is so-called "noise penalty" [2]. In addition, a possible minimum relative to the shot noise level in out-of-loop is also limited by the uncorrelated vacuum, $\delta\hat{a}_2$. Thus, the power injected to the photodetector (PD1; in-loop) used for the intensity stabilization was two-times larger than the power injected to the photodetector (PD2; out-of-loop) for monitoring the intensity fluctuation. This power balance allows intensity stabilization of the beam at a relative shot-noise level of 1.8 dB. There were picomotors-actuated mirrors before these two PDs so as to adjust the position of the beam spot on the detectors in order to find the spot position where the effect of the beam jitter is minimized. The incident angles to these two PDs were adjusted to the Brewster angle in order to minimize the effect of the back scattering. The detailed analysis will be presented in Appendix.

Technical Features

There are two main technical features in our experiment: an extremely thin suspension wire, and the triangular geometry of the optical cavity. The thin wire assures that the amount of energy stored in the pendulum is dominated by the gravitational potential over the elastic bending energy of the wire [3]. Since any loss of the energy is only associated with the elastic part of the stored energy, the total mechanical loss of

the pendulum is diluted with gravity by a factor of $k_{\mathrm{grav}}/k_{\mathrm{el}} = 4l\sqrt{mg/\pi Y}/r^2 = 6 \times 10^2$, where k_{grav} and k_{el} are the gravitational and elastic spring constants of the pendulum, r is the radius of the wire, l is the length of the wire, m is the mass of the mirror, Y is the Young's module of the wire, and g is the gravitational acceleration. Any reduction of the loss results in a reduction of a thermal fluctuation force, which also drives the mechanical motion similarly to the quantum back-action, by a factor of $\sqrt{k_{\mathrm{grav}}/k_{\mathrm{el}}}$.

The radiation pressure of the light induces a torque on the mirror when it is rotated. In a suspended linear cavity, this torque works as an optical anti-torsional spring, which causes a mechanical instability (so-called Sidles-Sigg instability [4, 5]). This is especially a serious issue because the mirror is suspended by the thin wire in order to reduce the thermal noise, which provides a small mechanical torsional spring constant ($k_{\mathrm{t,m}} \simeq 3 \times 10^{-11}$ Nm/rad) to compete against the optical anti-torsional spring. Because the gravitational dilution is increased with decreasing the radius of the wire, the trade-off relationship between the intra-cavity power (the quantum back-action level) and the radius of the suspension wire (suspension thermal noise level). The detailed expression of the above trade-off is given in Chap. 4. In order to circumvent this limitation, we used a triangular cavity, which has a positive optical torsional spring, and exhibits no instability in the rotation around the suspension axis. In our setup, the optical torsional spring constant is $k_{\mathrm{t,opt}} = +1 \times 10^{-9}$ Nm/rad, whereas it is $k_{\mathrm{t,opt}}^{(\mathrm{linear})} = -1 \times 10^{-9}$ Nm/rad for a linear cavity with otherwise the same scale and power. We succeed in storing about 50-times higher optical power in our cavity than the instability limit for the linear cavity, while the dilution factor becomes about 600.

5.2 Partial Aspects of the Experiment

In this section, we present a mechanical oscillator (a suspended mirror consisting of a mirror and a tungsten wire), an optical system (geometry of the cavity and the laser source), calibration, a detection system, and a vacuum system.

5.2.1 Mechanical Oscillator

- **Details of the mechanical oscillator**
  The mechanical oscillator is one of the key components in our experiment because it mainly determines the magnitude of the quantum back-action in terms of both the mechanical susceptibility and the optical power gain inside the cavity. In addition to the signal level, it also determines the noise level of the suspension thermal noise through material dissipation and gravitational dilution (shown in Fig. 5.1). It is the main noise source driving the mechanical oscillator, similarly to the quantum back-action. To reduce the difficulty for detection, the mechanical oscillator was

designed to have a low mass (5.0 mg), a high (power) reflectivity (the designed values are 0.99957 for p-polarized light and 0.99997 for s-polarized light), and a low mechanical loss of the pendulum (the measured value is $Q_{\mathrm{pend}} = (3.2 \pm 1.0) \times 10^5$; see in Chap. 6). The low mass was achieved using a thin (the radius was 0.2 mm) flat mirror. [Furthermore, the flat mirror reduces the noise, which is leaked from the residual side-motion (i.e., orthogonal to the pendulum).] Unlike a conventional *linear* optical cavity, the geometrical advantages of a *triangular* cavity enables us to stably trap the flat mirror due to the optical torsional spring effect. (In general, the dissipation of substrate material, which is related to the mirror thermal noise, increases as the object becomes thin due to only surface loss. Thus, we estimate that its mechanical quality factor of the substrate is 10^5. This is relatively lower, but is sufficient to observe the quantum back-action, partially because of an enhancement of the quantum back-action through the lightening.) The low mechanical loss of the pendulum was achieved by using an ultra-thin wire (the radius was 1.5 um) to suspend the mirror, and high reflectivity was achieved using Ion Beam Sputtering (IBS) to coat it.

- **Dimensions and spot size**
  The dimensions of the triangular cavity and the spot size on the movable mirror are important factors in terms of frequency noise of the laser and any mirror thermal noise, respectively. By designing the path length (the spot size) to be as small (large) as possible, there sensing noises are depressed. We set the cavity round-trip length as short as possible, about 9 cm, from the viewpoint of easy handling. The beam radii on the movable mirror and on the controlled mirror, as determined by the cavity parameters, were 110 um and 178 um, respectively. Based on the choices of the cavity length, the substrates of the thin mirror and of the beam spot sizes, the theoretical frequency and thermal noise levels are shown in Fig. 5.1.
- **Vibration isolation system**
  Seismic noise is the most serious problem in the low-frequency region (i.e., the vibration level is about $10^{-7}/f^2$ m/$\sqrt{\mathrm{Hz}}$ above 1 Hz on our laboratory) because it is not only increased, but also becomes difficult to be mitigated using passive filter, such as a pendulum. The other seismic motions, such as a bobbing motion of the pendulum, leaks into the direction of the beam axis through asymmetries of the isolation system. Therefore, a sufficient level of attenuations for all degrees of freedom has to be achieved as well. To meet this criteria, the isolation system was made of two parts: a double pendulum and a double stack.
  Figure 5.5 shows the suspension system designed for this experiment. The triangular cavity was placed on a platform made of aluminum, which was suspended by the double pendulum on a double stage pre-isolation stack. Common-mode rejection of seismic noise is expected by using the common platform for the triangular cavity. The intermediate ring mass (made of copper) of the double pendulum was also suspended with three tungsten wires (radius of 150 um) and vertical coil springs. For the purpose of damping, another larger intermediate ring mass (made of steel) with strong magnets was suspended next to the (smaller) intermediate mass of copper. In order to avoid any re-injection of seismic noise from the

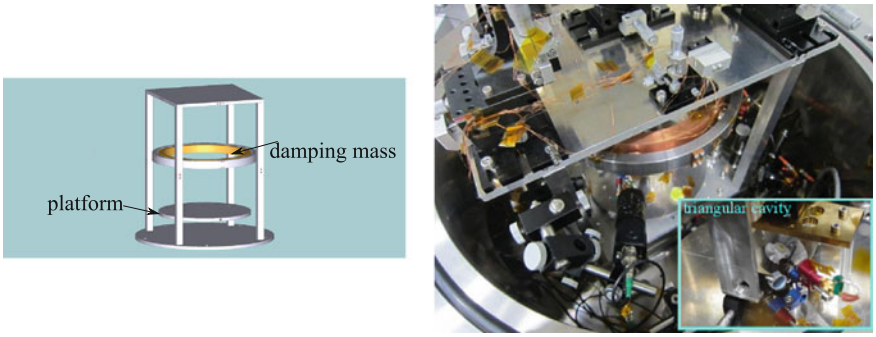

Fig. 5.5 Double-pendulum system

damping magnet, the intermediate mass of steel was also isolated from any seismic motion. In order to decouple the seismic motion from other degrees of freedom, the slope of the platform of aluminum was adjusted using x-y-z stages, which were attached onto stages located on the top of the double pendulum. Then, the slope of the intermediate mass of steel was also adjusted by using the other x-y-z stages, which were attached on stages in order to decouple the eddy-current damping from other degrees of freedom. The double-pendulum system theoretically provides 160 dB of isolation at the resonant frequency (around hundred Hz) of the movable mirror in the horizontal plane. In the vertical plane, the coil springs provide 80 dB of isolation at the resonance.

The pre-isolation stack, designed and constructed by Kenji Numata [7], can provide further isolation for all degrees of freedoms, although the double pendulum ensures sufficient isolation. The stack was composed of two stainless-steel blocks, separated by isolation rubbers. The isolation performance of this stack was also measured by Numata using a vibration exciter. It was better than 70 dB for the vertical direction, and 80 dB for horizontal direction at resonance [7].

The total performance of this suspension and the stack system is estimated by multiplying the simulated isolation ratio of the suspension and the measured isolation ratio of the stack to 150 and 240 dB. The required level of displacement noise was very likely achieved.

5.2.2 Laser Source

As a laser source we used a monolithic non-planar Nd:YAG ring laser with 2 W continuous wave single-mode output power at 1064 nm [8]. The wavelength is the most common choice in the current GW detectors. Nonplanar ring oscillators (NPROs) are monolithic lasers where the laser radiation circulates along a nonplanar ring in a single laser crystal. This is believed to give the best performance as a continuous-wave

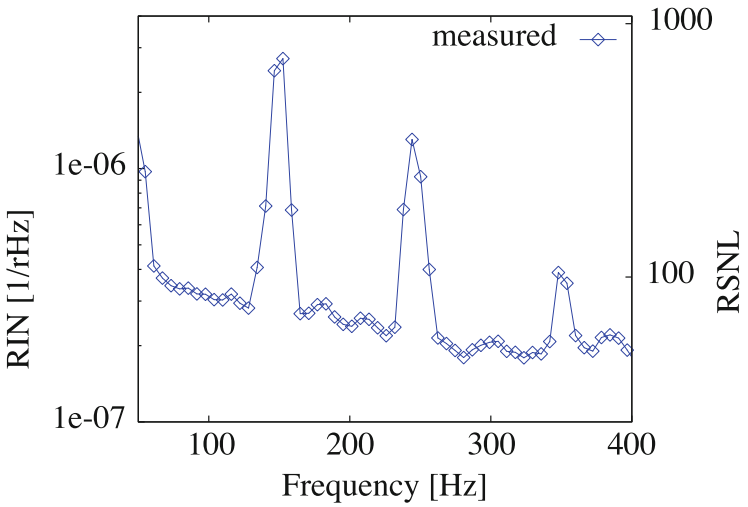

Fig. 5.6 Intensity fluctuations of the laser. The measured spectra of the intensity fluctuation of the input laser. Left vertical axis indicates the relative intensity noise level (RIN), and the right side indicates the relative shot noise level (RSNL). Spectral peaks are identified as power line harmonic. Reprinted with permission from Ref. [1]. Copyright 2015 by American Physical Society

laser. The laser intensity can be modulated by applying a voltage signal to its current actuator. Our intensity stabilization shown in Appendix was done by using this actuator. The tuning efficiency was measured before its installation into the injection bench of our setup.

Figure 5.6 shows the measured intensity fluctuations of the free-running laser, which is divided by the incident laser power and its shot-noise-level, respectively.

5.2.3 Calibration

Here, we present calibration of the pendulum's displacement (or force acting on the pendulum), which is based on the three points: (i) efficiency of the coil-magnet actuator for the cavity-length control (from the voltage to force conversion factor); (ii) relationship between the round-trip length and the pendulum motion of the suspended mirror; and (iii) open-loop compensation of the cavity-length control system.

- **Actuator efficiency**. In order to calibrate the displacement noise spectrum from the voltage signal, we measured the actuator efficiency and determined the voltage-to-force conversion factor. Here, we present measurement of the factor using a Michelson interferometer.
  Figure 5.7a shows the configuration used to measure the actuation efficiencies. We locked the Michelson interferometer using a PD, an appropriate servo circuit

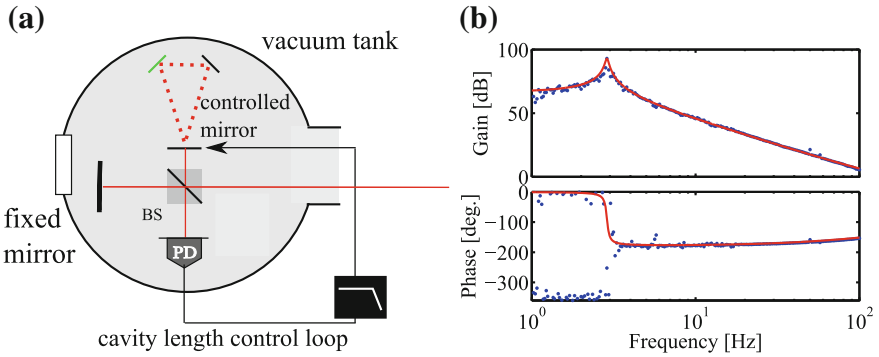

Fig. 5.7 Measurement of the efficiency of the coil-magnet actuator. **a** Experimental setup. The laser beam was fed into the Michelson interferometer (MI). Light was detected using a photodetector (PD), and the MI was locked at the mid-fringe point. **b** Measured open loop transfer functions of the displacement control are shown as blue points, while the red solid lines are the fitting curves. From this measurement, the actuation efficiency, $(2.1 \pm 0.1) \times 10^{-5}$ N/V, was estimated. Reprinted with permission from Ref. [1]. Copyright 2015 by American Physical Society

and the same coil-magnet actuator as the main measurement, and measured the open-loop gain as shown in Fig. 5.7b. From the fitting to the measured date, we could estimate the voltage-to-force conversion factor of the actuator, because the others composing the loop, such as the response of the Michelson interferometer, the mechanical susceptibility of the pendulum (controlled mirror), PD, and servo filter, had been measured by other experiments. As a result, we experimentally determined the actuation efficiency to be $(2.1 \pm 0.1) \times 10^{-5}$ N/V.

- **Relationship between the round-trip length and the pendulum's displacement** Let us consider the triangular cavity shown in Fig. 5.8, whose round-trip length L_r is given by

$$L_\mathrm{r} = L_\mathrm{PQ} + L_\mathrm{QR} + L_\mathrm{RP}, \tag{5.1}$$

where L_PQ is the length of the line segment PQ, L_QR is the length of the line segment QR, and L_RP is the length of the line segment RP. The round-trip length is also given by

$$L_\mathrm{r} = R(\sin 2\mathrm{A} + \sin 2\mathrm{B} + \sin 2\mathrm{C}), \tag{5.2}$$

where circumradius of $\triangle$ABC is defined as R.

Here, as shown in Fig. 5.9, we consider the displacement of the pendulum (5-mg flat mirror) given by dx, which induces the change of the beam spot on the curved mirror given by $d\theta$. After the displacement is denoted by prime (e.g., $R \to R'$), (first-order) change of the round-trip length, $dL_\mathrm{r} \equiv L'_\mathrm{r} - L_\mathrm{r}$, is given by

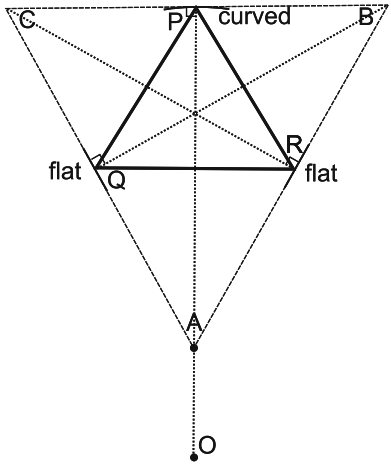

Fig. 5.8 Top view of the triangular cavity. The orthic triangle of △ABC is △PQR. A: a point where two straight lines to which the flank of the respective flat mirrors is extended are crossed; O: center of curvature of the curved mirror; P: a point where the straight line AO and the curved mirror are crossed; B (C): a point where the tangent line at the point P and (each) straight line to which the flank of the (each respective) flat mirror is extended are crossed; and Q (R): a perpendicular line from B (C) to AC (AB)

Fig. 5.9 The displacement of the pendulum. α: incident angle

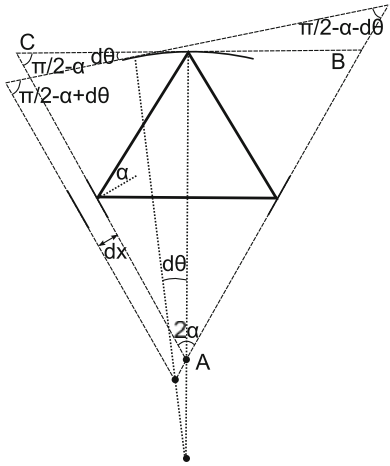

$$
\begin{aligned}
dL_{\mathrm{r}} &= R'[\sin 4\alpha + \sin(\pi - 2\alpha - 2d\theta) + \sin(\pi - 2\alpha + 2d\theta)] \\
&\quad -R[\sin 4\alpha + \sin(\pi - 2\alpha) + \sin(\pi - 2\alpha)], \\
&\simeq R'(\sin 4\alpha + 2\sin 2\alpha) - R(\sin 4\alpha + 2\sin 2\alpha), \\
&= 2dR\sin 2\alpha(1 + \cos 2\alpha). \qquad (5.3)
\end{aligned}
$$

By using law of sines given by

$$R = \frac{L_{\mathrm{BC}}}{2\sin 2\alpha}, \tag{5.4}$$

and thus $dR \equiv R' - R$ is given by the change of the length of the line segment BC, since $\angle$ A does not change with the displacement of the pendulum.
In order to obtain the expression of dR, followings are respectively obtained by using law of sines for $\triangle$C'ST and $\triangle$BB'S in Fig. 5.10

$$\begin{cases} \dfrac{a_1}{\sin\left(\dfrac{\pi}{2}+\alpha\right)} = \dfrac{a + r\dfrac{d\theta}{2}}{\sin\left(\dfrac{\pi}{2}-\alpha-d\theta\right)}, \\ \dfrac{a_2}{\sin\left(\dfrac{\pi}{2}-\alpha\right)} = \dfrac{a - r\dfrac{d\theta}{2} + \dfrac{dx}{\cos\theta}}{\sin\left(\dfrac{\pi}{2}+\alpha-d\theta\right)}, \end{cases} \tag{5.5}$$

where $r \equiv L_{\mathrm{OP}} (= 0.2\ \mathrm{m})$ is the radius of curvature of the curved mirror, a is defined as the length of the line segment BP (CP), a_1 is defined as the length of the line segment B'S, and a_2 is defined as the length of the line segment C'S as shown in Fig. 5.10. Thus, the change of the length of the line segment BC is given by

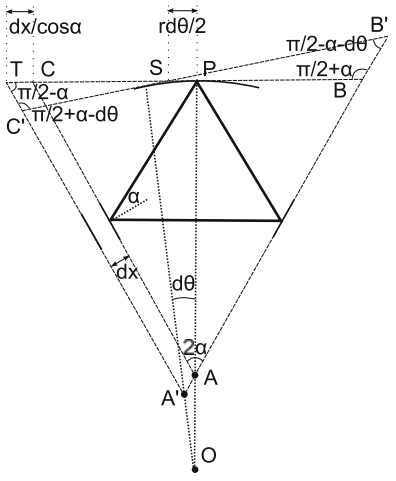

Fig. 5.10 Detailed figure of the displacement of the pendulum. S (T): a point where the straight line BC (BC) and the straight line B'C' (A'C') are crossed

$$\begin{aligned}
\mathrm{B'C'} - \mathrm{BC} &= a_1 + a_2 - 2a, \\
&= \left(a + r\frac{d\theta}{2}\right)\frac{\cos\alpha}{\cos(\alpha + d\theta)} \\
&\quad + \left(a - r\frac{d\theta}{2} + \frac{dx}{\cos\alpha}\right)\frac{\cos\alpha}{\cos(-\alpha + d\theta)} - 2a, \\
&\simeq \left(a + r\frac{d\theta}{2}\right)(1 + \tan\alpha d\theta) \\
&\quad + \left(a - r\frac{d\theta}{2} + \frac{dx}{\cos\alpha}\right)(1 - \tan\alpha d\theta) - 2a, \\
&\simeq \frac{dx}{\cos\alpha}. \qquad (5.6)
\end{aligned}$$

Using this equation, dR is given by

$$\begin{aligned}
dR &= \frac{\mathrm{B'C'} - \mathrm{BC}}{2\sin 2\alpha}, \\
&= \frac{dx}{2\sin 2\alpha\cos\alpha}. \qquad (5.7)
\end{aligned}$$

The relationship between the round-trip length and the displacement of the pendulum (flat mirror) is given by

$$\begin{aligned}
dL_\mathrm{r} &= 2dR\sin 2\alpha(1 + \cos 2\alpha), \\
&= \frac{1 + \cos 2\alpha}{\cos\alpha}dx, \\
&= 2dx\cos\alpha. \qquad (5.8)
\end{aligned}$$

In addition to the displacement of the flat mirror, we consider the displacement of the curved mirror also given by dx, as shown in Fig. 5.11. The round-trip length is given by

$$\begin{aligned}
L_\mathrm{r} &= R[\sin 2\gamma + \sin(\pi - \gamma) + \sin(\pi - \gamma)], \\
&= 2R\sin\gamma(1 + \cos\gamma), \qquad (5.9)
\end{aligned}$$

where we define γ as $\pi/2 - \alpha$. By using law of sines again,

$$R = \frac{\mathrm{BC}}{2\sin\gamma}. \qquad (5.10)$$

Thus, $dR \equiv R' - R$ is given by the change of the length of the line segment BC, which is written by

$$\mathrm{B'C'} - \mathrm{BC} = 2dx\tan\frac{\gamma}{2}. \qquad (5.11)$$

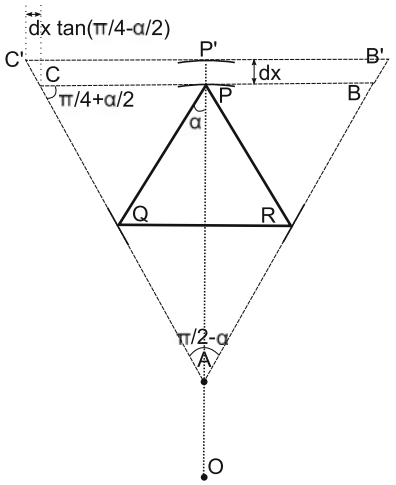

Fig. 5.11 The displacement of the curved mirror. α: incident angle to the curved mirror

Thus, dR is given by

$$\begin{aligned} dR &= \frac{\mathrm{B'C'} - \mathrm{BC}}{2\sin\gamma}, \\ &= \frac{dx}{2\cos^2\dfrac{\gamma}{2}}. \end{aligned} \tag{5.12}$$

The relationship between the round-trip length and the displacement of the curved mirror is given by

$$\begin{aligned} dL_\mathrm{r} &= 2dR\sin\gamma(1+\cos\gamma), \\ &= 2dx\sin\gamma, \\ &= 2dx\cos\alpha. \end{aligned} \tag{5.13}$$

From the above, the relationship between the round-trip length and the displacement of the any mirror is given by

$$dL_\mathrm{r} = 2dx\cos\alpha. \tag{5.14}$$

From Eq. (5.14), the optomechanical coupling constant defined as $\partial\omega_\mathrm{c}/\partial x$ is given by $\omega_\mathrm{c}/L_\mathrm{r} \times 2\cos\alpha$. In the limit of $\alpha \to 0$, Eq. (5.14) will be equal to $dL_\mathrm{r} = 2dx$, which is the case of the linear cavity is considered. Also, in the limit of $\alpha \to \pi/2$, dL_r becomes zero since the beam does not be reflected on the mirror.

- **Servo system for the cavity length control**
  The detected signal at the PD3 was demodulated by the DBM, and then sent to a control servo circuit. The displacement/force fluctuation can be extracted from error/feedback signals (labeled v_{er} and v_{fb}, respectively) of the servo loop. In the following, we describe the open-loop transfer function of the triangular cavity loop.

  – **The simplified model shown in Fig. 5.12a:**
    Figure 5.12a shows a simplified model of the triangular cavity servo system. The displacement of the movable mirror, δx, is converted by the PDH method into a voltage thorough a displacement-to-voltage conversion factor, H [V/m] (consists of the transfer function of the optical cavity and the RF photodetector), producing an error signal, V_{er} [V]. It is filtered by an electric servo circuit, F [V/V], producing a feedback signal, V_{fb} [V]. The feedback signal pushes the movable mirror χ_m [m/N] through the coil with an efficiency of A [N/V]. Here, an open-loop transfer function of the triangular cavity loop, $G = HFA\chi_m$, is obtained. From the error signal, the displacement can be estimated as

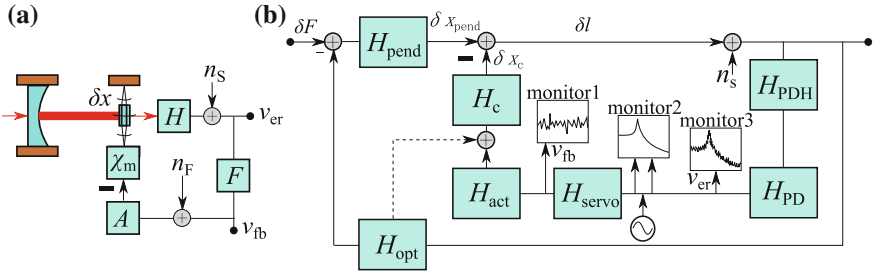

Fig. 5.12 The detailed and simplified block diagram of the triangular cavity servo. **a** The simplified block diagram, which is characterized by follow parameters; δx, displacement of the movable mirror; H, displacement-to-voltage conversion factor; F, servo filter; A, the efficiency of the actuator; χ_m, mechanical susceptibility; v_{er}, error signal; v_{fb}, feedback signal; n_S, sensor noise; n_F, filter noise. In practice, the PDH signal was extracted by the reflected light and the actuator was attached not to the movable mirror, but the controlled mirror (see in Chap. 6). **b** The detailed block diagram, which is characterized by follow parameters; δF [N], force fluctuation imposed on the 5-mg pendulum; δl [m], displacement fluctuation of the cavity length; δx_{pend} [m], displacement of the pendulum; δx_c [m], displacement of the controlled mirror; H_{PDH} [W/m], power-to-displacement conversion factor; H_{PD} [V/W], voltage-to-power conversion factor; H_{servo} [V/V], servo filter; H_{act} [N/V] (it is measured to be $(2.1 \pm 0.1) \times 10^{-5}$ N/V by using a simple Michelson interferometer), the efficiency of the actuator; H_{pend} [m/N], mechanical susceptibility of the pendulum; H_c [m/N], mechanical susceptibility of the controlled mirror; H_{opt} [N/m], the optical spring effect; and n_S [m], the sensing noise. Force fluctuation imposed on the 5-mg pendulum is respectively monitored as force and displacement power spectrum at the monitor1 and the monitor3. The dashed line shows the optical spring effect to the controlled mirror, but it is negligible because the controlled mirror is too massive to be moved by the optical force. Reprinted with permission from Ref. [1]. Copyright 2015 by American Physical Society

$$\delta^{(\mathrm{er})}x = \frac{1+G}{H}v_{\mathrm{er}} \xrightarrow{G \to 0} \frac{1}{H}v_{\mathrm{er}} = \delta x + \frac{n_{\mathrm{S}}}{H} + A\chi_{\mathrm{m}}n_{\mathrm{F}}. \tag{5.15}$$

On the other hand, based on the feedback signal, it is given by

$$\begin{aligned}\delta^{(\mathrm{fb})}x = \frac{1+G}{FH}v_{\mathrm{fb}} &= \delta x + \frac{n_{\mathrm{S}}}{H} + \frac{A\chi_{\mathrm{m}}}{G}n_{\mathrm{F}} \\ &\xrightarrow{G \to \infty} A\chi_{\mathrm{m}}v_{\mathrm{fb}} = \delta x + \frac{n_{\mathrm{s}}}{H}.\end{aligned} \tag{5.16}$$

Based on the viewpoint of the filter noise, the estimation from the feedback signal is appropriate.

From Eqs. (5.15) and (5.16), the error and the feed-back signal respectively give us displacement spectrum of the oscillator and force spectrum ($\delta x/\chi_{\mathrm{m}}$) imposed on the oscillator. Force spectrum differs from displacement spectrum in that it is not be affected by the changeable susceptibility of the pendulum due to the dynamical back-action of the optical field, as it is independent on the mechanical dynamics of the pendulum. Displacement spectrum, on the other hand, gives us the information of the mechanical susceptibility, and thus is tolerant of sensing noise–dummy signal that limits the sensitivity for measurement, which is independent from mechanical motion—at the resonance.

– **The detailed model shown in Fig. 5.12b:**

The detailed expression is given by using the parameters written in the caption of Fig. 5.12b. The monitor1 gives the force fluctuation as

$$\frac{G_2 H_{\mathrm{pend}}}{H_{\mathrm{c}} H_{\mathrm{act}}} \times \frac{\delta F + n_s/H_{\mathrm{c}}}{1 - G_1 - G_2}\ [\mathrm{V}], \tag{5.17}$$

where $G_1 = H_{\mathrm{pend}}H_{\mathrm{opt}}$ and $G_2 = H_{\mathrm{PDH}}H_{\mathrm{PD}}H_{\mathrm{servo}}H_{\mathrm{act}}H_{\mathrm{c}}$, while the monitor3 gives the displacement fluctuation as

$$(\delta x_{\mathrm{pend}} + n_{\mathrm{s}})H_{\mathrm{PDH}}H_{\mathrm{PD}}\ [\mathrm{V}], \tag{5.18}$$

where G_2 is supposed to be negligibly small. Note that, in the limit of the large (electrical) open-loop gain, the feed-back signal given by Eq. (5.17) is proportional to $M/m \times \delta F/H_{\mathrm{act}}$, where m is mass of the pendulum and M is mass of the controlled mirror, while the feed-back signal given by Eq. (5.16) is only proportional to $\delta F/A$. The difference given by a factor of M/m is came from the fact that the (5-mg) pendulum and the controlled mirror is connected via the optical spring, in the detailed model.

5.2.4 Detection System and Vacuum System

In this section, we describe the signal detection system and the vacuum system. The signal detection system is composed of a modulator, a RF photo detector, and a demodulator.

- **Modulator**
  We used the Pound-Drever-Hall technique to control the triangular cavity. The laser beam was phase modulated by an EOM (New Focus Inc., model 4003) on the injection bench. The EOM is made up of a LiNbO3 crystal and a tank circuit tuned at 15 MHz. The EOM was driven by a commercial oscillator at 15.000 MHz. We set the output voltage of the oscillator at 1 V, and the modulation depth was about 0.1 rad.

- **RF photo detector and demodulator**
  The PDH error signal was extracted at PD3 (HAMAMATSU, G10899-01K), which detected the intensity changes at the modulation frequency in the reflected light. The PD3 was followed by an RLC circuit that converted its photocurrent to voltage with high efficiency, and pre-amplifiers. The Q-value of the circuit was measured to be about 30. The detected RF signal was demodulated and down-converted to an AF signal by a Double Balanced Mixer (DBM; Mini Circuit, SBL-1).
  The output voltage noise from the demodulator, V_{n}, represents the sum of the shot noise and of the detector noise in general [7]. The equivalent photo current noise, I_{det}, is defined by

$$V_{\mathrm{n}}^2 = 2eR_{\mathrm{det}}^2(I_{\mathrm{DC}} + I_{\mathrm{det}}). \tag{5.19}$$

  Here, R_{det} is the equivalent resistance for the current-to-voltage conversion, and I_{DC} is the DC photocurrent. To make the noise of the detection system negligible compared to the shot-noise level, I_{det} has to be smaller than I_{DC}. In our case, the shot noise is not a serious problem because the input laser power was increased such that the radiation pressure shot noise dominates. On the other hand, an equivalent resistance is necessary to check the consistency of a calibration. Figure 5.13 shows the measured demodulated output voltage of PD3 as a function of the DC photocurrent. The response was fitted by Eq. 5.19. The noise equivalent photocurrents, I_{det}, were estimated to be 6.8 mA. The equivalent resistance was estimated to be 583 Ω. Typical photocurrents operations occurs at 4 mA, which is slightly less than the noise equivalent photocurrents; however, the photodetector and demodulation system does not limit the sensitivity.

- **Vacuum system**
  Every component of the system, except for the input optics on the injection bench, was housed in a vacuum system in order to reduce the effect of sound, air motion, changes in the refraction index along the optical path, and so on. Figures 5.3 and 5.5 show the vacuum system used in this experiment. Two almost identical vacuum tanks were used for the intensity stabilization and for the observation

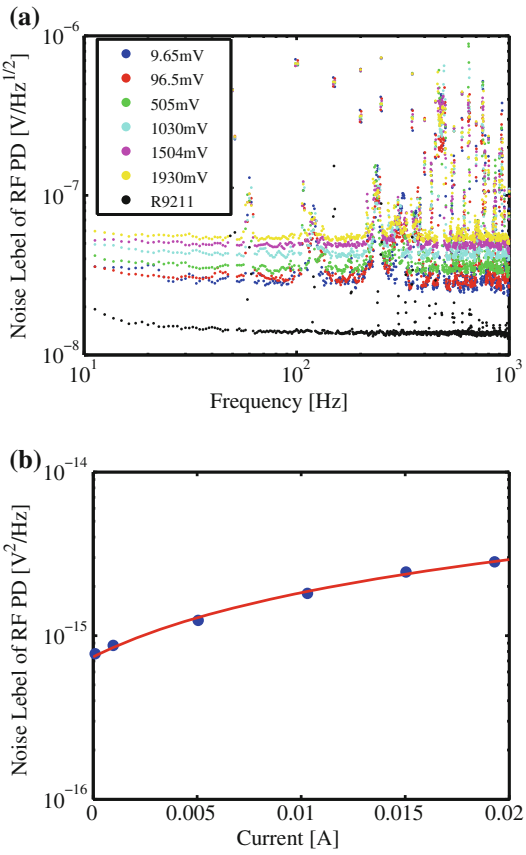

Fig. 5.13 Characterization of the RF PD. **a** Observed spectra for various input laser power. **b** PD3 output noise at the modulation frequency

of quantum back-action. The system is relatively compact—their inner diameter is about 50 cm. Every component was designed to fit inside. The system was evacuated with a rotary pump and a turbomolecular pump connected to the tank in which the intensity stabilization signal was extracted. The typical vacuum level was 10^{-3} Pa.

References

1. Matsumoto, N., Komori, K., Michimura, Y., Hayase, G., Aso, Y., Tsubono, K.: 5-mg suspended mirror driven by measurement-induced backaction. Phys. Rev. A **92**, 033825 (2015)
2. Taubman, M.S., Wiseman, H., McClelland, D.E., Bachor, H.-A.: Intensity feedback effects on quantum-limited noise. J. Opt. Soc. Am. **12**, 10 (1995)
3. Saulson, P.R.: Thermal noise in mechanical experiments. Phys. Rev. D. **42**, 8 (1990)
4. Sidles, J.A., Sigg, D.: Optical torques in suspended Fabry-perot interferometers. Phys. Lett. A. **354**, 167–172 (2006)

5. Sakata, S., Miyakawa, O., Nishizawa, A., Ishizaki, H., Kawamura, S.: Measurement of angular antispring effect in optical cavity by radiation pressure. Phys. Rev. D. **81**, 064023 (2010)
6. Corbitt, T., et al.: An all-optical trap for a gram-scale mirror. Phys. Rev. Lett. **98**, 150802 (2007)
7. Numata, K. Direct measurement of mirror thermal noise. Ph.D. thesis, Department of Physics, Faculty of Science, University of Tokyo, Tokyo, Japan, (2002)
8. https://www.coherent.com/downloads/Mephisto_DS_1013revA_2.pdf, (Accessed March 9, 2015)

Chapter 6
Experimental Results

Abstract In this chapter, we present the development of the 5-mg suspended mirror driven by the quantum back-action larger than the thermal fluctuating force. The origin of quantum back-action is momentum transferred to the mirror by light upon its reflection. Concerning the coherent light, the photon number fluctuates according to a Poisson distribution, which caused the radiation pressure fluctuation, termed radiation pressure shot noise (RPSN). The pendulum mode excited by this force fluctuation was estimated to be larger than the thermal fluctuating force by a factor of 1.4 ± 0.2 at 325 Hz. To explain our estimation based on the noise analysis, we also present the optical, the mechanical, and the optomechanical characterization of our system. The relevant publication is Phys. Rev. A **92**, 033825 (2015) [1].

Keywords Pendulum with the long relaxation · Structure damping · Displacement and force measurement

6.1 Optical Characterization

From Eqs. (2.79) to (2.81), the optical total (amplitude) decay rate κ and the decay rate for the fixed mirror (into which the laser is injected) given by κ_{in1} are necessary for estimating the power spectrum of the quantum and classical back-action. Here, we present estimations of these parameters.

The experimental setup for the optical characterization is shown in Fig. 5.2.We measured the transmittance of the triangular cavity using the two beams: (i) the (p-polarized) beam written as the red (controlling beam) line in Fig. 5.2 was used to control the cavity length; and (ii) the (p-polarized) beam written as the blue line (signal beam) in Fig. 5.2 was used to measure the transmittance of the triangular cavity.

The shifted frequency of the controlling beam was changed within the range from $\Delta_{\mathrm{AOM}} = 77\,\mathrm{MHz} - 83\,\mathrm{MHz}$ by the AOM, while the blue beam was shifted at 80 MHz by the other AOM. Thus the transmittance of the cavity for the broadband frequency could be measured using PD6 and PD7. Figure 6.1 shows the result. Fitting to the Lorentzian, given by $a \cdot b^2/(b^2 + (\Delta_{\mathrm{AOM}} - c)^2)$, the red line shown in Fig. 6.1 is

N. Matsumoto, *Classical Pendulum Feels Quantum Back-Action*,
Springer Theses, DOI 10.1007/978-4-431-55882-8_6

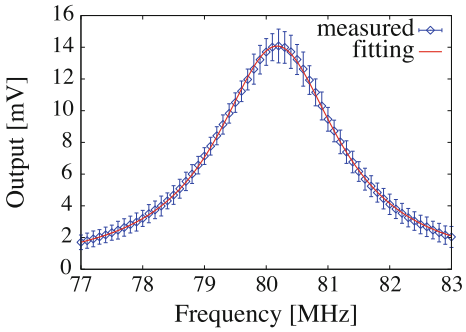

Fig. 6.1 Cavity scan. The optical characterization of our devices was done by sweeping the laser frequency across the optical resonance while detecting the transmitted light in a photo-detector. The blue circles are measured values and the vertical blue lines are the statistical errors; the red line is the fitting line. From this measurement, the total (amplitude) decay rate, $\kappa/2\pi = (1.181 \pm 0.003) \times 10^6$ Hz (i.e. finesse, $\mathscr{F}_\mathrm{p} = (1.47 \pm 0.03) \times 10^3$) was estimated against the p-polarized light. Reprinted with permission from Ref. [1]. Copyright 2015 by American Physical Society

obtained by a least-squares technique, and the following result is obtained.

$$a = (1.407 \pm 0.003) \times 10^{-2}\ \mathrm{V}, \tag{6.1}$$

$$b = (1.181 \pm 0.003) \times 10^{6}\ \mathrm{Hz}, \tag{6.2}$$

$$c = (80.176 \pm 0.002) \times 10^{6}\ \mathrm{Hz}. \tag{6.3}$$

Thus,

$$\frac{\kappa}{2\pi} = (1.181 \pm 0.003) \times 10^{6}\ \mathrm{Hz}, \tag{6.4}$$

can be obtained. Because the power reflectance at the resonance for the controlling beam, given by $(2\kappa_{\mathrm{in}1}/\kappa - 1)^2$, was measured to be 0.22 ± 0.04, the decay rate for the fixed mirror $\kappa_{\mathrm{in}1}$ is given by

$$\frac{\kappa_{\mathrm{in}1}}{2\pi} = (8.7 \pm 0.3) \times 10^{5}\ \mathrm{Hz},\ \text{or}\ (3.1 \pm 0.3) \times 10^{5}\ \mathrm{Hz}. \tag{6.5}$$

To obtain the decay for the controlled mirror, the power *transmittance* for the signal beam, given by $4\kappa_{\mathrm{in}1}\kappa_{\mathrm{in}2}/\kappa^2$, was measured to be 0.11 ± 0.01. Thus, the decay rate for the controlled mirror $\kappa_{\mathrm{in}2}$ is given by

$$\frac{\kappa_{\mathrm{in}2}}{2\pi} = (0.44 \pm 0.05) \times 10^{5}\ \mathrm{Hz},\ \text{or}\ (1.2 \pm 0.3) \times 10^{5}\ \mathrm{Hz}. \tag{6.6}$$

To distinguish, we used information from the measurement of the optomechanical coupling constant, see also in Sect. 6.3.

To obtain the finesse, the free spectral range (FSR) of the cavity $\nu_{\rm FSR}$ was measured by followings: (i) the controlling and the signal beams were injected into the cavity; (ii) the frequency of the controlling (signal) beam was shifted to 82 MHz (80 MHz), whose difference was used to calibration; and (iii) freely swinging pendulum ($\sim$2 Hz) made many of the detected power peaks, whose interval was used to determine the FSR, which is given by

$$\nu_{\rm FSR} = (3.47 \pm 0.07) \times 10^9 \text{ Hz}. \tag{6.7}$$

Note that the period at which the velocity of the pendulum is nearly constant was selected to measure the FSR, such that the FSR is not over estimated. From this, the cavity round-trip length L, and the finesse $\mathscr{F}$ are respectively given by

$$L = 8.7 \pm 0.2 \text{ cm}, \tag{6.8}$$

$$\mathscr{F} = (1.47 \pm 0.03) \times 10^3. \tag{6.9}$$

To conclude, $\kappa/2\pi = (1.181 \pm 0.003) \times 10^6$ Hz (i.e. finesse, $\mathscr{F}_{\rm p} = (1.47 \pm 0.03) \times 10^3$), ($\kappa_{\rm in1}/2\pi = (8.7 \pm 0.3) \times 10^5$ Hz, and $\kappa_{\rm in2}/2\pi = (0.44 \pm 0.05) \times 10^5$ Hz) were obtained. Note that the finesse can be further increased by using the s-polarized light, but we used the p-polarized light because the priority was given to the easiness of cavity control.

6.2 Mechanical Characterization

Here we present the details of the Q-value measurement of the mechanical oscillator. The mechanical Q-value can be written as $Q_{\rm m} = \omega_{\rm m}/2\gamma_{\rm m}$, using $\omega_{\rm m}$ and $\gamma_{\rm m}$ in Eq. (2.58). Also, from the fluctuation-dissipation theorem, the thermal noise can be written as

$$S^{(2)}_{\rm FF,th} = 4k_{\rm B}T_{\rm th}\gamma_{\rm m}m. \tag{6.10}$$

Thus, by measuring the Q-value of the pendulum, the (maximum) thermal noise level can be estimated. Here, T is the temperature of the thermal bath, and $k_{\rm B}$ is the Boltzmann constant. From Eq. (6.10), it follows that the (suspension) thermal noise level is proportional to the pendulum loss, $\gamma_{\rm pend}$, and so the displacement sensitivity can be improved by trapping the pendulum with the gravitational potential and diluting the loss. Our oscillator was also trapped by the optical fields. It is able to increase the effective resonant frequency of the pendulum without changing the thermal noise level, and the oscillator is effectively cooled down to

$$T_{\rm eff} = T\frac{\omega_{\rm pend}Q_{\rm eff}}{\omega_{\rm eff}Q_{\rm pend}}, \tag{6.11}$$

where ω_{pend} and Q_{pend} are respectively the natural resonant frequency and the Q-value of the pendulum and Q_{eff} is the effective quality factor of the pendulum via the optical spring. It is worth pointing out that this effective cooling reduces the thermal noise at the resonant frequency, but it does not change the signal-to-noise ratio (SNR) with respect to the quantum back-action (detailed discussion is seen in Chap. 2). This is because the reduction of the thermal noise at the resonant frequency is caused by the change in the susceptibility, not the reduction in the force fluctuation. The change in the susceptibility also reduces the quantum back-action, and therefore SNR remains the same.

In our experiment, we used a thin wire to suspend a mirror in order to dilute the mechanical loss by the gravitational potential and to increase the pendulum Q-value. Generally, a thin wire has a low material Q-value because the loss of a material comes mainly from the surface loss. Ultra-thin wires have been used for discharging test masses for inertia sensors. There is some literature that reports on measurements of the Q-value for golden thin wires; one example reports the Q-value of a 10 μm diameter golden wire at Q = 270 [2]. However, the Q-value of an ultra-thin tungsten wire, as far as we know, has not yet been reported.

Our experimental setup for the Q-value measurement was almost the same as that shown in Fig. 5.2, except that the fixed mirror was removed. The incident beam was aligned such that the beam would hit the movable mirror at its edge, and the mirror would block the portion of the beam before the beam could be detected by PD4. The amplitude of the resonant motion can be obtained by demodulating the output of PD4 with the resonant frequencies of the pendulum mode (2.2 Hz) and the torsional mode (0.23 Hz) because a small oscillation of the mirror creates amplitude modulation of

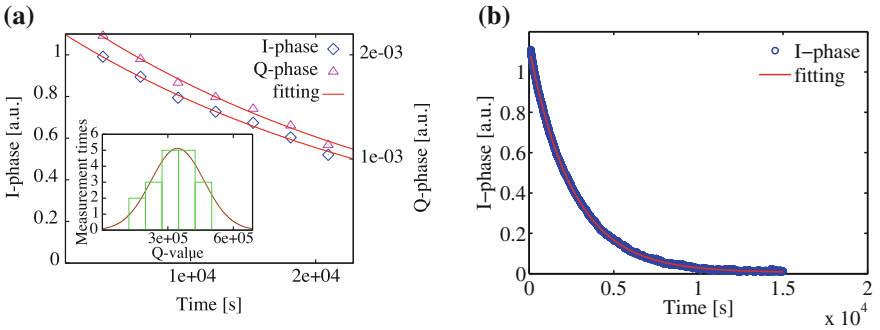

Fig. 6.2 Ringdown measurement. The measured damped oscillations for the pendulum and the yawing motion are shown, respectively. **a** The ringdown of the pendulum. Amplitude (I-phase) and phase quadrature (Q-phase) of the oscillation during a free decay were obtained by the optical shadow sensor. The inset shows the distribution of the measured mechanical quality factor, and was fitted by the Gaussian distribution. The mechanical Q-value of the pendulum, $Q_{\text{pend}} = (3.2 \pm 1.0) \times 10^5$, was measured. Reprinted with permission from Ref. [1]. Copyright 2015 by American Physical Society. **b** The ringdown of the yaw mode. Only amplitude quadrature of the oscillation during a free decay was obtained (*blue*) by the optical shadow sensor. The mechanical Q-value of the yaw, $Q_{\text{yaw}} = 1.9 \times 10^3$, was measured

the beam. The Q-values were measured by exciting the mirror motion and measuring the decay time of each mode.

Our pendulum had a very high Q-value, since the loss was diluted by the gravitational potential by a factor of 600. Therefore, the pendulum mode had a very long decay time, and measuring the Q-value without excitations was difficult. In order to prevent an overestimation of the Q-value (i.e. thermal noise), we also measured the Q-value of the yaw mode, which had a shorter decay time, to have estimated the maximum Q-value of the pendulum. In addition to the shorter decay time due to the no-dilution effect, the yaw mode has tolerance to the mechanical loss of the clamping mechanism, such as the epoxy due to its mode function, which represents the mechanical displacement patterns associated with mechanical motion. We can estimate the Q-value of the yaw mode as being the intrinsic (natural) mechanical Q-value of the wire. Thus, the measured pendulum Q-value should be smaller than the maximum Q-value of the pendulum estimated from $Q_{\mathrm{pend,max}} = Q_{\mathrm{yaw}} \times 600$.

The result of the ring-down measurement is shown in Fig. 6.2. The measured Q-value for the pendulum mode was $Q_{\mathrm{pend}} = (3.2 \pm 1.0) \times 10^5$ (the resonant frequency was $\omega/2\pi = 2.2$ Hz). The measured Q-value for the torsion mode was $Q_{\mathrm{yaw}} = 1.9 \times 10^3$ (the resonant frequency was $\omega_{\mathrm{yaw}}/2\pi = 0.23$Hz). This means that the upper limit of the Q-value for the pendulum mode would be $Q_{\mathrm{pend,max}} = 1.1 \times 10^6$, which is higher than the Q-value from the direct measurement mentioned above, by a factor of about 4. Thus, mechanical loss such as the clamping loss possibly reduces the Q-factor of the pendulum by a factor of 4.

We note that no one knows whether the dissipation is depend (structure damping) or independent (viscous damping) on the frequency a priori. If viscous damping model is valid, the ratio of the quantum back-action to the thermal fluctuating force becomes

$$\frac{S^{(2)}_{\mathrm{FF,q}}}{S^{(2)}_{\mathrm{FF,th}}} = \frac{N_{\mathrm{circ}} g^2}{n_{\mathrm{th}} \kappa} \times \frac{2 Q_{\mathrm{pend}}}{\omega_{\mathrm{pend}}}. \tag{6.12}$$

If structure damping model is valid, the ratio becomes

$$\frac{S^{(2)}_{\mathrm{FF,q}}}{S^{(2)}_{\mathrm{FF,th}}} = \frac{N_{\mathrm{circ}} g^2}{n_{\mathrm{th}} \kappa} \times \frac{2 Q_{\mathrm{pend}} \omega}{\omega^2_{\mathrm{pend}}}, \tag{6.13}$$

where nth is phonon number, $\omega_{\mathrm{m}}/2Q_{\mathrm{pend}}$ is the mechanical dissipation for the viscous case, and $\omega^2_{\mathrm{m}}/2Q_{\mathrm{pend}}\omega$ is for the structure case. Because our pendulum can be trapped by the optical spring, the ratio at the pendulum resonant frequency can be further increased with increased optical restoring force by a factor of $\omega_{\mathrm{eff}}/\omega_{\mathrm{pend}}$, if the dissipation of the pendulum is limited by the internal friction, i.e. the structure damping. To distinguish, we performed noise analysis in Chap. 6, Sect. 4, and the structure damping model is valid to our measurement.

6.3 Optomechanical Characterization

Here, we present the measurement of the optomechanical coupling constant from the optical spring effect. We measured the effective resonant frequency of the 5-mg suspended mirror by measuring the open-loop gain given by $G_2/(1-G_1)$ as shown in Fig. 5.12 (open-loop gain is proportional to $1/(\omega_{\rm eff}^2 - \omega^2)$), in order to estimate the optomechanical coupling constant, g, of the cavity using Eq. (2.76). Together with the measured value in Chap. 6, Sect. 1, we can determine the value of the optical decay rate for the fixed mirror $\kappa_{\rm in1}$ and the value of the optical decay rate for the controlled mirror $\kappa_{\rm in2}$.

The optical restoring force was measured using the same setup as shown in Fig. 5.2, at a higher pressure (1×10^3 Pa) than that for the main quantum back-action measurement. The beam shown as the red line in Fig. 5.2 at 0.54 mW was injected to the cavity, and the cavity length was controlled using the same light (PD3). Under these conditions, the decay rate from the gas damping is $\gamma_{\rm gas}/2\pi \simeq +1$ Hz, and the minimum decay rate from the optical spring was $\Gamma_{\rm opt,min}/2m \simeq -0.1$ Hz. Thus, the cavity stays sufficiently stable. After closing the cavity length control loop, a small electrical signal was injected into the loop in order to measure the resonant frequency of the movable mirror. Figure 6.3 shows the measured open-loop transfer function.

To measure the dependence of the effective resonant frequency on the cavity (normalized) detuning $\delta \equiv \Delta/\kappa$, the normalized detuning was monitored by

$$\delta = \sqrt{\frac{(r_{\rm d} - r_{\rm TEM})r_0^2}{r_{\rm TEM} - r_{\rm d} r_0^2}}, \tag{6.14}$$

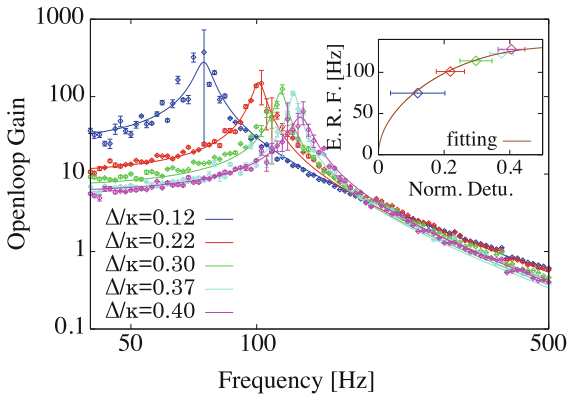

Fig. 6.3 Optical spring response for various detunings of the cavity. The effective mechanical frequency is measured by monitoring the open-loop function given by $G_2/(1-G_1)$ at the monitor2 as shown in Fig. 5.12. The inset shows the dependence of the effective resonant frequency (E. R. F.) on the cavity detuning normalized by the cavity linewidth. From this measurement, the optomechanical coupling constant, $g/2\pi = (2.8 \pm 0.2)\omega_c$ /m, was estimated. Reprinted with permission from Ref. [1]. Copyright 2015 by American Physical Society

$$r_0 \equiv \frac{2\kappa_{\mathrm{in1}}}{\kappa} - 1, \tag{6.15}$$

where r_{d} having the unit of V is the measured reflected power at PD3, r_{TEM} having the unit of V is the reflected power on the zero-detuning (i.e., on the resonance) at PD3, and r_0 is defined as the amplitude reflectance on the zero-detuning. By using the measured normalized detuning δ and the effective resonant frequency f_{eff}, fitting to the function, given by $f_{\mathrm{eff}}^2 - f_{\mathrm{m}}^2 = D \cdot \delta/(1+\delta^2)^2$ was performed by a least-squares technique, and the following result is obtained.

$$D \equiv \frac{P}{(2\pi)^3 m} \frac{2\omega_{\mathrm{c}}/(2\pi)}{(\kappa/(2\pi))^2} \left(\frac{g}{\omega_{\mathrm{c}}}\right)^2 (r_0+1) = (7.82 \pm 0.09) \times 10^4\ \mathrm{Hz}^2. \tag{6.16}$$

The inset of Fig. 6.3 as the red line is obtained using $D = 7.82 \times 10^4$. From Eq. (6.16), the incident angle of the laser β is given by

$$\cos^2\beta = \frac{0.834}{r_0+1}. \tag{6.17}$$

Because r_0 is calculated to be 0.47 or -0.469, from the value obtained in Chap. 6, Sect. 1, the decay rate for the fixed mirror κ_{in1} and the decay rate for the controlled mirror κ_{in2} are respectively determined by

$$\frac{\kappa_{\mathrm{in1}}}{2\pi} = (8.7 \pm 0.3) \times 10^5\ \mathrm{Hz}, \tag{6.18}$$

$$\frac{\kappa_{\mathrm{in2}}}{2\pi} = (0.44 \pm 0.05) \times 10^5\ \mathrm{Hz}, \tag{6.19}$$

and the $\cos\beta$ should be 0.75 ± 0.04. Thus, the optomechanical coupling constant g is given by

$$\frac{g}{2\pi} \equiv 2\cos\beta \frac{\omega_{\mathrm{c}}}{L} = (2.8 \pm 0.2)\omega_{\mathrm{c}}\ /\mathrm{m}. \tag{6.20}$$

6.4 Measurement of the Back-Action and Discussions

We measured two types of the back-action signal as shown in Fig. 5.12: the displacement fluctuations from the PDH signal with no feedback gain, i.e. the controlled 1×10^2-g mirror was *not* electrically trapped such that the displacement signal can be directly measured; and the force fluctuations from the PDH signal with some gain, i.e. the controlled mirror was electrically trapped with respect to the cavity length such that the controlled mirror works as a transducer of the force fluctuation acting on the 5-mg mirror.

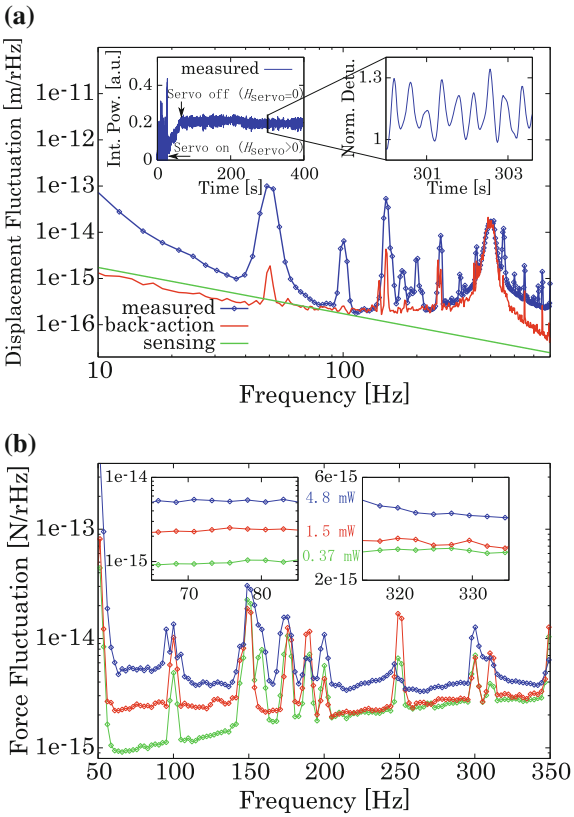

Fig. 6.4 A series of measurements of the back-action. **a** Observed spectra of displacement fluctuation at optical power, $P_{\mathrm{in}} = 7.6\,\mathrm{mW}$; the mean value of cavity detuning, $\Delta = 1.1 \times \kappa$; and open loop gain, $G_2 = 0$. Measured displacement spectral density (*blue*), estimated back-action contribution (*red*), and estimated sensing noise with f^{-1} (f^1 in the force fluctuation) spectral slope (*green*) are shown. Spectral peaks are identified as follows: at around 200 Hz, suspension wire violin mode; at around 400 Hz, pendulum motion trapped by the optical spring. The *left* inset shows the measured data in time-domain, and its vertical axis shows intracavity power (Int. Pow.). The *right* inset shows the enlarged view of the *left* inset, and its vertical axis shows cavity detuning normalized (Norm. Detu.) by the cavity linewidth. **b** Observed spectra of force fluctuation (*blue* input laser power of 4.8 mW; *red* 1.5 mW; *green* 0.37 mW). Reprinted with permission from Ref. [1]. Copyright 2015 by American Physical Society

As shown in the inset of Fig. 6.4a, the suspended mirror swung freely in about the first 30 s, and then cavity length fluctuations were controlled by increasing the gain of the servo filter. After the control was activated, the gain was gradually reduced until the electrical trap was lost. At about 70 s of the left inset, the gain became zero, and the cavity length was only optically controlled through the optical spring effect (note, it is not the double optical spring effect, and the stability might be generated by coupling to the optical torsional spring effect) such that the signal of displacement

fluctuations can be obtained. In Fig. 6.4a as blue dots, the measured (single-sided) amplitude spectral density (the square root of the power spectrum) of the optically trapped pendulum motion, with the input power of 7.6 mW and the cavity detuning of $1.1 \times \kappa$, is shown. The calibrated noise floor level agrees with the estimated classical back-action induced motion (red) at around 400 Hz, where the pendulum motion is included. The estimation was performed as follows: (i) fluctuated effective resonant frequency by the optical spring was calculated using measured detuning as shown in the insets of Fig. 6.4a; (ii) fluctuated effective mechanical loss was supposed to be 0.01 Hz; (iii) force fluctuation induced by the classical back-action given by Eq. (2.81) was estimated using measured classical intensity fluctuations shown in Fig. 5.6; and (iv) estimated displacement fluctuations shown in Fig. 6.4a (red) is given by $\sqrt{|\chi_{\rm eff}|^2 S^{(2)}_{\rm FF,cl}}$, where $\chi_{\rm eff}$ is decided by the estimated effective resonant frequency and the supposed effective mechanical loss.

The dependence of the measured force fluctuation shown in Fig. 6.4b at 75 and 325 Hz on the input laser power are respectively shown in Fig. 6.5a as blue and cyan dots. The results are also well fitted to the estimated dependence on the power over 2 mW (pink) and 5 mW (magenta) respectively, while the noise level below 0.8 mW at 75 Hz is clearly lower than the estimated thermal noise with the viscous model (gray). To guarantee the stationarity of our measurement, the chi square test was used to test whether a set of data fits a Rayleigh distribution. As shown in Fig. 6.5b, e.g., each curve is well close to Rayleigh distributions written by blue lines, since they exhibited stationary. To distinguish the measured noise below 0.8 mW from the thermal noise with the viscous model, Fig. 6.5c shows the dependence of the spectral slope on the input laser power. The result is well fitted to the structure model with f^{-1} spectral slope plus unknown noise with f^1 slope written as red area. Because the rms force noise must not diverge, stationary force noise has spectral slope smaller than 0; therefore roughly 93 % of the measured spectrum with no input-laser at 75 Hz is not force but sensing noise, with about f^1 spectral slope (e.g., frequency noise has such a dependence [3]). Thus the structure damping model is valid in our measurements. We can thus estimate the ratio of the quantum back-action to the thermal fluctuating force, and then the ratio is estimated to be larger than 1 over 325 Hz with input laser power of about 5 mW as shown in Fig. 6.5a.

To rule out calibration errors, correlation measurements proposed by Verlot et al. [4] is suitable; however, let us here focus on the following two sources. As for the back-action induced by the phase fluctuation (labeled by $\delta\phi$) of the laser [5], which is written by $S^{(2)}_{\rm FF,phase} = (S^{(2)}_{\rm FF,cl} + S^{(2)}_{\rm FF,q}) \times 2\Delta\omega_{\rm eff}\delta\phi/(\kappa^2 + \Delta^2)$, it is negligible because the cavity condition is the "bad" condition. In our measurements, roughly only 0.3 % of the force fluctuation is due to the phase noise. As for the photo-thermal shot noise given by $2\alpha^2(1+\sigma)^2\hbar\omega_{\rm c}T_{\rm abs}P_{\rm circ}m\omega^2/(\rho_{\rm m}C\pi r_0^2)^2$ [6, 7], it is maximumly only 0.2 % of the quantum back-action. Here, $\alpha(= 6\times10^{-7}/{\rm K})$ is thermal expansion coefficient, $\sigma(= 0.17)$ is the Poisson coefficient, $T_{\rm abs}$ is the absorption coefficient of the 5-mg mirror, $P_{\rm circ}(= 6.8\ {\rm W})$ is intra-cavity power, $\rho_{\rm m}(= 2.2 \times 10^3\ {\rm kg/m^3})$ is density, $C(= 750\ {\rm J/kg/K})$ is specific heat capacity, spot size (r_0) is designed as about 100 μm. The absorption coefficient is determined by using the decay rate

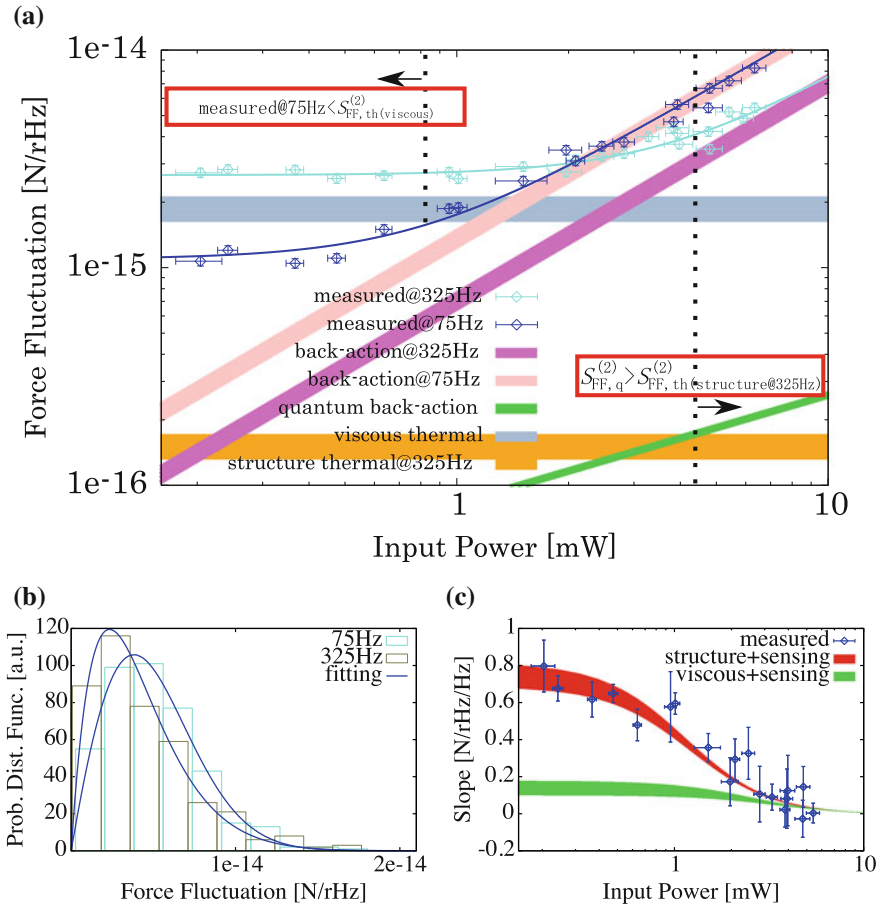

Fig. 6.5 A series of data analysis for estimating the ratio of the quantum back-action to the thermal fluctuating force. **a** Dependence of the measured force amplitude spectral density on the input laser power. Measured force fluctuation at 325 Hz (*blue*), measured force fluctuation at 75 Hz (*cyan*), theoretical thermal force due to the residual gas damping (*yellow*), theoretical thermal force spectrum with the viscous damping model (*gray*), theoretical thermal force spectrum with the structure damping model at 325 Hz (*orange*), and estimated back-action with the measured $B = 94 (A = 3.5 \times 10^{-7}/\sqrt{\text{Hz}})$ at 75 Hz and $B = 48 (A = 1.8 \times 10^{-7}/\sqrt{\text{Hz}})$ at 325 Hz (*pink* and *magenta*) are shown. Each area includes the 68 % confidence level. The error is due to the systematic error such as the uncertainty of the quantum efficiency and calibration factor, and the statistic error in measurement. **b** Distribution of force amplitude spectral density with input power of 4.8 mW for two representative frequencies within the measurement band. Each curve is a histogram of the spectrum at the specified frequency. Each of them is taken from the Fourier transform of 0.4 s of data; the equivalent noise bandwidth for each curve is 2.4 Hz. **c** Dependence of the spectrum slopes at 75 Hz on the input laser power. Measured slopes of the force amplitude spectral density (*blue*), theoretical estimation based on the structure damping model (*red*), and the theoretical estimation based on the viscous damping model (*green*) are shown

Table 6.1 Parameters

Parameter	Symbol	Unit	Measured value	Estimated value
Mass of the suspended mirror	m	kg	5.0×10^{-6}	–
Mass of the controlled mirror	M	kg	9.7×10^{-2}	–
Optomechanical coupling	$g/2\pi$	Hz/m	$(2.8 \pm 0.2)\omega_c$	(design) $2.84\omega_c$
Total optical (amplitude) decay rate	$\kappa/2\pi$	Hz	$(1.181 \pm 0.003) \times 10^6$	–
Optical decay rate (in1)	$\kappa_{in1}/2\pi$	Hz	$(8.7 \pm 0.3) \times 10^6$	–
Optical decay rate (in2)	$\kappa_{in2}/2\pi$	Hz	$(0.44 \pm 0.05) \times 10^5$	–
Finesse	$\mathscr{F}_p$	–	$(1.47 \pm 0.03) \times 10^3$	–
Round-trip length	L	m	$(8.7 \pm 0.2) \times 10^{-2}$	(design) 9×10^{-2}
Ffree spectral range	ν_{FSR}	Hz	$(3.4 \pm 0.2) \times 10^9$	–
Quality factor	Q_{pend}	–	$(3.2 \pm 1.0) \times 10^5$	$<1.1 \times 10^6$
Actuator efficiency	A	N/V	$(2.1 \pm 0.1) \times 10^{-5}$	–
Slope of the PDH signal	H_{PDH}	V/m	$(1.18 \pm 0.08) \times 10^{10}$	–
Signal to noise ratio	–	–	–	1.4 ± 0.2

for the absorption coefficient, κ_{abs}, which is supposed as $\kappa - \kappa_{in} - \kappa_{out}$, in order to estimate upper limit of the photo-thermal noise.

For reaching the SQL, the frequency where the quantum back-action and the shot noise are equal should be optimized by changing input laser power. In our measurements, it becomes about 1 kHz, which is already close to the analyzed frequency of 325 Hz. To reduce the classical laser noise and reach the quantum regime, the use of interferometer consisting of two optical cavities is necessary to introduce common mode rejection of the laser noise, and its requirement is about factors of 100. To reduce the residual gas damping sufficiently, the interferometer has to be set inside the vacuum chamber of 10^{-5} Pa, corresponding mechanical decay rate, γ_{gas}, is about 3×10^{-8} Hz (corresponding quality factor is about 10^8). Both improvements are experimentally feasible within the current technology.

Parameters are summarized in the Table 6.1.

References

1. Matsumoto, N., Komori, K., Michimura, Y., Hayase, G., Aso, Y., Tsubono, K.: 5-mg suspended mirror driven by measurement-induced backaction. Phys. Rev. A **92**, 033825 (2015)
2. Liu, L., et al.: Measurement of the effect of a thin discharging wire for an electrostatic inertial sensor with a high-quality-factor pendulum. Class. Quantum Gravity **29**, 055010 (8pp) (2012)
3. https://www.coherent.com/downloads/MephistoDS1013revA2.pdf. Accessed March 9, 2015

4. Verlot, P., Tavernarakis, A., Briant, T., Cohadon, P.-F., Heidmann, A.: Scheme to probe optomechanical correlations between two optical beams down to the quantum level. Phys. Rev. Lett. **102**, 103601 (2009)
5. Rabl, P., Genes, C., Hammerer, K., Aspelmeyer, M.: Phase-noise induced limitations on cooling and coherent evolution in optomechanical systems. Phys. Rev. A. **80**, 063819 (2009)
6. Braginsky, V.B., Gorodetsky, M.L., Vyatchanin, S.P.: Thermodynamical fluctuations and photothermal shot noise in gravitational wave antennae. Phys. Lett. A **264**, 1–10 (1999)
7. Restrepo, J., Gabelli, J., Ciuti, C., Favero, I.: Classical and quantum theory of photothermal cavity cooling of a mechanical oscillator. C.R. Physique **12**, 860–870 (2011)

Chapter 7
The Future

Abstract In this chapter, two possible future investigations are proposed: (i) to cool the massive 5-mg pendulum down to its ground-state; and (ii) to reach the standard quantum limit (SQL) for continuous force (displacement) measurement using the 5-mg pendulum. For these purposes, more higher Q-value pendulum than that developed in this thesis (suspended by the tungsten wire of 3 μm in diameter) is necessary. Also, the passive cavity-assisted cooling is necessary for increasing the resonant frequency but not sufficient to cool the pendulum down to its ground-state. In addition to the passive cooling, the feed-back cooling has to be used. Here, we present brief explain for our future plans, and the details will be submitted soon.

Keywords Ground-state cooling · SQL · High-Q pendulum using a CNT fiber for suspension

7.1 Future Improvement

First, as compared with the experiment described above, it is necessary to improve several parameters: (i) the mechanical quality factor of the pendulum; (ii) the mechanical quality factor of the substrate; and (iii) the finesse.

(i) The Q-value of the pendulum can be improved by: increasing the dilution factor by using a thinner wire from 3 to 1.5 μm; changing the lossy alminium clamp to a relative lossless steel clamp; and the degree of vacuum can be improved from 10^{-3} Pa to 10^{-4} Pa by changing the devices in the vacuum tank to devices with only little gas release. It is presumed that the Q-value of the pendulum can be increased from 3.2×10^5 to 5×10^6 at least by these improvements because the Q-value without only clamping loss was estimated to be 1.1×10^6 in Chap. 6, and further dilution enlarges the value by about 5 times. (Also, the use of the carbon nanotube (CNT) fiber further increases the Q-value of the pendulum, possibly. Because physical property of the CNT is suitable for increase the gravitational dilution: (i) the density and the young modulus of the CNT fiber are smaller then the tungsten, and thus the length of the wire can be increased without being contaminated by the violin mode; (ii) the withstand load of the CNT fiber is comparable with the tungsten such that the radius

N. Matsumoto, *Classical Pendulum Feels Quantum Back-Action*,
Springer Theses, DOI 10.1007/978-4-431-55882-8_7

of the wire can be decreased without decreasing the mass of the pendulum; and (iii) the natural quality factor is also comparable with the tungsten wire with the radius of about a few micro meter [1]).

(ii) We estimated the mechanical quality factor of the substrate to be 10^5 by taking the thinness of the mirror into consideration. Although it may be a slight overestimation, we estimate the Q-value of the substrate to be 10^6 here. If this is an overestimate, it may be necessary to change the lossy thin form of the mirror.

(iii) In this thesis, we used p-polarized light because it enabled us to easily control the optical cavity. Here, we assume that by using s-polarized light and an input coupler for the input beam better reflectivity is possible. By making these changes, the finesse would rise to 10000.

Under these assumptions, we propose the followings.

7.2 Towards Ground-State Cooling

To test of the quantum mechanics, the simplest way is to demonstrate the quantum coherence of the macroscopic objects, which is cooled down to its ground state. Ground-state cooling has been realized [2–4]; however, it has not been realized on the macroscopic mass scale.

From Eqs. (1.1) and (6.10), the relationship between the thermal fluctuation force and the SQL is given by

$$\frac{S^{(2)}_{\mathrm{FF,th}}}{S^{(2)}_{\mathrm{FF,SQL}}} = \frac{4k_{\mathrm{B}}T\gamma_{\mathrm{m}}m}{\hbar|\chi_{\mathrm{m}}(\omega)|^{-1} + 2\hbar\omega_{\mathrm{m}}\gamma_{\mathrm{m}}m} \xrightarrow{\omega \to \omega_{\mathrm{m}}} \frac{k_{\mathrm{B}}T}{\hbar\omega_{\mathrm{m}}}. \tag{7.1}$$

Therefore, the occupation number becomes (about) unity when the thermal noise and the SQL are equal. (Correctly, the occupation number, $1/(\exp(\hbar\omega_{\mathrm{m}}/k_{\mathrm{B}}T) - 1)$, becomes about 0.58, in this case.)

In our case, due to the bad cavity condition, reducing the quantum back-action is challenging via the passive (cavity-assisted) cooling; however, the thermal excitation can be sufficiently removed. The phonon occupation number, $\langle n \rangle = 0.22$, is reachable, as shown in Fig. 7.1. To reduce the effect of back-action, one can use the QND method like the variational readout. The feed-back cooling, on the other hand, is able to cool the optomechanical oscillator with the bad cavity condition down to its ground state. In our case, the actuator for feed-back cooling can not be attached with the suspended small mirror. But it is possible to use the feed-back cooling by feeding back to the other mirror consisting the cavity, when the both of mirrors is optically combined by the optical spring [5].

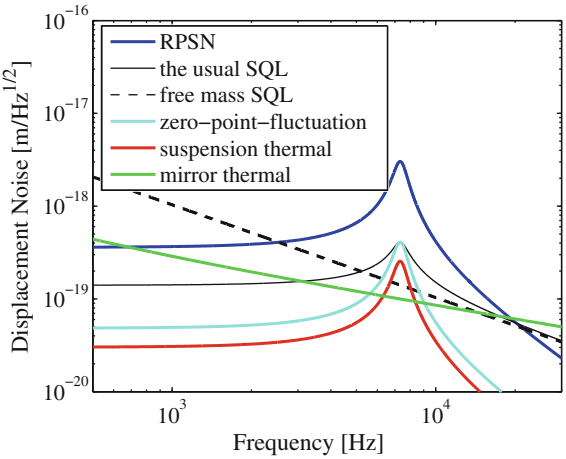

Fig. 7.1 **Plan1**. The quantum back-action (*blue*), the suspension thermal noise (*red*), the mirror thermal noise (*green*), the zero-point fluctuation (*cyan*), the SQL for the free mass (*dotted black*) and the usual (for the people belonged to GW detectors) SQL for the modified mirror (*black line*) are shown. The parameters are listed in Table 7.1

Table 7.1 Parameter list of Fig. 7.1

Parameter	Value	Unit
Finesse	1.0×10^4	–
Cavity decay rate	0.9	MHz
Q-value of the pendulum	5.0×10^6	–
Q-value of the substrate	1.0×10^6	–
Effective resonant frequency	7.4	kHz
Effective Q-value	8.4	–
Input power (driving)	250	mW
Input power (spring)	1500	mW
Normalized detuning (driving)	-1.0	–
Normalized detuning (spring)	2.5	–

7.3 Towards Beating the SQL

In order to develop the gravitational-wave astronomy and testing quantum mechanics, respectively, it is necessary to overcome the SQL. To meet the criteria, we firstly have to realize the condition of $\Omega_x/\Omega_F > 2$. Under this condition, there is a nonzero frequency band (in between Ω_F and Ω_x) in which the classical noise is completely below the SQL.

Figure 7.2 shows the possible sensitivity ($\Omega_F \sim 2700$, $\Omega x \sim 15000$). The criteria can easily be realized, and thereby this is a suitable platform to experimentally study the QND technique.

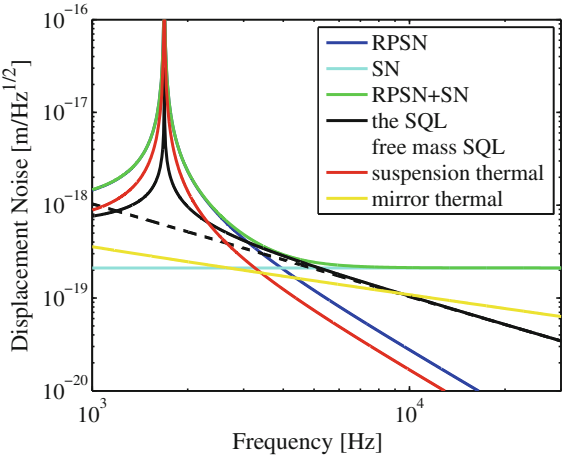

Fig. 7.2 Plan2. The quantum back-action (*blue*), the shot noise (*cyan*), the suspension thermal noise (*red*), the mirror thermal noise (*yellow*), the SQL for the free mass (*dotted black*) and the SQL for the modified mirror (*black line*) are shown. Ω_F, Ω_q, and Ω_x are the frequencies at which the classical force noise (i.e., suspension thermal noise), quantum back-action, and classical sensing noise (i.e., the mirror thermal noise) intersect the free-mass SQL, respectively. The parameters are listed in Table 7.2

Table 7.2 Parameter list of Fig. 7.2

Parameter	Value	Unit
Finesse	4400	–
Cavity decay rate	2.1	MHz
Q-value of the pendulum	5.0×10^6	–
Q-value of the substrate	1.0×10^6	–
Effective resonant frequency	1.7	kHz
Effective Q-value	1700	–
Input power (driving)	10	mW
Input power (spring)	100	mW
Normalized detuning (driving)	−0.06	–
Normalized detuning (spring)	3	–

References

1. Matsumoto, N., Komori, K.: (to be submitted)
2. O'Connell, A.D., et al.: Quantum ground state and single-phonon control of a mechanical resonator. Nature **464**, 697–703 (2010)
3. Teufel, J.D., et al.: Sideband cooling of micromechanical motion to the quantum ground state. Nature **475**, 359–363 (2011)
4. Chan, J., et al.: Laser cooling of a nanomechanical oscillator into its quantum ground state. Nature **478**, 89–92 (2011)
5. Matsumoto, N., Kuwahara, Y., Ushiba, T., Karita, M., Inoue, Y.: (to be submitted)

Chapter 8
Conclusions

This thesis presented the observation of measurement-induced back-action imposed on the massive 5-mg suspended mirror (pendulum) in classical regime, whose quantum component was estimated to be also larger than thermal fluctuating force at room temperature. The quantum back-action is one of the most significant issues to be investigated regarding the interferometric gravitational-wave (GW) detectors because it will directly limit the sensitivity in next-generation detectors. Although the quantum back-action is just a noise for weak-force measurements such as GW detectors, it is one of the key milestones towards testing the quantum mechanics in macroscopic domain to explore the boundaries between classical and quantum world, which might solve the measurement problem at the fundamental level (Chap. 3). Until now, no one had observed the quantum back-action using the massive mechanical oscillator because it is generally masked by thermal fluctuating force (Chap. 1). To increase the optomechanical coupling and to reduce the thermal fluctuating force, an optical cavity with high circulating optical power must consist of a freely suspended mirror. However, the fundamental instability, called the Siddles-Sigg instability (i.e., optical anti-torsional spring effect), prevents their coexistence.

We developed an optical triangular cavity to overcome this limitation. When the triangular cavity is used, the anti-torsional spring in pitch motion still occurs without any dependence on the isolation of the pendulum from the thermal bath. On the other hand, the anti-torsional spring in yaw motion changes the stable positive torsional spring (Chap. 4). The geometrical advantages of the triangular cavity enables for the mirror to be isolated from the thermal bath with higher intracavity power than the stability limit for the liner optical cavity (Chaps. 2 and 6). We succeed in storing about 50-times higher optical power in our cavity than the instability limit for the linear cavity, while the dilution factor becomes about 600 (measured improvement was a factor of 150), and the ratio of the quantum back-action to the thermal fluctuating force was estimated to be 1.4 ± 0.2 at 325 Hz (Chaps. 5 and 6). Our result opens a new route to investigate ultra-sensitive force measurements and macroscopic quantum mechanics (Chaps. 3 and 7). Both of them certainly go toward beating the

N. Matsumoto, *Classical Pendulum Feels Quantum Back-Action*,
Springer Theses, DOI 10.1007/978-4-431-55882-8_8

standard quantum limit (SQL), and the only difference is the viewpoint from them. The former regards it as significant noise, and the latter regards it as a benchmark. Although reaching the SQL at the resonant point (so-called ground state cooling) is still challenging via the passive cooling due to the bad cavity condition, it can be reached at off-resonance by using our method in the future (Chap. 7). This condition is necessary to experimentally study the QND scheme for GW detectors, and to generate macroscopic Gaussian entanglement states between two macroscopic masses. It is, therefore, a critical step toward gravitation wave astronomy and of macroscopic quantum measurements.

Appendix A
Intensity Stabilization

All's well that ends well

Here, we describe intensity stabilization using active feed-back control. When the intensity is stabilized by the feed-back technique, reachable stability is limited over the shot-noise level (i.e., minimum uncertainty level), because the intensity monitor is always contaminated with the vacuum fluctuation injected from the pick-off mirror (and any kind of optical loss, e.g. loss of the quantum efficiency). To mitigate the contamination named noise penalty, we measured relatively higher optical power in the in-loop (i.e., signal fed back to the actuator) than that in the out-of-loop (i.e., signal for monitoring the actual stability of the laser). Although the achieved stability via the feed-back control alone did not meet the demand for reaching the shot noise level, it could be satisfied by the passive stabilization using the interferometer, in addition to the feed-back control.

To start with, let us consider the simplest case, as shown in Fig. A.1a. Since we only pay attention to the amplitude fluctuation of the electromagnetic field, only the amplitude quadrature is considered. The input laser and the vacuum fluctuation entering the unused port of the beam-splitter (BS) can be given by $\delta\hat{a}$, $\delta\hat{b}_1$, respectively. A fluctuation component of a transmitted light from the BS labeled as $\delta\hat{E}_\mathrm{t}$ is given by

$$\delta\hat{E}_\mathrm{t} = t_1\delta\hat{a} + r_1\delta\hat{b}_1, \tag{A.1}$$

where r_1 represents the amplitude reflectivity of the BS and t_1 represents the amplitude transmittivity of the BS. On the other hand, the reflected light $\delta\hat{E}_\mathrm{r}$ is given by

$$\delta\hat{E}_\mathrm{r} = -r_1\delta\hat{a} + t_1\delta\hat{b}_1. \tag{A.2}$$

If the transmitted light is used for stabilization, the negative-feed-back system ideally reduces $\delta\hat{E}_\mathrm{t}$ to zero, and then

$$\delta\hat{a} = -\frac{r_1}{t_1}\delta\hat{b}_1 \tag{A.3}$$

N. Matsumoto, *Classical Pendulum Feels Quantum Back-Action*,
Springer Theses, DOI 10.1007/978-4-431-55882-8

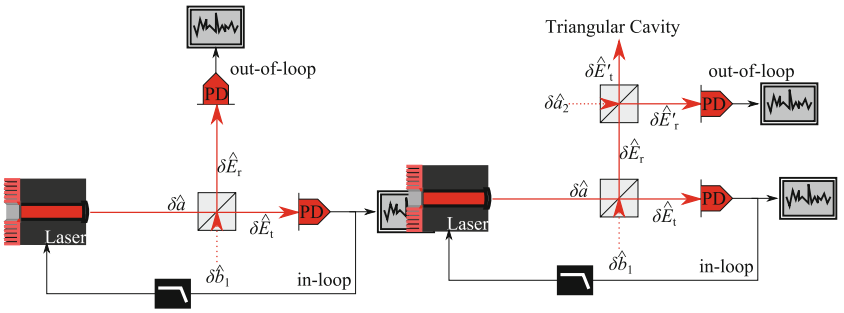

Fig. A.1 Intensity stabilization system. **a** Simplest case. **b** Our case

is obtained. The anti-correlation between $\delta\hat{a}$ and $\delta\hat{b}$ increases the noise level in the out-of-loop (i.e., the reflected field). It is given by

$$\delta\hat{E}_r = \frac{1}{t_1}\delta\hat{b}_1. \tag{A.4}$$

Therefore, the maximum stability in the out-of-loop is $1/t_1$-times larger than the vacuum fluctuation. This effect is called the "noise penalty". In our case, we used two half-BSs shown in Fig. A.1b. Then, the maximum stability can be calculated as

$$\delta\hat{E}'_r = \sqrt{\left(\frac{r_2}{t_1}\right)^2 + t_2^2}\,\delta\hat{b}_1 \xrightarrow{t_1, t_2 \to 1/\sqrt{2}} \sqrt{\frac{3}{2}}\delta\hat{b}_1. \tag{A.5}$$

Therefore, the achievable relative shot-noise level is reduced to about 1.8 dB.

A.1 Intensity Stabilized Laser

One of the main noise sources for the quantum back-action measurement is the classical back-action force generated by the classical intensity noise of the laser. By making a high finesse cavity (i.e., high optical power gain inside the cavity), we can decrease the power of the input beam, such that the requirement of the classical intensity noise level is reduced in terms of the relative *intensity* noise level. Note that the requirement of the noise level in terms of the relative *shot*-noise level is unchanged.

In this section, the photodetectors for the feed-back control using the current actuator (tuning efficiency is shown in Fig. A.2a) and monitoring the achieved stability, the stabilization servo system, and the achieved stability will be explained.

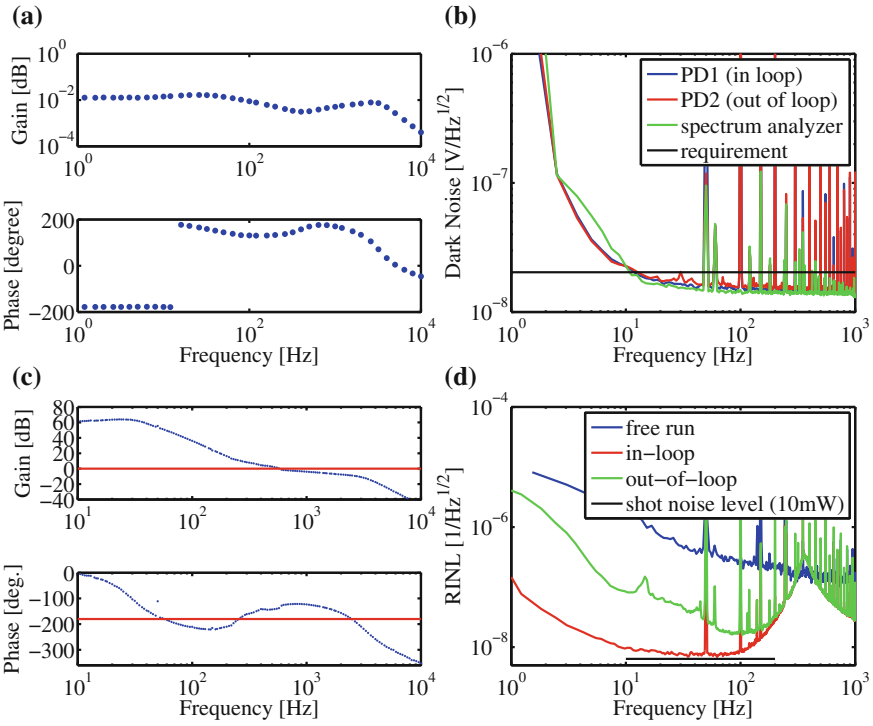

Fig. A.2 A series of measurements for intensity stabilization. **a** Transfer function from the intensity modulation of the laser to the PD1. **b** Dark noise of photodetectors. Observed spectra of the voltage fluctuation of the photodetectors. Both detectors satisfy the requirement (*black*). **c** Open-loop transfer function of the intensity stabilization. The unity-gain frequency was approximately at 600 Hz. **d** Measured intensity fluctuation. Observed spectra of intensity fluctuation of the input driving beam. The measured intensity fluctuation (*blue*), measured intensity fluctuation before the stabilization (*red*), and the requirement for achieving the shot-noise level inside the cavity (*green*) are shown

- **Photodetectors for intensity stabilization**
  The two beam-splitter output fields were focused onto Perkin Elmer C30642 InGaAs photodiodes with an active diameter of 2 mm. The electronics was designed by referring to that specified in Ref. [1]. Since intensity stabilization is performed by measuring the intensity fluctuation, the dark noise of the detectors has to be under the required intensity noise level. To confirm this, we measured the dark noise as shown in Fig. A.2b.

- **Servo system**
  We designed the servo system to have a comparable gain to achieve the goal sensitivity at about 10−100 Hz. The control signal was fed back to a current actuator of the laser head. Figure A.2c shows the measured openloop transfer function of the stabilization loop. The unity gain frequency was about 600 Hz, and

phase margin was 55°. The measured stabilization gain by the in-loop signal was about 30 dB at 100 Hz, which is comparable with the required gain.

- **Achieved stability**
  Figure A.2d shows the measured intensity noise. The actual stability of the stabilized laser was measured by the error signal of the non-stabilization loop (out-of-loop). The achieved stability does not satisfy our requirement by the active stabilization alone. To meet the demand, the passive common mode rejection by the interferometer can be used.

Reference

1. Kwee, P., Willke, B., Danzmann, K.: Shot-noise-limited laser power stabilization with a high-power photodiode array. Opt. Lett. **34**, 19 (2009)

Curriculum Vitae

Nobuyuki Matsumoto

Current affiliation address:
Sendai,
980-8578,
Japan
e-mail: nobuyuki.matsumoto.e7@tohoku.ac.jp

Appointments

- Assistant Professor,
  Tohoku University, Frontier Research Institute for Interdisciplinary Sciences and Research Institute of Electrical Communication (April 2015)
- JSPS Research Fellowship for Young Scientists (PD),
  The University of Tokyo (April 2014–May 2015)
- JSPS Research Fellowship for Young Scientists (DC),
  The University of Tokyo (April 2013–May 2014)

Education

- Doctor of Philosophy (Ph.D.) in Physics,
  The University of Tokyo (2011–2014), advisor: Dr. M. Ando
- Master of Science in Physics,
  The University of Tokyo (2009–2011), advisor: Dr. K. Tsubono
- Bachelor of Science in Physics,
  Keio University (2005–2009), advisor: Dr. Y. Ohashi

N. Matsumoto, *Classical Pendulum Feels Quantum Back-Action*,
Springer Theses, DOI 10.1007/978-4-431-55882-8